Studies on the Behavior of Nonequilibrium Gas Mixtures on the Basis of Kinetic Theory

Shingo Kosuge

2001

Studies on the Behavior of Nonequilibrium Gas Mixtures on the Basis of Kinetic Theory

Shingo Kosuge

2001

Preface

In aerospace engineering and in vacuum engineering connected with various advanced technologies, the understanding of the behavior of low-density gas flows is one of the important research subjects. On the other hand, in connection with the recent remarkable progress in micromechanical engineering, the control as well as the understanding of gas flows in microscales becomes increasingly important. The common feature of these two types of flow is the fact that the molecular mean free path is not negligibly small compared with the characteristic size of the systems, so that the states of the gas deviate from local equilibrium states. Nonequilibrium states also arise in the gas flows with evaporation and condensation which are commonly encountered in various fields of engineering and science. To be more specific, even when the molecular mean free path is negligibly small, the state of the gas is nonequilibrium in the vicinty of the boundary (or interface) on which evaporation or condensation is taking place.

For these nonequilibrium gas flows, the classical fluid or gas dynamics is not applicable, and a microscopic approach based on kinetic theory of gases is required. Such an approach is called the molecular gas dynamics or rarefied gas dynamics. Since the fundamental equation of the molecular gas dynamics, which is called the Boltzmann equation, is a nonlinear integro-differential equation that is much more complicated than the equations of classical fluid dynamics, its analysis is not an easy matter. Nevertheless, for single-component gases, there is a rich accumulation of successful and useful results. For instance, a general theory to describe the behavior of slightly rarefied gas flows (i.e., the gas flows in which the molecular mean free path is relatively small) by the use of fluid-dynamic type systems has been established by means of a systematic asymptotic analysis of the Boltzmann equation. At the same time, the validity of the classical fluid dynamics was examined in the light of this theory, and as a result an essential defect contained in the fluid dynamics was revealed. Further, accurate numerical methods for solving the Boltzmann and related kinetic equations have been developed, and various problems of fundamental importance have been clarified for wide ranges of gas rarefaction. However, for multicomponent gaseous mixtures, the accumulation of the results is much poorer because of more serious complexity of the

Boltzmann equation intrinsic to this case.

In the present study, therefore, we consider binary gas mixtures in nonequilibrium states and try to clarify the behavior of the mixture in some problems that appear to be of basic as well as of practical importance by means of asymptotic and numerical analyses of the Boltzmann equation. The content of the present thesis is as follows.

In Chap. 1, we consider flows of a vapor caused by evaporation and condensation on its two parallel plane condensed phases in the situation that another gas which neither evaporates nor condenses (a noncondensable gas) is contained in the vapor. Our main interest here is to clarify the behavior of the mixture in the continuum limit with respect to the vapor (i.e., the limit where the mean free path of the vapor molecules vanishes). By means of a systematic asymptotic analysis of the Boltzmann equation, it is shown that there are two types of the continuum limit depending on the amount of the noncondensable gas contained in the system. One of the limits exhibits a striking feature that an infinitesimal amount of the noncondensable gas gives a substantial effect on the vapor flows. These results are also confirmed by a numerical analysis of the Boltzmann equation using the direct simulation Monte Carlo (DSMC) method.

In Chap. 2, we investigate the structure of a shock wave for a binary mixture, which is one of the most fundamental nonequilibrium flows. First, we develop an accurate finite-difference method for the Boltzmann equation for hard-sphere molecules, in which a precise method for the computation of the complicated collision integrals is devised. Then, applying the method, we clarify the transition from the upstream equilibrium state to the downstream one through the shock wave in the level of the molecular velocity distribution function for a wide range of concentrations of the two components.

Finally in Chap. 3, we consider another fundamental problem, the problem of heat transfer in a binary rarefied mixture between two parallel plates with different temperatures. We analyze the problem numerically by using the finite-difference method developed in Chap. 2 and clarify the temperature and density distributions as well as the heat flow for typical cases of small to large mean free path. The behavior of the molecular velocity distribution function is also clarified.

Contents

Chapter 1

Evaporation and condensation between two parallel condensed phases in the presence of a noncondensable gas [1]

1.1 Introduction

Vapor flows with evaporation and condensation on the boundary are one of the main subjects in modern kinetic theory, and for single-component systems (composed of a pure vapor and its own condensed phase) many successful results have been obtained. For instance, a new type of gasdynamics (i.e., fluid-dynamic equations and their boundary conditions) describing such flows around arbitrarily shaped boundaries in the continuum limit (the limit as the Knudsen number tends to zero) has been established by means of a systematic asymptotic analysis of the Boltzmann equation for small Knudsen numbers.[2–6] At the same time, its higher-order correction due to the effect of gas rarefaction has also been obtained.[2–4] On the other hand, various problems, such as an evaporating flow from a spherical or cylindrical condensed phase[7–10] and a vapor flow past a spherical condensed phase,[11] have been investigated by accurate numerical analyses for the entire range of the Knudsen number, and the detailed structure of the vapor flows has been clarified.

Among these problems, the flow caused by evaporation and condensation between two parallel plane condensed phases (say, the two-surface problem) would be one of the most fundamental problems. In spite of the fact that the problem appears to be very simple, it contains some nontrivial features, such as the phenomenon of negative temperature gradient.[12,2] Therefore, it has been investigated by many authors,[12,2,13–23] and, as a result, some interesting behavior has been clarified. For example, in the continuum limit, the flow field becomes uniform except in the vanishingly thin Knudsen layers adjacent to the condensed phases, irrespective of the strength of evaporation and condensation.[5,21] Furthermore, this limiting behavior cannot be described correctly by the linearized Boltzmann equation, however weak the evaporation and condensation may be, and therefore a fully nonlinear treatment is always

necessary.[21]

In practical situations, however, evaporation and condensation often take place in the presence of another gas that neither evaporates nor condenses (say, a noncondensable gas). In the two-surface problem, in view of the above-mentioned behavior in the continuum limit for the (much simpler) single-component system, some nontrivial and essentially nonlinear behavior is expected in this limit when a noncondensable gas is contained in the vapor flow. The two-surface problem in the presence of a noncondensable gas has also been investigated in several papers.[24–31] However, only the case of weak evaporation and condensation has been considered on the basis of linearized equations or weakly nonlinear approaches for small Knudsen numbers. In addition, these works are mainly based on model Boltzmann equations. In fact, various model equations have been employed because the models for a mixture proposed so far are not so satisfactory as the BGK model[32–34] for a single-component gas. Consequently, the fully nonlinear behavior of the vapor and of the noncondensable gas, in particular, that in the continuum limit, has not been understood correctly.

The aim of this chapter is to obtain a clear understanding of the point mentioned above. That is, we investigate the two-surface problem of evaporation and condensation for a mixture of a vapor and a noncondensable gas in nonlinear situations on the basis of the Boltzmann equation. After the formulation of the problem in Sec. 1.2, we carry out an asymptotic analysis of the problem for small values of the Knudsen number (associated with vapor-vapor collisions) in Sec. 1.3, where the fundamental features of the continuum limit (with respect to the vapor) are clarified. Then, in Sec. 1.4, the problem is analyzed numerically by means of the direct simulation Monte Carlo method[35,36] for a wide range of the Knudsen number. Here, special attention is focused on the behavior of the system for small Knudsen numbers and in the continuum limit, and the basic features clarified by the asymptotic analysis are confirmed numerically.

The two-surface problem of evaporation and condensation (for the pure vapor case) is a physical example of the so-called slab problem which has also been an important subject of mathematical study[37–40] because it is the simplest boundary-value problem of the Boltzmann equation. Notable progress has been achieved in this field, and the existence of a solution of the (nonlinear) Boltzmann equation in a slab has been proved under some conditions.[38,40]

1.2 Formulation of problem and basic equation

1.2.A Problem and assumptions

We consider a vapor in the gap $0 < X_1 < D$ between two parallel plane surfaces at rest of its condensed phase, one located at $X_1 = 0$ and kept at temperature T_I and the other located at $X_1 = D$ (> 0) and kept at temperature T_{II}, where X_i is a space rectangular coordinate system. We suppose that a noncondensable gas is also contained in the gap. We investigate the steady flow of the vapor caused by evaporation and condensation and the behavior of the noncondensable gas under the following assumptions.

(i) The behavior of the vapor and that of the noncondensable gas are described by the Boltzmann equation for a binary mixture.

(ii) The molecules of the vapor and those of the noncondensable gas are hard (or rigid) spheres, and all the collisions between the molecules are completely elastic.

(iii) The vapor molecules leaving each surface of the condensed phase are distributed according to the corresponding part of the Maxwellian distribution describing the stationary saturated state at the temperature of the surface (the complete condensation condition).

(iv) The noncondensable gas molecules are reflected diffusely on the surfaces of the condensed phase.

1.2.B Basic equations

Let ξ_i (or $\boldsymbol{\xi}$) be the molecular velocity, $F^A(X_1, \boldsymbol{\xi})$ the velocity distribution function of the vapor molecules, and $F^B(X_1, \boldsymbol{\xi})$ that of the noncondensable gas molecules. The Boltzmann equation in the present problem is written in the following form.[41,42]

$$\xi_1 \frac{\partial F^\alpha}{\partial X_1} = J^{A\alpha}(F^A, F^\alpha) + J^{B\alpha}(F^B, F^\alpha), \qquad (\alpha = A, B), \tag{1.1}$$

where, with $\alpha = A, B$ and $\beta = A, B$,

$$J^{\beta\alpha}(F, G) = \frac{1}{2}(d^{\beta\alpha})^2 \int [F(\boldsymbol{\xi}_*^{\beta\alpha}) G(\boldsymbol{\xi}^{\beta\alpha}) - F(\boldsymbol{\xi}_*) G(\boldsymbol{\xi})] |\boldsymbol{\alpha} \cdot \mathbf{V}| d\Omega(\boldsymbol{\alpha}) d\boldsymbol{\xi}_*, \tag{1.2}$$

$$\boldsymbol{\xi}^{\beta\alpha} = \boldsymbol{\xi} + (\mu^{\beta\alpha}/m^{\alpha})(\boldsymbol{\alpha}\cdot\mathbf{V})\boldsymbol{\alpha}, \tag{1.3a}$$

$$\boldsymbol{\xi}_*^{\beta\alpha} = \boldsymbol{\xi}_* - (\mu^{\beta\alpha}/m^{\beta})(\boldsymbol{\alpha}\cdot\mathbf{V})\boldsymbol{\alpha}, \tag{1.3b}$$

$$\mathbf{V} = \boldsymbol{\xi}_* - \boldsymbol{\xi}, \tag{1.3c}$$

$$d^{\beta\alpha} = (d^{\alpha} + d^{\beta})/2, \tag{1.3d}$$

$$\mu^{\beta\alpha} = 2m^{\alpha}m^{\beta}/(m^{\alpha} + m^{\beta}). \tag{1.3e}$$

Here, $\boldsymbol{\xi}_*$ is the integration variable for $\boldsymbol{\xi}$, $\boldsymbol{\alpha}$ is a unit vector, $d\boldsymbol{\xi}_* = d\xi_{*1}d\xi_{*2}d\xi_{*3}$, and $d\Omega(\boldsymbol{\alpha})$ is the solid-angle element; m^A and d^A are the mass and the diameter of a vapor molecule, and m^B and d^B are those of a noncondensable-gas molecule; the domain of integration with respect to $\boldsymbol{\alpha}$ is all the directions, and that with respect to $\boldsymbol{\xi}_*$ is the whole space of $\boldsymbol{\xi}_*$.

The boundary conditions on the surfaces, the complete condensation condition for the vapor and the diffuse reflection for the noncondensable gas, are, with $\alpha = A, B$,

$$F^{\alpha} = \sigma_I^{\alpha}(m^{\alpha}/2\pi\kappa T_I)^{3/2}\exp(-m^{\alpha}\xi_i^2/2\kappa T_I), \quad \text{for} \quad \xi_1 > 0, \quad \text{at} \quad X_1 = 0, \tag{1.4}$$

$$\sigma_I^A = n_I, \tag{1.5a}$$

$$\sigma_I^B = -(2\pi m^B/\kappa T_I)^{1/2}\int_{\xi_1<0}\xi_1 F^B(0,\boldsymbol{\xi})d\boldsymbol{\xi}, \tag{1.5b}$$

and

$$F^{\alpha} = \sigma_{II}^{\alpha}(m^{\alpha}/2\pi\kappa T_{II})^{3/2}\exp(-m^{\alpha}\xi_i^2/2\kappa T_{II}), \quad \text{for} \quad \xi_1 < 0, \quad \text{at} \quad X_1 = D, \tag{1.6}$$

$$\sigma_{II}^A = n_{II}, \tag{1.7a}$$

$$\sigma_{II}^B = (2\pi m^B/\kappa T_{II})^{1/2}\int_{\xi_1>0}\xi_1 F^B(D,\boldsymbol{\xi})d\boldsymbol{\xi}, \tag{1.7b}$$

where n_I and n_{II} are the saturation number density of the vapor molecules at temperature T_I and that at temperature T_{II}, respectively, κ is the Boltzmann constant, and $d\boldsymbol{\xi} = d\xi_1 d\xi_2 d\xi_3$. Physically, the saturation vapor pressure (or number density) is a function of the temperature only, which depends on the substance of the vapor (the Clausius-Clapeyron equation[43]); thus, n_I and n_{II} are determined by T_I and T_{II}, respectively. In the following, however, such a relation is never used, and n_I and n_{II} are assumed to be parameters independent of T_I and T_{II}.

Now let us define the macroscopic variables of each component in terms of its velocity distribution function as follows. With $\alpha = A$ and B,

$$n^\alpha = \int F^\alpha d\boldsymbol{\xi}, \tag{1.8a}$$

$$u^\alpha = (1/n^\alpha) \int \xi_1 F^\alpha d\boldsymbol{\xi}, \tag{1.8b}$$

$$p^\alpha = \kappa n^\alpha T^\alpha = (1/3) \int m^\alpha (\xi_i - u^\alpha \delta_{i1})^2 F^\alpha d\boldsymbol{\xi}, \tag{1.8c}$$

where n^A, $\boldsymbol{v}^A = (u^A, 0, 0)$, p^A, and T^A are the molecular number density, the flow velocity, the *pressure*, and the *temperature* of the vapor, and n^B, $\boldsymbol{v}^B = (u^B, 0, 0)$, p^B, and T^B are the corresponding quantities of the noncondensable gas.[44] The domain of the integration with respect to $\boldsymbol{\xi}$ in Eqs. (1.8a) – (1.8c) and in what follows is the whole space of $\boldsymbol{\xi}$ unless otherwise stated. On the other hand, the molecular number density n, the density ρ, the flow velocity $\boldsymbol{v} = (u, 0, 0)$, the pressure p, and the temperature T of the total mixture of the vapor and the noncondensable gas are defined by

$$n = \int (F^A + F^B) d\boldsymbol{\xi}, \tag{1.9a}$$

$$\rho = \int (m^A F^A + m^B F^B) d\boldsymbol{\xi}, \tag{1.9b}$$

$$u = (1/\rho) \int \xi_1 (m^A F^A + m^B F^B) d\boldsymbol{\xi}, \tag{1.9c}$$

$$p = \kappa n T = (1/3) \int (\xi_i - u\delta_{i1})^2 (m^A F^A + m^B F^B) d\boldsymbol{\xi}. \tag{1.9d}$$

Therefore, they are expressed in terms of the macroscopic variables of individual components as follows.

$$n = n^A + n^B, \tag{1.10a}$$

$$\rho = m^A n^A + m^B n^B, \tag{1.10b}$$

$$u = (1/\rho)(m^A n^A u^A + m^B n^B u^B), \tag{1.10c}$$

$$p = p^A + m^A n^A (u^A - u)^2/3 + p^B + m^B n^B (u^B - u)^2/3. \tag{1.10d}$$

It should be noted that the solution to the boundary-value problem, Eqs. (1.1), (1.4), and (1.6), is not unique. In order to obtain a unique solution, we have to specify a quantity associated with the amount of the noncondensable gas. Here, we choose the average number

density

$$n_{av}^B = D^{-1}\int_0^D n^B(X_1)dX_1 = D^{-1}\int_0^D \int F^B d\boldsymbol{\xi} dX_1, \tag{1.11}$$

as the parameter to be specified.

Integrating both sides of Eq. (1.1) with respect to $\boldsymbol{\xi}$ over its whole space, we obtain

$$n^\alpha u^\alpha = \int \xi_1 F^\alpha d\boldsymbol{\xi} = const, \qquad (\alpha = A, B), \tag{1.12}$$

which expresses the mass conservation for each component. Since $n^B u^B = 0$ at $X_1 = 0$ and D because of the diffuse reflection condition for the noncondensable gas, we have

$$n^B u^B = 0, \qquad (0 \le X_1 \le D). \tag{1.13}$$

1.2.C Nondimensionalization

We now introduce the following nondimensional variables. With $\alpha = A$ and B,

$$x_1 = X_1/D, \quad \zeta_i = \xi_i(2\kappa T_I/m^A)^{-1/2}, \tag{1.14a}$$

$$\hat{F}^\alpha = F^\alpha(2\kappa T_I/m^A)^{3/2}/n_I, \tag{1.14b}$$

$$\hat{n}^\alpha = n^\alpha/n_I, \quad \hat{u}^\alpha = u^\alpha(2\kappa T_I/m^A)^{-1/2}, \tag{1.14c}$$

$$\hat{p}^\alpha = p^\alpha/p_I, \quad \hat{T}^\alpha = T^\alpha/T_I, \tag{1.14d}$$

$$\hat{n} = n/n_I, \quad \hat{\rho} = \rho/\rho_I, \tag{1.14e}$$

$$\hat{u} = u(2\kappa T_I/m^A)^{-1/2}, \quad \hat{p} = p/p_I, \tag{1.14f}$$

$$\hat{T} = T/T_I, \tag{1.14g}$$

where $\rho_I = m^A n_I$ and $p_I = \kappa n_I T_I$ are, respectively, the density and the pressure of the vapor in the saturated equilibrium state at rest at temperature T_I. In what follows, the symbol $\boldsymbol{\zeta}$ is also used for ζ_i.

The Boltzmann equation (1.1) is then nondimensionalized as follows.

$$\zeta_1 \frac{\partial \hat{F}^\alpha}{\partial x_1} = \frac{1}{k}[C^{A\alpha}\hat{J}^{A\alpha}(\hat{F}^A, \hat{F}^\alpha) + C^{B\alpha}\hat{J}^{B\alpha}(\hat{F}^B, \hat{F}^\alpha)], \qquad (\alpha = A, B), \tag{1.15}$$

where, with $\alpha = A, B$ and $\beta = A, B$,

$$\hat{J}^{\beta\alpha}(\hat{F}, \hat{G}) = \frac{1}{4\sqrt{2\pi}}\int [\hat{F}(\boldsymbol{\zeta}_*^{\beta\alpha})\hat{G}(\boldsymbol{\zeta}^{\beta\alpha}) - \hat{F}(\boldsymbol{\zeta}_*)\hat{G}(\boldsymbol{\zeta})]|\boldsymbol{\alpha}\cdot\hat{\mathbf{V}}|d\Omega(\boldsymbol{\alpha})d\boldsymbol{\zeta}_*, \tag{1.16}$$

$$\boldsymbol{\zeta}^{\beta\alpha} = \boldsymbol{\zeta} + (\hat{\mu}^{\beta\alpha}/\lambda^{\alpha})(\boldsymbol{\alpha}\cdot\hat{\mathbf{V}})\boldsymbol{\alpha}, \tag{1.17a}$$

$$\boldsymbol{\zeta}_*^{\beta\alpha} = \boldsymbol{\zeta}_* - (\hat{\mu}^{\beta\alpha}/\lambda^{\beta})(\boldsymbol{\alpha}\cdot\hat{\mathbf{V}})\boldsymbol{\alpha}, \tag{1.17b}$$

$$\hat{\mathbf{V}} = \boldsymbol{\zeta}_* - \boldsymbol{\zeta}, \tag{1.17c}$$

$$C^{AA} = 1, \quad C^{BA} = C^{AB} = (1 + d^B/d^A)^2/4, \quad C^{BB} = (d^B/d^A)^2, \tag{1.17d}$$

$$\hat{\mu}^{\beta\alpha} = 2\lambda^{\alpha}\lambda^{\beta}/(\lambda^{\alpha} + \lambda^{\beta}), \quad \lambda^A = 1, \quad \lambda^B = m^B/m^A, \tag{1.17e}$$

$$k = (\sqrt{\pi}/2)\mathrm{Kn} = (\sqrt{\pi}/2)(\ell/D), \tag{1.17f}$$

$$\ell = [\sqrt{2}\pi(d^A)^2 n_I]^{-1}. \tag{1.17g}$$

Here, $\boldsymbol{\zeta}_*$ is the integration variable for $\boldsymbol{\zeta}$, $d\boldsymbol{\zeta}_* = d\zeta_{*1}d\zeta_{*2}d\zeta_{*3}$, the domain of integration with respect to the unit vector $\boldsymbol{\alpha}$ is all the directions, and that with respect to $\boldsymbol{\zeta}_*$ is its whole space; ℓ is the mean free path of the vapor molecules in the equilibrium state at rest with temperature T_I and molecular number density n_I, and thus Kn is the Knudsen number based on ℓ and D.

The nondimensional form of the boundary conditions at $x_1 = 0$ and 1, corresponding to Eqs. (1.4) – (1.7b), is written as, with $\alpha = A, B$,

$$\hat{F}^{\alpha} = \pi^{-3/2}\hat{\sigma}_w^{\alpha}(\lambda^{\alpha})^{3/2}\hat{T}_w^{-3/2}\exp(-\lambda^{\alpha}\hat{T}_w^{-1}\zeta_i^2), \quad \text{for} \quad \zeta_i a_i > 0, \tag{1.18}$$

$$\hat{\sigma}_w^A = \hat{n}_w, \tag{1.19a}$$

$$\hat{\sigma}_w^B = -2\sqrt{\pi}(m^B/m^A)^{1/2}\hat{T}_w^{-1/2}\int_{\zeta_j a_j<0}\zeta_i a_i \hat{F}^B d\boldsymbol{\zeta}, \tag{1.19b}$$

where

$$\hat{T}_w = 1, \quad \hat{n}_w = 1, \quad a_i = (1,0,0), \quad \text{at} \quad x_1 = 0, \tag{1.20a}$$

$$\hat{T}_w = T_{II}/T_I, \quad \hat{n}_w = n_{II}/n_I, \quad a_i = (-1,0,0), \quad \text{at} \quad x_1 = 1. \tag{1.20b}$$

The nondimensional form of the relations between the macroscopic variables and the

velocity distribution functions, Eqs. (1.8a) – (1.10d), is given by

$$\hat{n}^\alpha = \int \hat{F}^\alpha d\boldsymbol{\zeta}, \quad \hat{u}^\alpha = (\hat{n}^\alpha)^{-1} \int \zeta_1 \hat{F}^\alpha d\boldsymbol{\zeta}, \tag{1.21a}$$

$$\hat{p}^\alpha = \hat{n}^\alpha \hat{T}^\alpha = (2/3)\lambda^\alpha \int (\zeta_i - \hat{u}^\alpha \delta_{i1})^2 \hat{F}^\alpha d\boldsymbol{\zeta}, \tag{1.21b}$$

$$\hat{n} = \int (\hat{F}^A + \hat{F}^B) d\boldsymbol{\zeta} = \hat{n}^A + \hat{n}^B, \tag{1.21c}$$

$$\hat{\rho} = \int (\hat{F}^A + \frac{m^B}{m^A} \hat{F}^B) d\boldsymbol{\zeta} = \hat{n}^A + \frac{m^B}{m^A} \hat{n}^B, \tag{1.21d}$$

$$\hat{u} = \hat{\rho}^{-1} \int \zeta_1 (\hat{F}^A + \frac{m^B}{m^A} \hat{F}^B) d\boldsymbol{\zeta} = \hat{\rho}^{-1} (\hat{n}^A \hat{u}^A + \frac{m^B}{m^A} \hat{n}^B \hat{u}^B), \tag{1.21e}$$

$$\begin{aligned} \hat{p} = \hat{n}\hat{T} &= (2/3) \int (\zeta_i - \hat{u}\delta_{i1})^2 (\hat{F}^A + \frac{m^B}{m^A} \hat{F}^B) d\boldsymbol{\zeta} \\ &= \hat{p}^A + \frac{2}{3} \hat{n}^A (\hat{u}^A - \hat{u})^2 + \hat{p}^B + \frac{2}{3} \frac{m^B}{m^A} \hat{n}^B (\hat{u}^B - \hat{u})^2. \end{aligned} \tag{1.21f}$$

Here and in what follows, the domain of integration with respect to $\boldsymbol{\zeta}$ is its whole space unless otherwise stated.

Equation (1.15) and boundary conditions (1.18) – (1.19b) contain the following nondimensional parameters to be specified (cf. the second paragraph in Sec. 1.2.B).

$$\frac{T_{II}}{T_I}, \quad \frac{n_{II}}{n_I}, \quad k \text{ (or Kn)}, \quad \frac{m^B}{m^A}, \quad \frac{d^B}{d^A}. \tag{1.22}$$

In addition, we have to specify the parameter

$$\frac{n^B_{av}}{n_I} = \int_0^1 \hat{n}^B dx_1, \tag{1.23}$$

corresponding to Eq. (1.11), to obtain a unique solution of the problem. On the other hand, from Eqs. (1.12) and (1.13) , we have the following mass conservation relation,

$$\hat{n}^A \hat{u}^A = const \quad \text{and} \quad \hat{n}^B \hat{u}^B = 0, \quad \text{for} \quad 0 \le x_1 \le 1. \tag{1.24}$$

Here, we mention other Knudsen numbers. Let us consider the equilibrium state at rest with temperature T_I of the mixture of the vapor with number density n_I and the noncondensable gas with number density n^B_{av}. We denote by ℓ^{BA} the mean free path of the vapor molecules with respect to their collisions with the noncondensable gas, by ℓ^{AB} that of the noncondensable-gas molecules with respect to their collisions with the vapor, and by ℓ^{BB} that of the noncondensable-gas molecules with respect to the collisions among themselves.

Then, ℓ^{BA}, ℓ^{AB}, and ℓ^{BB} are given as

$$\ell^{BA} = [\pi(d^{AB})^2 n_{av}^B]^{-1}[m^B/(m^A+m^B)]^{1/2}, \tag{1.25a}$$

$$\ell^{AB} = [\pi(d^{AB})^2 n_I]^{-1}[m^A/(m^A+m^B)]^{1/2}, \tag{1.25b}$$

$$\ell^{BB} = [\sqrt{2}\pi(d^B)^2 n_{av}^B]^{-1}. \tag{1.25c}$$

Therefore, if we introduce the following Knudsen numbers:

$$\mathrm{Kn}^{BA} = \ell^{BA}/D, \quad \mathrm{Kn}^{AB} = \ell^{AB}/D, \quad \mathrm{Kn}^{BB} = \ell^{BB}/D, \tag{1.26}$$

they are expressed in terms of the parameters in Eqs. (1.22) and (1.23), namely,

$$\mathrm{Kn}^{BA} = 4\sqrt{2}\left(\frac{n_{av}^B}{n_I}\right)^{-1}\left(1+\frac{d^B}{d^A}\right)^{-2}\left(\frac{m^B/m^A}{1+m^B/m^A}\right)^{1/2}\mathrm{Kn}, \tag{1.27a}$$

$$\mathrm{Kn}^{AB} = 4\sqrt{2}\left(1+\frac{d^B}{d^A}\right)^{-2}\left(\frac{1}{1+m^B/m^A}\right)^{1/2}\mathrm{Kn}, \tag{1.27b}$$

$$\mathrm{Kn}^{BB} = \left(\frac{n_{av}^B}{n_I}\right)^{-1}\left(\frac{d^B}{d^A}\right)^{-2}\mathrm{Kn}. \tag{1.27c}$$

1.3 Asymptotic analysis for small Knudsen numbers

In this section, we investigate the asymptotic behavior of the gases for small Knudsen numbers (Kn or $k \ll 1$) with special interest in the continuum limit (Kn or $k \to 0$).

1.3.A Hilbert expansion

To begin with, we seek a moderately varying solution $\hat{F}_H^A$ and $\hat{F}_H^B$ of Eq. (1.15) [i.e., $\partial \hat{F}_H^{A,B}/\partial x_1 = O(\hat{F}_H^{A,B})$] by the simple power series expansion (Hilbert expansion), namely,

$$\hat{F}_H^\alpha = \hat{F}_{H0}^\alpha + \hat{F}_{H1}^\alpha k + \hat{F}_{H2}^\alpha k^2 + \cdots, \qquad (\alpha = A, B). \tag{1.28}$$

If we substitute Eq. (1.28) for $\hat{F}^\alpha$ in Eqs. (1.21a)–(1.21f), we obtain the corresponding power series expansions of the macroscopic variables of each component and of the total mixture, namely,

$$h_H^\alpha = h_{H0}^\alpha + h_{H1}^\alpha k + h_{H2}^\alpha k^2 + \cdots, \qquad (\alpha = A, B), \tag{1.29a}$$

$$h_H = h_{H0} + h_{H1} k + h_{H2} k^2 + \cdots, \tag{1.29b}$$

where h_H^α represents $\hat{n}_H^\alpha$, $\hat{u}_H^\alpha$, $\hat{T}_H^\alpha$, etc., h_H represents $\hat{n}_H$, $\hat{u}_H$, $\hat{T}_H$, etc., and the subscript H indicates the quantities corresponding to the moderately varying solution $\hat{F}_H^\alpha$. Substituting

Eq. (1.28) into Eq. (1.15) and equating the coefficients of k^m $(m = 0, 1, ...)$, we obtain a sequence of integral equations for $\hat{F}^{\alpha}_{Hm}$, i.e., with $\alpha = A, B$,

$$C^{A\alpha}\hat{J}^{A\alpha}(\hat{F}^{A}_{H0}, \hat{F}^{\alpha}_{H0}) + C^{B\alpha}\hat{J}^{B\alpha}(\hat{F}^{B}_{H0}, \hat{F}^{\alpha}_{H0}) = 0, \tag{1.30}$$

$$\sum_{l=0}^{m}[C^{A\alpha}\hat{J}^{A\alpha}(\hat{F}^{A}_{Hm-l}, \hat{F}^{\alpha}_{Hl}) + C^{B\alpha}\hat{J}^{B\alpha}(\hat{F}^{B}_{Hm-l}, \hat{F}^{\alpha}_{Hl})] = \zeta_1 \frac{\partial \hat{F}^{\alpha}_{Hm-1}}{\partial x_1}, \quad (m = 1, 2, ...). \tag{1.31}$$

As is well known,[41,42] the solution of Eq. (1.30) is given by local Maxwellian distributions

$$\hat{F}^{\alpha}_{H0} = \pi^{-3/2}\hat{n}^{\alpha}_{H0}\left(\frac{\hat{T}^{\alpha}_{H0}}{\lambda^{\alpha}}\right)^{-3/2} \exp\left(-\frac{\lambda^{\alpha}}{\hat{T}^{\alpha}_{H0}}(\zeta_i - \hat{u}^{\alpha}_{H0}\delta_{i1})^2\right), \quad (\alpha = A, B), \tag{1.32}$$

with the condition

$$\hat{u}^{A}_{H0} = \hat{u}^{B}_{H0} = \hat{u}_{H0}, \quad \hat{T}^{A}_{H0} = \hat{T}^{B}_{H0} = \hat{T}_{H0}. \tag{1.33}$$

On the other hand, Eq. (1.24) gives

$$\hat{n}^{B}_{H0}\hat{u}^{B}_{H0} \equiv 0, \tag{1.34}$$

which implies $\hat{n}^{B}_{H0} \equiv 0$ or $\hat{u}^{B}_{H0} \equiv 0$ (with $\hat{n}^{B}_{H0} \not\equiv 0$). We investigate these two cases separately.

1 The case of $\hat{u}^{B}_{H0} \equiv 0$ with $\hat{n}^{B}_{H0} \not\equiv 0$

In this case, from Eq. (1.33), we have

$$\hat{u}^{A}_{H0} = \hat{u}_{H0} \equiv 0. \tag{1.35}$$

Therefore, $\hat{F}^{A}_{H0}$ and $\hat{F}^{B}_{H0}$ are given by

$$\hat{F}^{\alpha}_{H0} = \pi^{-3/2}\hat{n}^{\alpha}_{H0}\left(\frac{\hat{T}_{H0}}{\lambda^{\alpha}}\right)^{-3/2} \exp\left(-\frac{\lambda^{\alpha}\zeta_i^2}{\hat{T}_{H0}}\right), \quad (\alpha = A, B). \tag{1.36}$$

Now let us assume that $\hat{n}^{A}_{H0}$ and $\hat{T}_{H0}$ take the following values on the surfaces of the condensed phase.

$$\hat{n}^{A}_{H0} = 1, \quad \hat{T}_{H0} = 1, \quad \text{at} \quad x_1 = 0, \tag{1.37a}$$

$$\hat{n}^{A}_{H0} = n_{II}/n_I, \quad \hat{T}_{H0} = T_{II}/T_I, \quad \text{at} \quad x_1 = 1. \tag{1.37b}$$

Then, $\hat{F}^{A}_{H0}$ and $\hat{F}^{B}_{H0}$ of Eq. (1.36) satisfy boundary conditions (1.18) – (1.20b) at the order of k^0. In order to determine $\hat{n}^{A}_{H0}$, $\hat{n}^{B}_{H0}$, and $\hat{T}_{H0}$ in the gas, we need to proceed to the higher

order in k. However, Eqs. (1.35), (1.37a), and (1.37b) show the following behavior in the continuum limit: As $k \to 0$,

$$\hat{u}_H^A \to 0, \tag{1.38}$$

and

$$\hat{n}_H^A \to 1, \quad \hat{T}_H \to 1, \qquad \text{at} \quad x_1 = 0, \tag{1.39a}$$

$$\hat{n}_H^A \to n_{II}/n_I, \quad \hat{T}_H \to T_{II}/T_I, \qquad \text{at} \quad x_1 = 1. \tag{1.39b}$$

Since the condition $\hat{n}_{H0}^B \not\equiv 0$ corresponds to $n_{av}^B/n_I \neq 0$ irrespective of the values of k, Eq. (1.38) shows the following important result: For any (non-zero) fixed value of n_{av}^B/n_I, evaporation and condensation stop in the continuum limit. In other words, the vapor flow ($\hat{u}^A$), which is controlled by the diffusion caused by the nonuniformity of $\hat{n}_{H0}^A$, $\hat{n}_{H0}^B$, and $\hat{T}_{H0}$, is of $O(\mathrm{Kn})$ and becomes vanishingly small in this limit. It is seen from Eqs. (1.27a) – (1.27c) that, in this limit, all the Knudsen numbers Kn^{BA}, Kn^{AB}, and Kn^{BB} tend to zero in proportion to k (or Kn).

2 The case of $\hat{n}_{H0}^B \equiv 0$

In this case, $\hat{u}_{H0}^A$ is not identically zero, and $\hat{F}_{H0}^A$ and $\hat{F}_{H0}^B$ are given by

$$\hat{F}_{H0}^A = \pi^{-3/2} \hat{n}_{H0}^A (\hat{T}_{H0}^A)^{-3/2} \exp\left(-\frac{(\zeta_i - \hat{u}_{H0}^A \delta_{i1})^2}{\hat{T}_{H0}^A} \right), \tag{1.40a}$$

$$\hat{F}_{H0}^B = 0. \tag{1.40b}$$

First, we show that $\hat{F}_{Hm}^B \equiv 0$ for any m. Let us assume that $\hat{F}_{H0}^B$, ..., $\hat{F}_{Hm-1}^B \equiv 0$. Then, from Eq. (1.31) with $\alpha = B$, we have

$$\hat{J}^{AB}(\hat{F}_{H0}^A, \hat{F}_{Hm}^B) = 0. \tag{1.41}$$

The solution to this equation is given by the form[45]

$$\hat{F}_{Hm}^B = C_m(x_1) \exp\left(-\frac{m^B}{m^A} \frac{(\zeta_i - \hat{u}_{H0}^A \delta_{i1})^2}{\hat{T}_{H0}^A} \right), \tag{1.42}$$

where $C_m(x_1)$ is an arbitrary function of x_1. On the other hand, we have, from Eq. (1.24),

$$\int \zeta_1 \hat{F}_{Hm}^B d\boldsymbol{\zeta} = 0. \tag{1.43}$$

The substitution of Eq. (1.42) into Eq. (1.43) leads to $C_m(x_1) \equiv 0$, i.e., $\hat{F}^B_{Hm} \equiv 0$. Therefore, it follows from Eq. (1.40b) that

$$\hat{F}^B_{Hm} \equiv 0, \qquad (m = 1, 2, ...). \tag{1.44}$$

Next, we consider $\hat{F}^A_{Hm}$. As is seen from Eq. (1.40a), $\hat{F}^A_{H0}$ does not fit to boundary condition (1.18) with $\alpha = A$. In order to obtain a solution satisfying the boundary condition, we have to introduce the Knudsen layers, with thickness of the order of the mean free path, adjacent to the surfaces of the condensed phase. The discussion about the Knudsen layers being left in Sec. 1.3.B, let us suppose, for the moment, that we have obtained the k^0-order solution (for $\hat{F}^A$ and $\hat{F}^B$) that satisfies boundary condition (1.18) at the order of k^0 and coincides with Eqs. (1.40a) and (1.40b) except in the Knudsen layers. Then, for the higher-order terms, boundary condition (1.18) with $\alpha = A$ becomes $(\hat{F}^A)_m = 0$ ($\zeta_i a_i > 0$; $m \geq 1$), where $(\hat{F}^A)_m$ indicates the k^m-order term of $\hat{F}^A$. It should also be noted that Eq. (1.44) satisfies boundary condition (1.18) with $\alpha = B$ at the order of k^m. We are going to show that $\hat{n}^A_{H0}$, $\hat{T}^A_{H0}$, and $\hat{u}^A_{H0}$ are constants and that $\hat{F}^A_{Hm} \equiv 0$ ($m \geq 1$) is a consistent solution except for a special case. With Eqs. (1.40b) and (1.44), Eq. (1.31) is reduced to a sequence of inhomogeneous linear integral equations for $\hat{F}^A_{Hm}$ ($m \geq 1$), i.e.,

$$\begin{aligned} &\hat{J}^{AA}(\hat{F}^A_{Hm}, \hat{F}^A_{H0}) + \hat{J}^{AA}(\hat{F}^A_{H0}, \hat{F}^A_{Hm}) \\ &= \zeta_1 \frac{\partial \hat{F}^A_{Hm-1}}{\partial x_1} - \sum_{l=1}^{m-1} \hat{J}^{AA}(\hat{F}^A_{Hm-l}, \hat{F}^A_{Hl}), \qquad (m = 1, 2, ...), \end{aligned} \tag{1.45}$$

where $\sum_{l=1}^{0}$ is understood to be zero. The homogeneous equation of Eq. (1.45) [i.e., Eq. (1.45) with the right-hand side being put to be zero] has the five independent nontrivial solutions $\hat{F}^A_{H0}$, $\hat{F}^A_{H0}\zeta_i$, and $\hat{F}^A_{H0}\zeta_j^2$.[46,45] Therefore, the inhomogeneous term of Eq. (1.45) should satisfy the following solvability condition to have a solution:

$$\int (1, \zeta_1, \zeta_j^2)[\text{RHS of Eq. (1.45)}] d\boldsymbol{\zeta} = 0, \tag{1.46}$$

which reduces to

$$\int (1, \zeta_1, \zeta_j^2)\zeta_1 \frac{\partial \hat{F}^A_{Hm-1}}{\partial x_1} d\boldsymbol{\zeta} = 0. \tag{1.47}$$

And the solution of Eq. (1.45) is expressed as

$$\hat{F}^A_{Hm} = \hat{F}^A_{H0}(C_{0m} + C_{1m}\zeta_1 + C_{4m}\zeta_j^2) + \Psi_m, \tag{1.48}$$

where C_{0m}, C_{1m}, and C_{4m} are undetermined functions of x_1, and Ψ_m is a particular solution of Eq. (1.45) orthogonal to $\hat{F}^A_{H0}$, $\hat{F}^A_{H0}\zeta_1$, and $\hat{F}^A_{H0}\zeta_j^2$. Here, we have taken into account the fact that we are looking for the solution which is even in ζ_2 and ζ_3 (note that the X_2 and X_3 components of $\boldsymbol{v}^A$ are assumed to be zero). From Eq. (1.40a) and Eq. (1.47) with $m = 1$, it follows that $\hat{n}^A_{H0}$, $\hat{T}^A_{H0}$, and $\hat{u}^A_{H0}$ are all (undetermined) constants (this corresponds to the compressible Euler equations[5]). Therefore, Eq. (1.45) with $m = 1$ reduces to the homogeneous equation, and its solution is given by Eq. (1.48) ($m = 1$) with $\Psi_1 = 0$. Using this solution in Eq. (1.47) with $m = 2$, we obtain simultaneous, linear, and homogeneous equations for dC_{01}/dx_1, dC_{11}/dx_1, and dC_{41}/dx_1. These equations give the (trivial) solution $dC_{01}/dx_1 = dC_{11}/dx_1 = dC_{41}/dx_1 = 0$ (i.e., C_{01}, C_{11}, and C_{41} are constants) if $\hat{u}^A_{H0} \neq \pm(5\hat{T}^A_{H0}/6)^{1/2}$. When $\hat{u}^A_{H0} = \pm(5\hat{T}^A_{H0}/6)^{1/2}$, that is, the flow speed corresponding to $\hat{u}^A_{H0}$ is sonic, there exists a nontrivial solution for dC_{01}/dx_1, dC_{11}/dx_1, and dC_{41}/dx_1, and therefore C_{01}, C_{11}, and C_{41} can take nonconstant values. Let us restrict ourselves to the case $\hat{u}^A_{H0} \neq \pm(5\hat{T}^A_{H0}/6)^{1/2}$. If we assume that $C_{01} = C_{11} = C_{41} = 0$, that is, $\hat{F}^A_{H1} \equiv 0$, then it satisfies boundary condition (1.18) with $\alpha = A$ at the order of k (see the fourth sentence in this paragraph). Similarly, we can show that $\hat{F}^A_{Hm} \equiv 0$ ($m \geq 2$) is a solution to Eq. (1.45) satisfying boundary condition (1.18) with $\alpha = A$ at the order of k^m.

To summarize, Eq. (1.40a) (with $\hat{n}^A_{H0}$, $\hat{T}^A_{H0}$, and $\hat{u}^A_{H0}$ being undetermined constants) and Eq. (1.40b) are the k^0-order solution except in the Knudsen layers adjacent to the surfaces of the condensed phase; $\hat{F}^B_{Hm} \equiv 0$ ($m \geq 1$) is the k^m-order solution satisfying boundary condition (1.18) with $\alpha = B$; furthermore, $\hat{F}^A_{Hm} \equiv 0$ ($m \geq 1$) gives the k^m-order solution satisfying boundary condition (1.18) with $\alpha = A$ when $\hat{u}^A_{H0} \neq \pm(5\hat{T}^A_{H0}/6)^{1/2}$. Therefore, the remaining task is to find the Knudsen-layer solution at the k^0 order which can be connected to Eqs. (1.40a) and (1.40b) and satisfies boundary condition (1.18). The constants $\hat{n}^A_{H0}$, $\hat{T}^A_{H0}$, and $\hat{u}^A_{H0}$ are determined by this analysis.

Since $\hat{F}^B_{Hm} \equiv 0$ ($m \geq 0$), the noncondensable gas can exist only in the Knudsen layers. As will be seen in Sec. 1.3.B, it can exist only in the Knudsen layer at the condensing surface. Let us suppose that $\hat{n}^B$ is of the order of unity in the Knudsen layer. [This is confirmed by the numerical analysis of the half-space problem of condensation,[47,48] which is equivalent to the problem of the Knudsen layer at the condensing surface (see Sec. 1.3.B).] Then, the average number density n^B_{av} is estimated as $n^B_{av}/n_I = O(\mathrm{Kn})$ because the thickness of the

Knudsen layer is of the order of ℓ. In other words, if we consider the case of small Kn with the condition $n_{av}^B/n_I = O(\mathrm{Kn})$, then all the amount of the noncondensable gas is confined in the Knudsen layer at the condensing surface. From Eqs. (1.27a) – (1.27c), it is seen that $\mathrm{Kn}^{BA} = O(1)$, $\mathrm{Kn}^{AB} = O(\mathrm{Kn})$, and $\mathrm{Kn}^{BB} = O(1)$ in this case.

1.3.B Knudsen-layer analysis and determination of $\hat{F}_{H0}^A$ for the case of $\hat{n}_{H0}^B \equiv 0$

In this section, we try to obtain the k^0-order solution satisfying the boundary condition for the case of $\hat{n}_{H0}^B \equiv 0$ in Sec. 1.3.A. For this purpose, we assume that the physical quantities undergo significant changes in the thin layers with thickness of the order of the mean free path adjacent to the surfaces of the condensed phase. Let us denote the k^0-order velocity distribution functions in the layers by $\hat{F}_0^A$ and $\hat{F}_0^B$, introduce the stretched space coordinate η, i.e.,

$$\begin{aligned} &\eta = x_1/k, \qquad \text{(for the layer adjacent to } x_1 = 0), \qquad \text{or} \\ &\eta = (1 - x_1)/k, \qquad \text{(for the layer adjacent to } x_1 = 1), \end{aligned} \tag{1.49}$$

and assume that $\partial \hat{F}_0^{A,B}/\partial\eta = O(\hat{F}_0^{A,B})$ [or $\partial \hat{F}_0^{A,B}/\partial x_1 = O(\hat{F}_0^{A,B}/k)$]. The $\hat{F}_0^A$ and $\hat{F}_0^B$ are, respectively, supposed to approach $\hat{F}_{H0}^A$ and $\hat{F}_{H0}^B$ ($\equiv 0$) rapidly as η tends to infinity. Then, from Eq. (1.15) and boundary condition (1.18), we obtain the equations and boundary conditions for $\hat{F}_0^A$ and $\hat{F}_0^B$, namely, for $\alpha = A, B$,

$$\zeta_i a_i \frac{\partial \hat{F}_0^\alpha}{\partial \eta} = C^{A\alpha} \hat{J}^{A\alpha}(\hat{F}_0^A, \hat{F}_0^\alpha) + C^{B\alpha} \hat{J}^{B\alpha}(\hat{F}_0^B, \hat{F}_0^\alpha), \tag{1.50}$$

$$\hat{F}_0^\alpha = \pi^{-3/2} \hat{\sigma}_{w0}^\alpha (\lambda^\alpha)^{3/2} \hat{T}_w^{-3/2} \exp(-\lambda^\alpha \hat{T}_w^{-1} \zeta_i^2), \quad \text{for} \quad \zeta_i a_i > 0, \quad \text{at} \quad \eta = 0, \tag{1.51}$$

$$\hat{\sigma}_{w0}^A = \hat{n}_w, \tag{1.52a}$$

$$\hat{\sigma}_{w0}^B = -2\sqrt{\pi}(m^B/m^A)^{1/2} \hat{T}_w^{-1/2} \int_{\zeta_j a_j < 0} \zeta_i a_i \hat{F}_0^B(\eta = 0, \boldsymbol{\zeta}) d\boldsymbol{\zeta}, \tag{1.52b}$$

and

$$\hat{F}_0^A \to \hat{F}_{H0}^A, \quad \hat{F}_0^B \to 0, \qquad \text{as} \quad \eta \to \infty, \tag{1.53}$$

where

$$a_i = (1,0,0), \quad \hat{T}_w = 1, \quad \hat{n}_w = 1, \quad \text{(for the layer adjacent to } x_1 = 0), \tag{1.54a}$$

$$a_i = (-1,0,0), \quad \hat{T}_w = T_{II}/T_I, \quad \hat{n}_w = n_{II}/n_I, \quad \text{(for the layer adjacent to } x_1 = 1). \tag{1.54b}$$

This problem is nothing other than the problem of an evaporating or condensing flow in a half space (the so-called half-space problem) in the presence of a noncondensable gas.

For the case of evaporation ($\hat{u}^A_{H0} a_1 > 0$), there is a solution to Eqs. (1.50)–(1.53) only when $\hat{F}^B_0 \equiv 0$. Physically, this means that, if there is a noncondensable gas in the Knudsen layer, it cannot stay there and is blown away toward infinity by the vapor flow. An example of such transition process is investigated in Refs. 49 and 50. Therefore, the problem is reduced to that for a pure vapor studied in Refs. 51–54. In this problem, the solution exists only when the parameters $\hat{T}_w$, $\hat{n}_w$, $\hat{T}^A_{H0}$, $\hat{n}^A_{H0}$, and $\hat{u}^A_{H0}$ satisfy the following relation.

$$M \le 1, \qquad \frac{\hat{n}^A_{H0}}{\hat{n}_w} = \frac{h_1(M)}{h_2(M)}, \qquad \frac{\hat{T}^A_{H0}}{\hat{T}_w} = h_2(M), \tag{1.55}$$

where

$$M = (6/5)^{1/2} |\hat{u}^A_{H0}| (\hat{T}^A_{H0})^{-1/2}, \tag{1.56}$$

which is the Mach number at infinity (i.e., the Mach number based on $\hat{u}^A_{H0}$ and $\hat{T}^A_{H0}$). The numerical data of $h_1(M)$ and $h_2(M)$ as well as the profiles of the macroscopic variables in the Knudsen layer, obtained by an accurate numerical analysis of the BGK model, are given in Ref. 54 (see also Ref. 8). The analytical form of these functions for $M \ll 1$ is obtained in Ref. 51 (see also Ref. 55).

For the case of condensation ($\hat{u}^A_{H0} a_1 < 0$), the problem was studied in Refs. 47 and 48. In Ref. 47, by considering the case where the molecule of the noncondensable gas is mechanically identical with that of the vapor, the problem was successfully decomposed into two problems, one for the total mixture and the other for the noncondensable gas. The former problem is identical with the half-space problem of condensation for a pure vapor, which has extensively been investigated in the literature (e.g., Refs. 51,56–58,6, and 59–61). For example, the condition that allows a steady solution has been clarified in a series of analytical and numerical studies.[51,57,58,6,61] Therefore, the above decomposition enables us to

exploit the comprehensive results for the pure-vapor case obtained so far. Furthermore, this approach not only reduces the necessary amount of computation drastically, but also gives the clear understanding of the basic structure of the solution. According to Ref. 47, under the above condition that the molecules of the two components are identical (i.e., $m^B/m^A = 1$ and $d^B/d^A = 1$ for hard-sphere molecules), the solution to Eqs. (1.50) – (1.53) exists only when the parameters $\hat{T}_w$, $\hat{n}_w$, $\hat{T}^A_{H0}$, $\hat{n}^A_{H0}$, and $\hat{u}^A_{H0}$ satisfy the following relation.

$$\frac{\hat{n}^A_{H0}}{\hat{n}_w} = \left(\frac{\hat{T}^A_{H0}}{\hat{T}_w}\right)^{-1} \tilde{F}_s\left(M, \frac{\hat{T}^A_{H0}}{\hat{T}_w}, \Gamma\right), \qquad \text{for} \quad M < 1, \tag{1.57a}$$

$$\frac{\hat{n}^A_{H0}}{\hat{n}_w} > \left(\frac{\hat{T}^A_{H0}}{\hat{T}_w}\right)^{-1} \tilde{F}_b\left(M, \frac{\hat{T}^A_{H0}}{\hat{T}_w}, \Gamma\right), \qquad \text{for} \quad M \geq 1, \tag{1.57b}$$

where

$$\Gamma = (2/\sqrt{\pi})(N^B/n^A_\infty \ell_\infty). \tag{1.58}$$

Here, M is defined by Eq. (1.56); $n^A_\infty = \hat{n}^A_{H0} n_I$ is the dimensional number density of the vapor molecules corresponding to $\hat{n}^A_{H0}$; ℓ_∞ is the mean free path of the vapor molecules in the equilibrium state at rest with number density n^A_∞ and temperature $T_\infty = \hat{T}^A_{H0} T_I$; and N^B is the total number of the noncondensable-gas molecules per unit area of the surface of the condensed phase (to be more precise, the total number included in the column perpendicular to the surface whose base is a unit area on the surface). The Γ is a parameter to be specified and is a measure of the amount of the noncondensable gas contained in the half space. The functions $\tilde{F}_s$ and $\tilde{F}_b$ were constructed numerically in Refs. 47 and 48, where the numerical data of the corresponding functions for the pure-vapor case,[57,58,6] obtained by using the BGK model, were exploited, and additional computations were carried out by the use of the model Boltzmann equation for a mixture proposed in Ref. 62.[63] [It should be noted that the Γ-dependence of $\tilde{F}_s$ and $\tilde{F}_b$ is obtained explicitly. For the Knudsen-layer structure, see Refs. 47 and 48, where $\hat{n}^B$ is seen to be of $O(1)$ (cf. the last paragraph of Sec. 1.3.A).]

Let us consider the case where $T_I \leq T_{II}$ and $n_I < n_{II}$, that is, evaporation is taking place on the surface at $x_1 = 1$ and condensation at $x_1 = 0$ (i.e., $\hat{u}^A_{H0} < 0$). Then, Eq. (1.55), applied to the surface at $x_1 = 1$, gives

$$M \leq 1, \qquad \hat{n}^A_{H0} = \frac{n_{II}}{n_I} \frac{h_1(M)}{h_2(M)}, \qquad \hat{T}^A_{H0} = \frac{T_{II}}{T_I} h_2(M), \tag{1.59}$$

and Eqs. (1.57a) and (1.57b), applied to the surface at $x_1 = 0$, give

$$\hat{n}^A_{H0}\hat{T}^A_{H0} = \tilde{F}_s(M, \hat{T}^A_{H0}, \Gamma), \qquad \text{for} \quad M < 1, \tag{1.60a}$$

$$\hat{n}^A_{H0}\hat{T}^A_{H0} > \tilde{F}_b(M, \hat{T}^A_{H0}, \Gamma), \qquad \text{for} \quad M \geq 1. \tag{1.60b}$$

Equation (1.59) shows that a flow with $M > 1$ never occurs. In order to complete Eqs. (1.59) and (1.60a) [or (1.60b)], we need the relation between Γ and our original parameters, Eqs. (1.22) and (1.23). Since $\ell = c(2\kappa T_I/m^A)^{1/2}/n_I$ [instead of Eq. (1.17g) for hard-sphere molecules] and $\ell_\infty = c(2\kappa T_\infty/m^A)^{1/2}/n^A_\infty$, where c is a constant, for the model equations by the use of which h_1, h_2, and $\tilde{F}_s$ have been obtained, the relation $n^A_\infty \ell_\infty (T_\infty)^{-1/2} = n_I \ell (T_I)^{-1/2}$ holds. Applying this relation to Eq. (1.58), noting that N^B is given by $n^B_{av}D$ in the original two-surface problem, and making use of Eq. (1.59), we obtain

$$\Gamma = \frac{2}{\sqrt{\pi}}(\hat{T}^A_{H0})^{-1/2}\frac{n^B_{av}D}{n_I\ell} = \frac{2}{\sqrt{\pi}}\left[\frac{T_{II}}{T_I}h_2(M)\right]^{-1/2}\frac{n^B_{av}}{n_I}\frac{1}{\mathrm{Kn}}. \tag{1.61}$$

This relation, in principle, completes Eqs. (1.59) and (1.60a) [or (1.60b)]. Equation (1.61) implies that n^B_{av}/n_I should be of $O(\mathrm{Kn})$ because Γ should be finite in Eqs. (1.60a) and (1.60b). Thus, we confirm the statement in the last paragraph of Sec. 1.3.A that $n^B_{av}/n_I = O(\mathrm{Kn})$ in the present case. Taking this fact into account, let us put

$$n^B_{av}/n_I = \Delta \mathrm{Kn}, \tag{1.62}$$

and consider Δ as a given parameter instead of n^B_{av}/n_I. Then, from Eqs. (1.61) and (1.62), we have

$$\Gamma = \frac{2}{\sqrt{\pi}}\left[\frac{T_{II}}{T_I}h_2(M)\right]^{-1/2}\Delta. \tag{1.63}$$

In the case of $M < 1$, eliminating $\hat{n}^A_{H0}$, $\hat{T}^A_{H0}$, and Γ from Eqs. (1.59), (1.60a), and (1.63), we obtain the following equation for M:

$$\frac{n_{II}}{n_I}\frac{T_{II}}{T_I}h_1(M) = \tilde{F}_s\left(M, \frac{T_{II}}{T_I}h_2(M), \frac{2}{\sqrt{\pi}}\left[\frac{T_{II}}{T_I}h_2(M)\right]^{-1/2}\Delta\right). \tag{1.64}$$

That is, M is determined by Eq. (1.64) for a given set of the parameters (T_{II}/T_I, n_{II}/n_I, Δ). Then, $\hat{n}^A_{H0}$ and $\hat{T}^A_{H0}$ are obtained from Eq. (1.59), and $\hat{u}^A_{H0}$ from Eq. (1.56). On the other hand, if we eliminate $\hat{n}^A_{H0}$, $\hat{T}^A_{H0}$, and Γ from Eqs. (1.59), (1.60b), and (1.63), we obtain the condition for T_{II}/T_I, n_{II}/n_I, and Δ for which a sonic flow ($M = 1$) occurs.

Table 1.1: The constants $\hat{n}^A_{H0}$, $\hat{T}^A_{H0}$, $\hat{u}^A_{H0}$, and M for various values of the parameters T_{II}/T_I, n_{II}/n_I, and Δ when the molecule of the noncondensable gas is mechanically the same as that of the vapor. The values are obtained on the basis of the BGK model and the model in Ref. 62. The values in the parentheses are those obtained by the use of the conversion of Δ, Eq. (1.67), assuming that Δ is given for hard-sphere molecules.

T_{II}/T_I	n_{II}/n_I	Δ	$\hat{n}^A_{H0}$	$\hat{T}^A_{H0}$	$-\hat{u}^A_{H0}$	M
1	1.2	0	1.118	0.981	0.0423	0.0468
1	1.2	0.5	1.128 (1.131)	0.984 (0.984)	0.0367 (0.0351)	0.0405 (0.0387)
1	1.2	1	1.137 (1.142)	0.985 (0.986)	0.0321 (0.0298)	0.0354 (0.0329)
1	1.2	2	1.149 (1.154)	0.987 (0.988)	0.0259 (0.0233)	0.0285 (0.0257)
1	2	0	1.543	0.930	0.1564	0.1777
1	2	0.5	1.606 (1.622)	0.941 (0.944)	0.1318 (0.1257)	0.1489 (0.1417)
1	2	1	1.655 (1.679)	0.949 (0.953)	0.1136 (0.1048)	0.1278 (0.1176)
1	2	2	1.720 (1.747)	0.960 (0.964)	0.0902 (0.0810)	0.1009 (0.0904)
1.1	2	0	1.491	1.012	0.1858	0.2023
1.1	2	0.5	1.560 (1.577)	1.026 (1.029)	0.1570 (0.1499)	0.1699 (0.1619)
1.1	2	1	1.612 (1.639)	1.036 (1.041)	0.1359 (0.1253)	0.1463 (0.1345)
1.1	2	2	1.687 (1.718)	1.050 (1.055)	0.1068 (0.0954)	0.1142 (0.1018)
1.1	5	0	2.781	0.919	0.3789	0.4331
1.1	5	0.5	3.158 (3.245)	0.960 (0.969)	0.2942 (0.2761)	0.3289 (0.3073)
1.1	5	1	3.411 (3.533)	0.985 (0.996)	0.2436 (0.2206)	0.2689 (0.2422)
1.1	5	2	3.743 (3.881)	1.014 (1.024)	0.1833 (0.1601)	0.1994 (0.1733)
1.1	10	0	4.614	0.854	0.5069	0.6009
1.1	10	0.5	5.686 (5.913)	0.926 (0.939)	0.3641 (0.3378)	0.4145 (0.3819)
1.1	10	1	6.336 (6.632)	0.961 (0.976)	0.2921 (0.2620)	0.3265 (0.2906)
1.1	10	2	7.141 (7.470)	0.999 (1.013)	0.2138 (0.1847)	0.2344 (0.2010)
1.2	5	0	2.708	0.992	0.4144	0.4557
1.2	5	0.5	3.089 (3.178)	1.040 (1.050)	0.3225 (0.3028)	0.3465 (0.3238)
1.2	5	1	3.346 (3.470)	1.068 (1.080)	0.2675 (0.2427)	0.2836 (0.2559)
1.2	5	2	3.687 (3.827)	1.101 (1.113)	0.2017 (0.1764)	0.2106 (0.1832)
1.2	10	0	4.505	0.922	0.5468	0.6238
1.2	10	0.5	5.576 (5.804)	1.003 (1.018)	0.3940 (0.3658)	0.4309 (0.3972)
1.2	10	1	6.226 (6.526)	1.043 (1.059)	0.3171 (0.2846)	0.3402 (0.3030)
1.2	10	2	7.039 (7.378)	1.085 (1.101)	0.2330 (0.2013)	0.2451 (0.2102)
1.2	20	0	7.731	0.858	0.6610	0.7818
1.2	20	0.5	10.46 (10.99)	0.979 (0.998)	0.4395 (0.4043)	0.4865 (0.4435)
1.2	20	1	11.94 (12.61)	1.028 (1.047)	0.3462 (0.3083)	0.3741 (0.3301)
1.2	20	2	13.73 (14.46)	1.076 (1.094)	0.2503 (0.2149)	0.2644 (0.2251)
1.5	100	0	32.25	0.965	0.8968	1.0000
1.5	100	0.5	47.28 (50.24)	1.176 (1.205)	0.5720 (0.5233)	0.5777 (0.5221)
1.5	100	1	55.44 (59.03)	1.251 (1.280)	0.4450 (0.3958)	0.4358 (0.3833)
1.5	100	2	65.06 (68.96)	1.322 (1.347)	0.3207 (0.2761)	0.3055 (0.2606)

The constants $\hat{n}^A_{H0}$, $\hat{T}^A_{H0}$, and $\hat{u}^A_{H0}$ thus obtained by using the numerical data of h_1, h_2, and $\tilde{F}_s$ in Refs. 54,47,48, and 64 and interpolations are shown in Table 1.1 for various values of T_{II}/T_I, n_{II}/n_I, and Δ, where the numbers in the parentheses are the results obtained by the use of the conversion that will be explained in the last paragraph of this subsection. (Note that we are considering the case where the molecule of the vapor is identical with that of the noncondensable gas.)

It should be noted that, in the case of $M < 1$, the asymptotic solution for small k (or Kn) has only the k^0-order terms, i.e., the uniform solution $\hat{F}^A_{H0}$ and $\hat{F}^B_{H0}$ ($\equiv 0$) supplemented by the Knudsen-layer solution $\hat{F}^A_0$ and $\hat{F}^B_0$, and all the higher-order terms vanish. That is, the noncondensable gas is confined only in the Knudsen layer at the condensing surface, and except in the Knudsen layer at each surface, the vapor flow is uniform and is independent of Kn; only the thickness of the Knudsen layer is affected by Kn. The profiles of the macroscopic variables in the Knudsen layer are similar in the sense that they are the same if expressed in terms of the length scale of ℓ [cf. Eq. (1.49)]. Consequently, as Kn tends to zero, the Knudsen layers shrink, with the uniform flow of the vapor unchanged. In particular, in the limit as Kn $\to 0$, the Knudsen layers become vanishingly thin compared with the distance D.

The values of $\hat{n}^A_{H0}$, $\hat{T}^A_{H0}$, and $\hat{u}^A_{H0}$ obtained on the basis of the model equations are to be compared with the results of direct numerical analysis of the original two-surface problem for hard-sphere molecules in the next section. However, the way of comparison of the results obtained by using different molecular models is not unique. Here, we introduce the following conversion for the comparison. When the molecule of the vapor is identical with that of the noncondensable gas, the mutual-diffusion coefficient D^{AB} for temperature T_I, vapor number density n_I, and noncondensable-gas number density n^B_{av} is given by[42]

$$D^{AB} = \frac{\sqrt{\pi}}{2}\gamma\left(\frac{2\kappa T_I}{m}\right)^{1/2}\frac{n_I}{n_I + n^B_{av}}\ell, \tag{1.65}$$

where $m = m^A = m^B$, and γ is a constant depending on the molecular model, e.g., $\gamma = 0.764215339(\equiv \gamma_{HS})$ for hard-sphere molecules[65,66] (this value is the one recomputed with higher accuracy in the present study), and $\gamma = 1$ for the collision model of Ref. 62. If we suppose that D^{AB} is a basic and common quantity and eliminate it from Eq. (1.65) for

hard-sphere molecules and that for the model, we obtain the following conversion formula:

$$(\ell)_{Model} = \gamma_{HS}(\ell)_{HS}, \quad \text{or} \quad (\mathrm{Kn})_{Model} = \gamma_{HS}(\mathrm{Kn})_{HS}, \tag{1.66}$$

where $(\ )_{Model}$ and $(\ )_{HS}$ indicate the quantity corresponding to the model and hard-sphere molecules, respectively. Since n_{av}^B/n_I is an originally given quantity independent of the molecular model, it follows from Eq. (1.62) that

$$(\Delta\mathrm{Kn})_{Model} = (\Delta\mathrm{Kn})_{HS}, \quad \text{or} \quad (\Delta)_{Model} = (\Delta)_{HS}/\gamma_{HS}, \tag{1.67}$$

with $\gamma_{HS} = 0.764215339$. This gives the conversion formula for Δ between hard-sphere molecules and the model, i.e., if $\Delta = a$ for hard-sphere molecules, then $\Delta = a/\gamma_{HS}$ should be used in Eqs. (1.63) and (1.64). The values of $\hat{n}_{H0}^A$, $\hat{T}_{H0}^A$, and $\hat{u}_{H0}^A$ obtained by the use of this conversion are shown in the parentheses in Table 1.1.

1.3.C Summary of the behavior in the continuum limit

The asymptotic analysis in Secs. 1.3.A and 1.3.B gives the following behavior in the continuum limit as Kn (or k) $\to 0$.

(i) In the limit with $n_{av}^B/n_I = c$, where c is a nonzero constant, evaporation and condensation of the vapor stop, and the entire gas becomes stationary.

(ii) In the limit with $n_{av}^B/n_I = \Delta\mathrm{Kn}$, where Δ is a given constant, all the noncondensable gas is confined in the Knudsen layer with a vanishingly small thickness (compared with D) at the condensing surface, and the vapor flow becomes uniform. The uniform values of the macroscopic variables depend on Δ.

If $c = 0$ in the case (i) [or $\Delta = 0$ in the case (ii)], this corresponds to the continuum limit in the pure-vapor case, in which there is a steady vapor flow.[5] Therefore, the limit (i) is singular (discontinuous) at $n_{av}^B/n_I = 0$ with respect to the parameter n_{av}^B/n_I.

The limit in the case (ii) shows a striking feature that, although the average number density n_{av}^B of the noncondensable gas is vanishingly small compared with the reference number density n_I of the vapor, the vapor flow is still affected by the presence of the noncondensable gas. To appreciate the issue, let us consider the case where the vapor is water vapor, $T_I = 350$ K, and $D = 10$ cm. Then the saturated vapor pressure p_I corresponding to n_I ($p_I = \kappa n_I T_I$) is about 300 Torr, and thus $\ell \simeq 10^{-5}$ cm, i.e., Kn $\simeq 10^{-6}$. This situation is

almost the (mathematical) continuum limit. Therefore, if a very small amount of a noncondensable gas corresponding to a partial pressure about 3×10^{-4} Torr is contained in the gap, it gives a finite effect on the vapor flow.

This fact might appear to be strange or unphysical because a vanishingly small amount seems to give a finite effect. In this connection, one should realize that, in order to have a finite effect, the local number density of the noncondensable gas in the Knudsen layer should be as large as that of the vapor. If the total amount of the noncondensable gas is not sufficient to attain this situation, then its effect on the vapor flow is negligible. But one should also note that, even if the local number density of the noncondensable gas in the Knudsen layer is high enough, its average number density n_{av}^B over the gap is vanishingly small compared with n_I (Note that the noncondensable gas can exist only in the Knudsen layer, which is infinitely thin compared with the distance D between the two surfaces). To understand the difference in the two cases (i) and (ii) more clearly, let us consider the following example. Consider the gap with $D \simeq \ell$ and suppose that the amount of the noncondensable gas in the gap is of the same order as that of the vapor. If we let the distance D infinitely large (in comparison with ℓ) with the total amount of the noncondensable gas being fixed, then we have the case (ii). On the other hand, if we inject the noncondensable gas with the increase of D to keep its total amount of the same order as that of the vapor, we get the case (i).

In the present paper, in order to avoid the complexity of the parameters, we formulated the problem on the basis of assumptions (ii) – (iv) in Sec. 1.2.A for the molecular model and the boundary conditions.[67] However, as is seen from the course of the asymptotic analysis, these assumptions are not essential to the fundamental features of the continuum limit. To be more specific, the limiting behavior, Eqs. (1.38) – (1.39b), in the case (i) is true for the general molecular model and for the general boundary conditions [i.e., any boundary condition for the vapor which is satisfied by the stationary Maxwellian distribution whose temperature and density are, respectively, the temperature of the surface and the saturation density of the vapor at this temperature, and any boundary condition for the noncondensable gas (with the impermeability condition) which is satisfied by the stationary Maxwellian distribution whose temperature is that of the surface and whose density is arbitrary]. The limiting behavior in the case (ii) is also true for the above general case; however, the values of the constants $\hat{n}_{H0}^A$, $\hat{T}_{H0}^A$, and $\hat{u}_{H0}^A$ depend on the molecular model as well as the boundary conditions. The

behavior in the cases (i) and (ii) will be confirmed numerically for hard-sphere molecules in the next section.

1.4 Numerical analysis and results

In this section, we carry out direct numerical analysis of the original two-surface problem. Since our main interest is to see the effect of the Knudsen number Kn and that of the average number density of the noncondensable gas n_{av}^B/n_I, we fix all the other parameters in Eq. (1.22) as

$$\frac{T_{II}}{T_I} = 1, \quad \frac{n_{II}}{n_I} = 2, \quad \frac{m^B}{m^A} = 1, \quad \frac{d^B}{d^A} = 1. \tag{1.68}$$

The first two equations might appear to be inconsistent because $T_I = T_{II}$ implies $n_I = n_{II}$ physically. However, if we consider the fact that, for many substances and for a wide range of the temperature, a slight change in the temperature leads to a significant change in the saturation vapor pressure (or density), we can justify the above parameter setting as a physically reasonable one for our purpose. As the solution method, we adopt the standard direct simulation Monte Carlo (DSMC) method by Bird.[35,36] Since the method is a straightforward extension of that explained in Ref. 68 to the case of a binary mixture, we omit the description of the method and summarize the obtained results.

Let J be the mass-flow rate of the vapor from the evaporating to the condensing surface (per unit time and per unit area of the plane $X_1 = const$) and $\hat{J}$ be its dimensionless form, i.e.,

$$J = -m^A n^A u^A \quad \text{and} \quad \hat{J} = J/m^A n_I (2\kappa T_I/m^A)^{1/2} = -\hat{n}^A \hat{u}^A. \tag{1.69}$$

Here, we note that $n^A u^A$ (or $\hat{n}^A \hat{u}^A$) is independent of X_1 (or x_1)[see Eq. (1.12) or (1.24)]. The nondimensional mass-flow rate $\hat{J}$ versus n_{av}^B/n_I is shown in Fig. 1.1 for various values of Kn; Fig. 1.1(b) is a magnified figure of the part for $0 \le n_{av}^B/n_I \le 0.25$ in Fig. 1.1(a). The values of $\hat{J}$ corresponding to Fig. 1.1 are given in Table 1.2. In Fig. 1.1(a), the dot-dash lines are the curves that smoothly join the numerical data for the same Kn, and the dotted line for Kn $= \infty$ indicates the result for the free-molecular flow. As Kn decreases, the gradient of the curve with constant Kn becomes steep at small values of n_{av}^B/n_I, and except for this region the mass-flow rate tends to vanish. In this way, as Kn $\to 0$, the mass-flow rate approaches

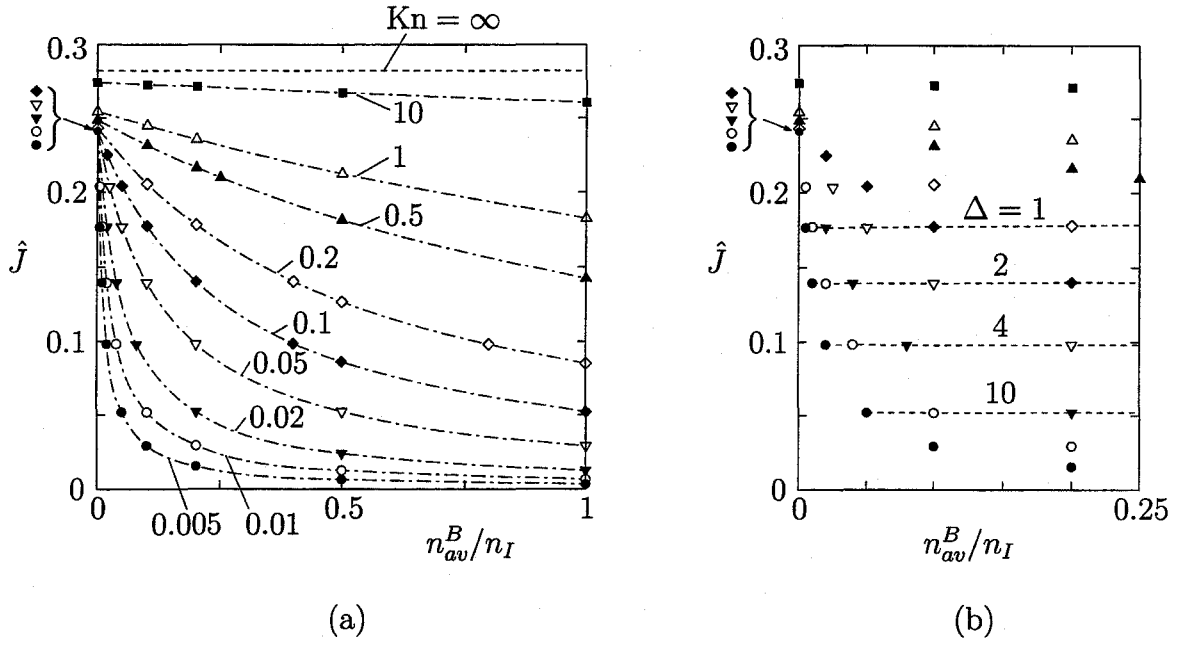

Figure 1.1: Nondimensional mass-flow rate of the vapor $\hat{J}$ [Eq. (1.69)] versus n_{av}^B/n_I for various values of Kn in the case $T_{II}/T_I = 1$, $n_{II}/n_I = 2$, $m^B/m^A = 1$, and $d^B/d^A = 1$. (a) $0 \le n_{av}^B/n_I \le 1$, (b) $0 \le n_{av}^B/n_I \le 0.25$. Here, ■ indicates the data for Kn = 10, △ for 1, ▲ for 0.5, ◇ for 0.2, ◆ for 0.1, ▽ for 0.05, ▼ for 0.02, ○ for 0.01, and ● for 0.005. In (a), the dot-dash line indicates a curve smoothly joining the data for the same Kn, and the dotted line for Kn = ∞ indicates the result for the free-molecular flow. In (b), the dotted line is the line joining the data for the same Δ [see the paragraph including Eq. (1.70)].

Table 1.2: Nondimensional mass-flow rate of the vapor $\hat{J}$ [Eq. (1.69)] for various values of n_{av}^B/n_I and Kn. Here, the other parameters are fixed as $T_{II}/T_I = 1$, $n_{II}/n_I = 2$, $m^B/m^A = 1$, and $d^B/d^A = 1$.

Kn	n_{av}^B/n_I	$\hat{J}$	Kn	n_{av}^B/n_I	$\hat{J}$
0.005	0	0.2406	0.1	0.02	0.2250
0.005	0.005	0.1765	0.1	0.05	0.2043
0.005	0.01	0.1396	0.1	0.1	0.1773
0.005	0.02	0.0983	0.1	0.2	0.1402
0.005	0.05	0.0520	0.1	0.4	0.0986
0.005	0.1	0.0293	0.1	0.5	0.0862
0.005	0.2	0.0155	0.1	1	0.0522
0.005	0.5	0.00646	0.2	0	0.2433
0.005	1	0.00329	0.2	0.1	0.2056
0.01	0	0.2409	0.2	0.2	0.1780
0.01	0.005	0.2040	0.2	0.4	0.1402
0.01	0.01	0.1770	0.2	0.5	0.1266
0.01	0.02	0.1394	0.2	0.8	0.0981
0.01	0.04	0.0984	0.2	1	0.0852
0.01	0.1	0.0520	0.5	0	0.2487
0.01	0.2	0.0294	0.5	0.1	0.2315
0.01	0.5	0.0126	0.5	0.2	0.2164
0.01	1	0.00660	0.5	0.25	0.2097
0.02	0	0.2408	0.5	0.5	0.1811
0.02	0.02	0.1766	0.5	1	0.1423
0.02	0.04	0.1394	1	0	0.2544
0.02	0.08	0.0980	1	0.02	0.2526
0.02	0.2	0.0522	1	0.1	0.2448
0.02	0.5	0.0240	1	0.2	0.2355
0.02	1	0.0126	1	0.5	0.2123
0.05	0	0.2406	1	1	0.1824
0.05	0.025	0.2037	10	0	0.2742
0.05	0.05	0.1766	10	0.1	0.2728
0.05	0.1	0.1395	10	0.2	0.2713
0.05	0.2	0.0983	10	0.5	0.2671
0.05	0.5	0.0522	10	1	0.2605
0.05	1	0.0291	∞		0.2821
0.1	0	0.2412			

the singular limit [case (i)] described in Sec. 1.3.C, i.e., $\hat{J} \to 0$ for $n_{av}^B/n_I = const(\neq 0)$, and $\hat{J} \to const(\neq 0)$ for $n_{av}^B/n_I = 0$.

The spatial distributions of the macroscopic variables for various Kn are shown in Fig. 1.2 for $n_{av}^B/n_I = 0.5$ and in Fig. 1.3 for $n_{av}^B/n_I = 1$. As Kn decreases from ∞ to 0.1 [Figs. 1.2(a) and 1.3(a)], the vapor flow speed decreases, and the gradient of n^A and that of n^B increase in the opposite directions. The limiting process of the case (i) in Sec. 1.3.C, which is expressed by Eqs. (1.38) – (1.39b), is seen in Figs. 1.2(b) and 1.3(b). That is, as Kn becomes small, the vapor flow velocity u^A tends to vanish; the vapor number density n^A approaches the saturation number densities n_I and n_{II} $(= 2n_I)$ at the condensing and evaporating surfaces, respectively; and the temperature of the total mixture T tends to approach the surface temperatures T_I and T_{II} $(= T_I)$ at the condensing and evaporating surfaces, respectively.[69] In Fig. 1.4, the flow speed of the vapor at three points versus Kn is shown for small Kn in the case $n_{av}^B/n_I = 0.5$ and 1. The flow velocity tends to vanish in proportion to Kn as Kn approaches zero, which is in agreement with Eq. (1.35) [or $\hat{u}_H^A = O(\mathrm{Kn})$]. The above behavior in the continuum limit can be explained physically as follows. In this limit, the vapor molecules evaporated from the surface at $X_1 = D$ are bounced back by frequent collisions with the noncondensable-gas molecules and accumulate at the surface. Their number density finally reaches the saturation density n_{II} $(= 2n_I)$, and evaporation stops. On the other hand, at the surface at $X_1 = 0$, the vapor molecules are removed by condensation, but the removed amount is not supplied because the flow of the vapor molecules toward the surface is blocked by frequent collisions with the noncondensable-gas molecules. Consequently, the number density of the vapor decreases to the saturation density n_I, and condensation stops.

The process of approach to the limit of the case (ii) in Sec. 1.3.C, namely,

$$\mathrm{Kn} \to 0, \quad \text{with} \quad n_{av}^B/n_I = \Delta \mathrm{Kn}, \tag{1.70}$$

(Δ is a given constant) is also included in Fig. 1.1 and Table 1.2. To be more specific, each dotted line in Fig. 1.1(b) indicates the line joining the data with common Δ ($\Delta = 1$, 2, 4, or 10), and therefore the data on it show the process of approach for $\Delta = 1$, 2, 4, or 10. As is also seen from the corresponding data in Table 1.2, the mass-flow rate $\hat{J}$ for a fixed Δ and for small Kn is almost constant, and the constant values depend on Δ. The behavior of the macroscopic variables in the limiting process for $\Delta = 0$ (pure vapor case), 1, and 2

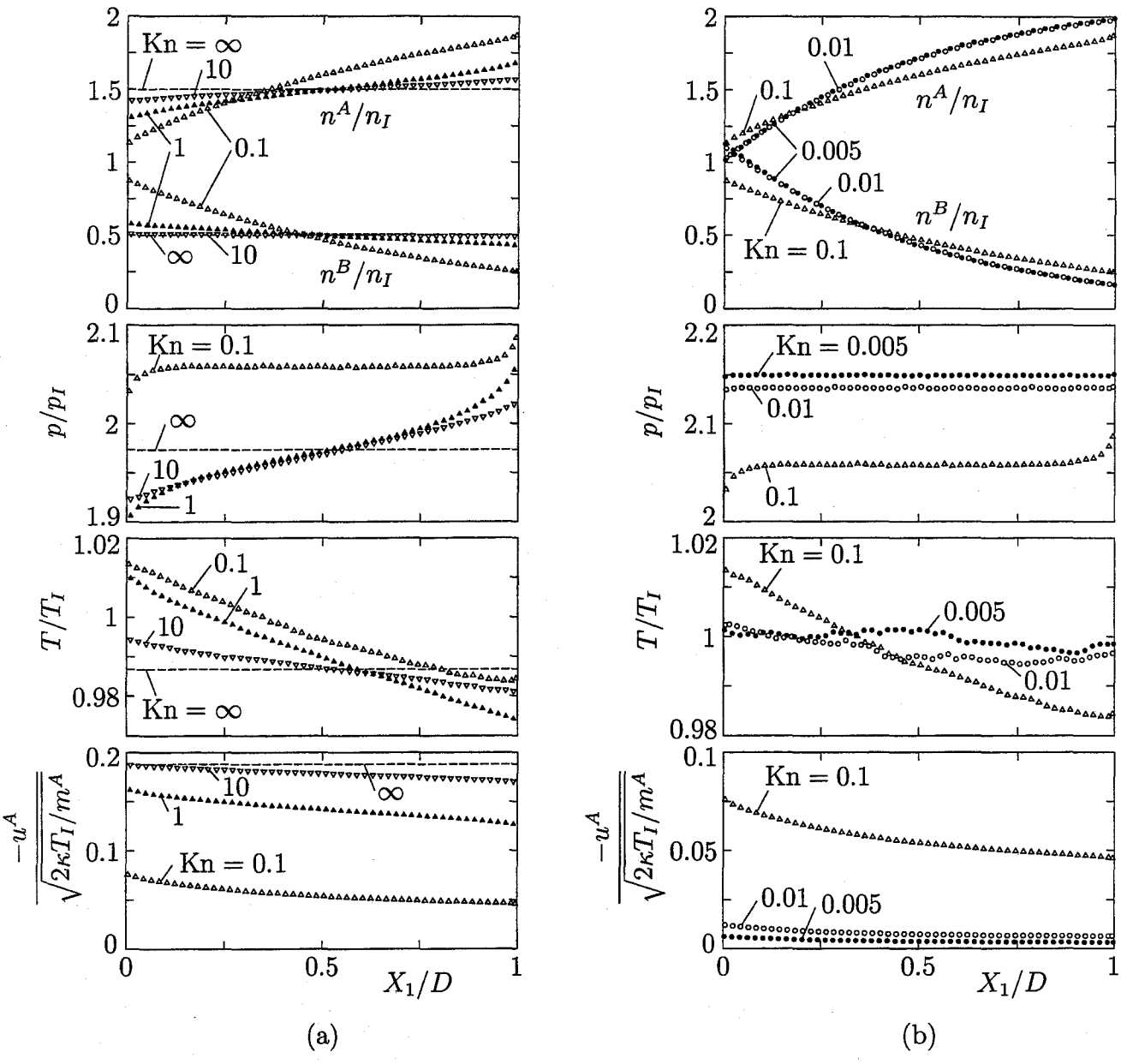

Figure 1.2: Profiles of the macroscopic variables n^A, n^B, p, T, and u^A for various Kn in the case $n^B_{av}/n_I = 0.5$. Here, the other parameters are fixed as $T_{II}/T_I = 1$, $n_{II}/n_I = 2$, $m^B/m^A = 1$, and $d^B/d^A = 1$. (a) Kn $= \infty$, 10, 1, and 0.1. (b) Kn $= 0.1$, 0.01, and 0.005. The dotted line for Kn $= \infty$ in (a) indicates the result for the free-molecular flow.

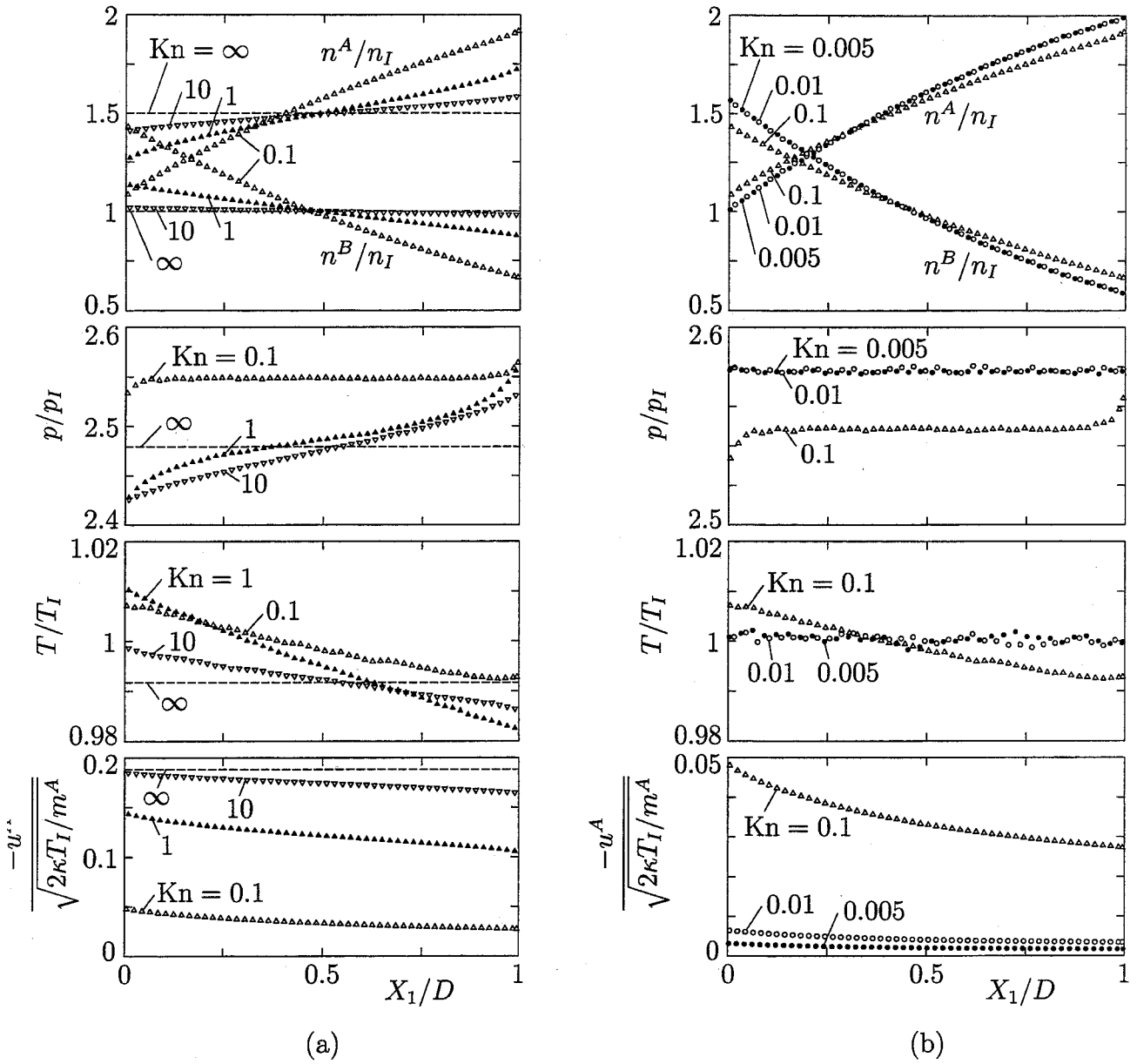

Figure 1.3: Profiles of the macroscopic variables n^A, n^B, p, T, and u^A for various Kn in the case $n^B_{av}/n_I = 1$. Here, the other parameters are fixed as $T_{II}/T_I = 1$, $n_{II}/n_I = 2$, $m^B/m^A = 1$, and $d^B/d^A = 1$. (a) Kn $= \infty$, 10, 1, and 0.1. (b) Kn $= 0.1$, 0.01, and 0.005. The dotted line for Kn $= \infty$ in (a) indicates the result for the free-molecular flow.

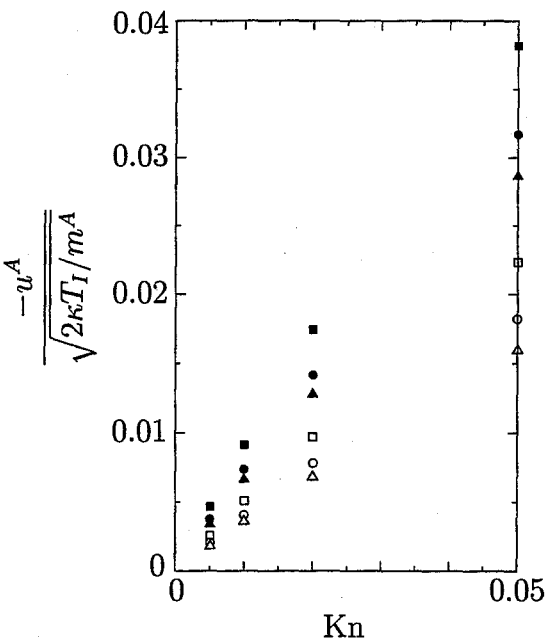

Figure 1.4: Flow speed of the vapor at three points versus Kn for small Kn in the case $n^B_{av}/n_I = 0.5$ and 1. Here, the other parameters are fixed as $T_{II}/T_I = 1$, $n_{II}/n_I = 2$, $m^B/m^A = 1$, and $d^B/d^A = 1$. The symbols ■, •, and ▲ indicate the data at $X_1/D = 0.2$, 0.5, and 0.8, respectively, for $n^B_{av}/n_I = 0.5$, and □, ○, and △ the corresponding data for $n^B_{av}/n_I = 1$.

are shown in Figs. 1.5, 1.6, and 1.7, respectively. The dotted lines in the figures indicate the constant values $\hat{n}^A_{H0}$, $\hat{T}^A_{H0}$ $(= \hat{T}_{H0})$, and $\hat{u}^A_{H0}$ in the parentheses in Table 1.1, which correspond to n^A/n_I, T/T_I, and $u^A/(2\kappa T_I/m^A)^{1/2}$, respectively. As shown by Fig. 1.6 ($\Delta = 1$), the noncondensable gas, which is distributed over the whole gap at Kn = 0.1, is confined near the condensing surface ($X_1 = 0$) at Kn = 0.01, and except for this region and for the vicinity of the evaporating surface ($X_1 = D$), the flow field of the vapor is uniform. At Kn = 0.005, the nonuniform regions, i.e., the Knudsen layer at $X_1 = 0$, where the noncondensable gas is confined, and that at $X_1 = D$, shrink, but the uniform flow of the vapor does not change. Such behavior is in agreement with the result of the asymptotic analysis in Sec. 1.3 (see the second paragraph from the last in Sec. 1.3.B). For larger Δ (Fig. 1.7), the vapor flow speed is decreased because larger amount of the noncondensable gas is included in the gap (or in the Knudsen layer) for the same Kn. It is seen from Figs. 1.5 – 1.7 that the constants $\hat{n}^A_{H0}$, $\hat{T}^A_{H0}$ $(= \hat{T}_{H0})$, and $\hat{u}^A_{H0}$ in the parentheses in Table 1.1, which are based on the model Boltzmann equations and the conversion (1.67), yield excellent prediction of the uniform state for hard-sphere molecules.

We now summarize the data concerning the simulation scheme used for the results presented in this section. The interval $0 \le X_1 \le D$ is divided into N_c cells of an equal size, where $N_c = 50$ ($0.2 \le$ Kn ≤ 10), 100 [Kn = 0.01 ($0.2 \le n^B_{av}/n_I \le 1$) and $0.02 \le$ Kn ≤ 0.1], 200 [Kn = 0.005 ($0.1 \le n^B_{av}/n_I \le 1$) and 0.01 ($0 \le n^B_{av}/n_I \le 0.1$)], and 400 [Kn = 0.005 (other n^B_{av}/n_I)]. The number of simulation particles N_p corresponding to $n_I D$ is 10^4 ($0.2 \le$ Kn ≤ 10), 2×10^4 [Kn = 0.01 ($0.005 \le n^B_{av}/n_I \le 0.1$ and $n^B_{av}/n_I = 0.5$) and $0.02 \le$ Kn ≤ 0.1], and 4×10^4 [Kn = 0.005 and 0.01 (other n^B_{av}/n_I)]. [Therefore, if $\hat{n}^A$ $(= n^A/n_I)$ $= c$ at a cell, then the number of the particles representing the vapor molecules in the cell is cN_p/N_c. The total number of the particles contained in the gap $0 \le X_1 \le D$ is larger than N_p since $\hat{n}^A$ is greater than unity; see Figs. 1.2, 1.3, and 1.5 – 1.7.] The total number of the particles representing the noncondensable-gas molecules (i.e., the number of the particles corresponding to $n^B_{av}D$) for the case of $n^B_{av}/n_I = c'$ is therefore given by $c'N_p$. The time step Δt, which is the interval between two successive times at which the collision processes are evaluated, is as follows: $D^{-1}(2\kappa T_I/m^A)^{1/2}\Delta t$ $[= (\sqrt{\pi}/2)(\text{Kn}/t_0)\Delta t$, where t_0 is the mean free time corresponding to ℓ] is 10^{-2} (Kn = 1 and 10), 5×10^{-3} (Kn = 0.2 and 0.5), 2×10^{-3} [Kn = 0.1 ($n^B_{av}/n_I = 0$, 0.02, 0.05, and 0.4)], 10^{-3} [Kn = 0.05 and 0.1 (other n^B_{av}/n_I)], 4×10^{-4} (Kn = 0.02), 2×10^{-4}

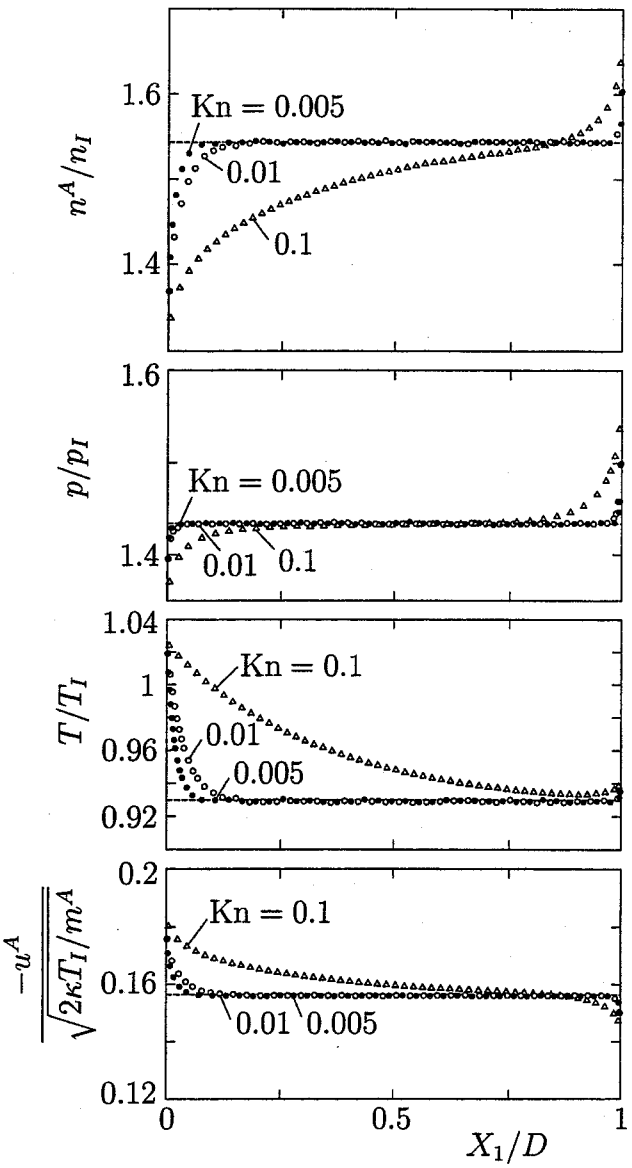

Figure 1.5: Profiles of the macroscopic variables n^A, p, T, and u^A for Kn = 0.1, 0.01, and 0.005 in the case $\Delta = 0$ (pure-vapor case). Here, the other parameters are fixed as $T_{II}/T_I = 1$ and $n_{II}/n_I = 2$. The dotted line indicates the corresponding result for the continuum limit given in Table 1.1.

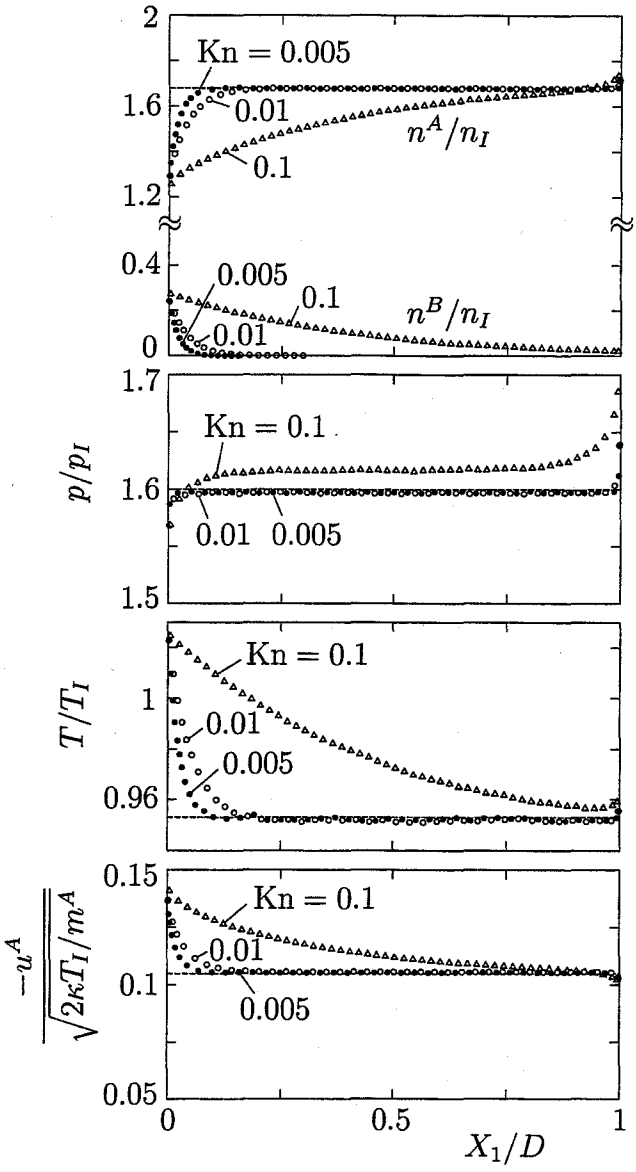

Figure 1.6: Profiles of the macroscopic variables n^A, n^B, p, T, and u^A for Kn = 0.1, 0.01, and 0.005 in the case $\Delta = 1$. Here, the other parameters are fixed as $T_{II}/T_I = 1$, $n_{II}/n_I = 2$, $m^B/m^A = 1$, and $d^B/d^A = 1$. The dotted line indicates the corresponding result for the continuum limit given in the parentheses in Table 1.1.

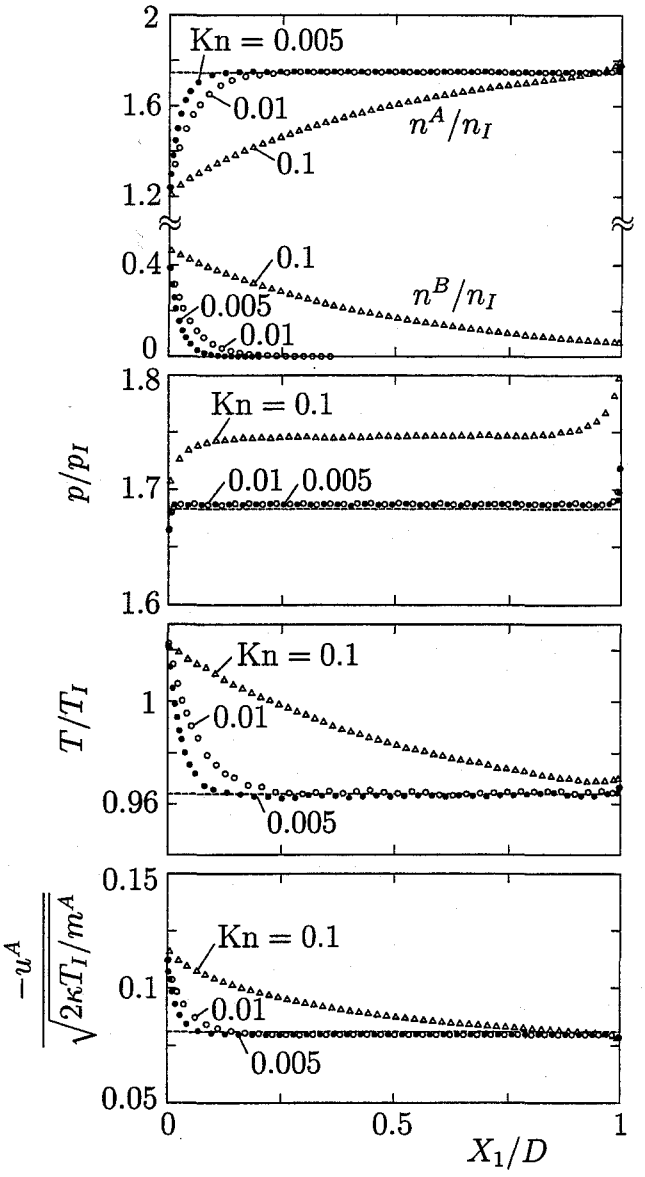

Figure 1.7: Profiles of the macroscopic variables n^A, n^B, p, T, and u^A for Kn = 0.1, 0.01, and 0.005 in the case $\Delta = 2$. Here, the other parameters are fixed as $T_{II}/T_I = 1$, $n_{II}/n_I = 2$, $m^B/m^A = 1$, and $d^B/d^A = 1$. The dotted line indicates the corresponding result for the continuum limit given in the parentheses in Table 1.1.

Table 1.3: Nondimensional mass-flow rate of the vapor $\hat{J}$ [Eq. (1.69)] obtained by the test computations (cf. Table 1.2) for $n_{av}^B/n_I = 0.01$ and 1 in the case Kn = 0.005. Here, the other parameters are fixed as $T_{II}/T_I = 1$, $n_{II}/n_I = 2$, $m^B/m^A = 1$, and $d^B/d^A = 1$.

$n_{av}^B/n_I = 0.01$			$n_{av}^B/n_I = 1$		
N_c	N_p	$\hat{J}$	N_c	N_p	$\hat{J}$
100	10^4	0.13947	100	10^4	0.003288
200	0.5×10^4	0.13944	200	0.5×10^4	0.003287
	10^4	0.13983		10^4	0.003303
	2×10^4	0.13971		2×10^4	0.003300
	4×10^4	0.13941		4×10^4	0.003287[a]
	8×10^4	0.13959	400	4×10^4	0.003296
400	4×10^4	0.13963[a]			

[a] The data included in Table 1.2.

[Kn = 0.01 (n_{av}^B/n_I = 0.005, 0.02, 0.04, 0.1, and 0.5)], and 10^{-4} [Kn = 0.01 (other n_{av}^B/n_I) and 0.005]. The data shown in Table 1.2 and Figs. 1.1 – 1.7 are the averages over more than $9 \times 10^5 \Delta t$ in most of the cases for $0.2 \leq$ Kn ≤ 10, more than $1.4 \times 10^6 \Delta t$ in most of the cases for $0.01 \leq$ Kn ≤ 0.1, and more than $2.5 \times 10^6 \Delta t$ in most of the cases for Kn = 0.005 after steady states are judged to be reached.

As noted above, the mass-flow rate J of the vapor in Eq. (1.69) does not depend on X_1 theoretically. However, the numerical result varies slightly with X_1 because of computational error. Therefore, the average values over $0 \leq X_1 \leq D$ are shown in Table 1.2. The variation, on the other hand, gives a measure of the error of the computation. The maximum relative deviation, $\max|J - J_{av}|/J_{av}$, in the region $0 \leq X_1 \leq D$, where J_{av} denotes the average of J, is less than 1.02×10^{-3} for the cases with $0.2 \leq \hat{J}$, less than 2.74×10^{-3} for the cases with $0.1 \leq \hat{J} < 0.2$, less than 5.07×10^{-3} for the cases with $0.05 \leq \hat{J} < 0.1$, less than 6.96×10^{-3} for the cases with $0.01 \leq \hat{J} < 0.05$, and less than 2.72×10^{-2} for the cases with $\hat{J} < 0.01$.

In order to confirm the reliability of the results presented in this section, some additional computations with different numbers of cells and particles are also carried out for typical cases. In general, accurate DSMC computation becomes increasingly difficult as the Knudsen number becomes small. Therefore, we give, in Table 1.3, some of the results of the mass-flow rate obtained by such computations for small Kn (Kn = 0.005) (cf. Table 1.2). The accurate computation of the mass-flow rate in the case of $n_{av}^B/n_I = 1$ is particularly difficult because

it is small.

The computations have mainly been carried out on DEC Alpha 600 5/333 and VT-Alpha 433AXP computers in the Section of Dynamics in Aeronautics and Astronautics, Department of Aeronautics and Astronautics, Graduate School of Engineering, Kyoto University.

1.5 Concluding remarks

In this chapter, we have investigated the effect of the presence of a noncondensable gas in the two-surface problem of evaporation and condensation, which is one of the most fundamental problems of a vapor flow caused by evaporation and condensation, by means of asymptotic analysis of the Boltzmann equation as well as numerical analysis based on the DSMC method. Our special attention is focused on the behavior in the continuum limit with respect to the vapor (i.e., Kn $\to$ 0). As the result of the asymptotic analysis, it is shown that there are two completely different types of behavior in the limit, the cases (i) and (ii) in Sec. 1.3.C, depending on the amount of the noncondensable gas included in the system. In particular, in the latter case, it is found that, although the average number density of the noncondensable-gas molecules is infinitesimally small compared with that of the vapor molecules (or the saturation number density of the vapor molecules at a reference state), the noncondensable gas gives a finite effect on the vapor flow. The process of approach to these two types of continuum limit is demonstrated by the numerical result obtained by the DSMC analysis.

Chapter 2

Shock-wave structure for a binary gas mixture[70]

2.1 Introduction

The analysis of the structure of a normal shock wave in a single component gas is one of the classical problems in modern kinetic theory and has been tackled by various methods, including moment methods,[71] model Boltzmann equations,[72] and the direct simulation Monte Carlo (DSMC) method,[73] since the beginning of 1950's (see, e.g., Refs. 36, 45, 74, 75, and their references). However, an accurate numerical result by means of a finite-difference (or discrete-ordinate) analysis of the Boltzmann equation was reported only in 1993.[76]

The main difficulty in analyzing the Boltzmann equation by a finite-difference method is to perform accurate computations of the complicated collision integrals. In 1989, Sone and coworkers[77] proposed an accurate and efficient method (numerical kernel method) for computing the collision integrals of the linearized Boltzmann equation for hard-sphere molecules. The method has successfully been applied to the finite-difference analyses of various fundamental problems of rarefied gas dynamics, such as the Knudsen-layer problems,[77–79] the plane Poiseuille flow and the thermal transpiration,[80] the plane Couette flow,[81] uniform flows past a sphere,[82,11] and the thermophoresis,[83] and the results to be regarded as the standards for these problems have been established. Subsequently, a similar method was developed for the nonlinear Boltzmann equation by Ohwada in the above-mentioned work on the shock-wave structure,[76,84] in which an accurate numerical result was obtained for relatively weak to moderately strong shock waves. The method has also been applied to the analysis of heat transfer between parallel plates.[85,86]

The problem of shock-wave structure for a binary gas mixture has also been a popular subject and has been investigated experimentally[87–89] as well as theoretically. The latter approach includes approximate analyses based on moment methods[90,91] and fluid-dynamic models,[92,93] and numerical analyses based on kinetic models[94,95] and the DSMC method.[96,97]

(See also Ref. 36 and its references.) In this chapter, we try to extend the method of Ohwada[76] to the case of a binary mixture of hard-sphere gases and investigate the structure of a normal shock wave for the mixture by an accurate finite-difference analysis of the Boltzmann equation. Our aim is to establish the result that can be the standard for the problem. It should be mentioned that a numerical result by another direct method was reported recently.[98] However, only one case of a rather weak shock is analyzed, and no information is given about the size and accuracy of the computation.

2.2 Problem and basic equation

2.2.A Problem

We consider a steady flow of a binary gas mixture (say, the mixture of A-component and B-component) through a standing normal shock wave. Let us take the X_1 axis of the space coordinates X_i in the direction of the flow. The mixture is in a uniform equilibrium state with speed U_-, temperature T_-, and molecular number densities n_-^A (A-component) and n_-^B (B-component) at upstream infinity ($X_1 = -\infty$), whereas it is in another equilibrium state with speed U_+, temperature T_+, and molecular number densities n_+^A (A-component) and n_+^B (B-component) at downstream infinity ($X_1 = \infty$). The conservations of the molecular number of each component, the total momentum, and the total energy lead to the expressions of the downstream parameters in terms of the upstream ones (the Rankine–Hugoniot relation), which can be arranged in the following form:

$$\frac{n_+^\alpha}{n_-^\alpha} = \frac{4M_-^2}{M_-^2+3}, \qquad (\alpha = A, B), \tag{2.1a}$$

$$\frac{U_+}{U_-} = \frac{M_-^2+3}{4M_-^2}, \tag{2.1b}$$

$$\frac{T_+}{T_-} = \frac{(5M_-^2-1)(M_-^2+3)}{16M_-^2}. \tag{2.1c}$$

Here M_- is the Mach number at upstream infinity defined by

$$M_- = U_-/(5R_-T_-/3)^{1/2}, \tag{2.2a}$$

$$R_- = k/(m^A\chi_-^A + m^B\chi_-^B), \tag{2.2b}$$

where k is the Boltzmann constant, m^A the mass of a molecule of the A-component, and m^B that of the B-component; χ_-^A and χ_-^B are the concentrations of the A-component and

the B-component at upstream infinity, i.e.,

$$\chi_-^\alpha = n_-^\alpha / n_-, \qquad (\alpha = A, B), \tag{2.3a}$$

$$n_- = n_-^A + n_-^B. \tag{2.3b}$$

It is seen from Eq. (2.1a) that the concentration of each component at downstream infinity, $\chi_+^\alpha = n_+^\alpha / n_+$ ($n_+ = n_+^A + n_+^B$), is the same as χ_-^α. Therefore, the Mach number at downstream infinity is given by $M_+ = U_+/(5R_-T_+/3)^{1/2}$ and is expressed as

$$M_+ = \left(\frac{M_-^2 + 3}{5M_-^2 - 1}\right)^{1/2}, \tag{2.4}$$

with the aid of Eqs. (2.1b)–(2.2a).

We investigate the transition from the upstream to the downstream state through the shock wave on the basis of the Boltzmann equation for a binary mixture under the assumption that the molecules of each component are hard (or rigid) spheres.

2.2.B Basic equations

Let ξ_i (or $\boldsymbol{\xi}$) be the molecular velocity, $F^A(X_1, \boldsymbol{\xi})$ the velocity distribution function of the molecules of the A-component, and $F^B(X_1, \boldsymbol{\xi})$ that of the B-component. The Boltzmann equation in the present problem is written in the following form.[41,42]

$$\xi_1 \frac{\partial F^\alpha}{\partial X_1} = \sum_{\beta=A,B} \left\{ G^{\beta\alpha}[F^\beta, F^\alpha] - \nu^{\beta\alpha}[F^\beta] F^\alpha \right\}, \qquad (\alpha = A, B), \tag{2.5}$$

where

$$G^{\beta\alpha}[f, g] = \frac{(d_m^{\beta\alpha})^2}{2} \int f(X_1, \boldsymbol{\xi}_*^{\beta\alpha}) g(X_1, \boldsymbol{\xi}^{\beta\alpha}) |\boldsymbol{a} \cdot \boldsymbol{V}| d\Omega(\boldsymbol{a}) d\boldsymbol{\xi}_*, \tag{2.6}$$

$$\nu^{\beta\alpha}[f] = \frac{(d_m^{\beta\alpha})^2}{2} \int f(X_1, \boldsymbol{\xi}_*) |\boldsymbol{a} \cdot \boldsymbol{V}| d\Omega(\boldsymbol{a}) d\boldsymbol{\xi}_*, \tag{2.7}$$

$$\boldsymbol{\xi}^{\beta\alpha} = \boldsymbol{\xi} + \frac{\mu^{\beta\alpha}}{m^\alpha} (\boldsymbol{a} \cdot \boldsymbol{V}) \boldsymbol{a}, \quad \boldsymbol{\xi}_*^{\beta\alpha} = \boldsymbol{\xi}_* - \frac{\mu^{\beta\alpha}}{m^\beta} (\boldsymbol{a} \cdot \boldsymbol{V}) \boldsymbol{a}, \quad \boldsymbol{V} = \boldsymbol{\xi}_* - \boldsymbol{\xi}, \tag{2.8}$$

$$d_m^{\beta\alpha} = (d_m^\alpha + d_m^\beta)/2, \qquad \mu^{\beta\alpha} = 2m^\alpha m^\beta / (m^\alpha + m^\beta). \tag{2.9}$$

Here, d_m^A and d_m^B are the diameter of a molecule of the A-component and that of the B-component, respectively; $\boldsymbol{\xi}_*$ is the integration variable for $\boldsymbol{\xi}$, $\boldsymbol{a}$ is a unit vector, $d\boldsymbol{\xi}_* = d\xi_{*1} d\xi_{*2} d\xi_{*3}$, and $d\Omega(\boldsymbol{a})$ is the solid-angle element around $\boldsymbol{a}$; the domain of integration is the whole space of $\boldsymbol{\xi}_*$ and all directions of $\boldsymbol{a}$.

The boundary condition at upstream infinity is

$$F^\alpha \to n_-^\alpha \left(\frac{m^\alpha}{2\pi k T_-}\right)^{3/2} \exp\left(-\frac{m^\alpha[(\xi_1 - U_-)^2 + \xi_2^2 + \xi_3^2]}{2kT_-}\right),$$
$$\text{for} \quad \xi_1 > 0 \quad \text{as} \quad X_1 \to -\infty, \tag{2.10}$$

and that at downstream infinity is

$$F^\alpha \to n_+^\alpha \left(\frac{m^\alpha}{2\pi k T_+}\right)^{3/2} \exp\left(-\frac{m^\alpha[(\xi_1 - U_+)^2 + \xi_2^2 + \xi_3^2]}{2kT_+}\right),$$
$$\text{for} \quad \xi_1 < 0 \quad \text{as} \quad X_1 \to \infty, \tag{2.11}$$

with $\alpha = A$ and B.

Let n^α be the molecular number density, v_i^α the flow velocity, p^α the *pressure*, T^α the *temperature*, p_{ij}^α the *stress* tensor, and q_i^α the *heat-flow* vector of α-component ($\alpha = A, B$), and let n be the molecular number density, ρ the density, v_i the flow velocity, p the pressure, T the temperature, p_{ij} the stress tensor, and q_i the heat-flow vector of the total mixture. Then these macroscopic variables are defined as the moments of the velocity distribution functions as follows:

$$\begin{aligned}
n^\alpha &= \int F^\alpha d\boldsymbol{\xi}, \qquad v_i^\alpha = (1/n^\alpha)\int \xi_i F^\alpha d\boldsymbol{\xi}, \\
p^\alpha &= kn^\alpha T^\alpha = (1/3)\int m^\alpha(\xi_i - v_i^\alpha)^2 F^\alpha d\boldsymbol{\xi}, \\
p_{ij}^\alpha &= \int m^\alpha(\xi_i - v_i^\alpha)(\xi_j - v_j^\alpha) F^\alpha d\boldsymbol{\xi}, \\
q_i^\alpha &= (1/2)\int m^\alpha(\xi_i - v_i^\alpha)(\xi_j - v_j^\alpha)^2 F^\alpha d\boldsymbol{\xi},
\end{aligned} \tag{2.12}$$

$$\begin{aligned}
n &= \int \sum_{\alpha=A,B} F^\alpha d\boldsymbol{\xi} = \sum_{\alpha=A,B} n^\alpha, \qquad \rho = \int \sum_{\alpha=A,B} m^\alpha F^\alpha d\boldsymbol{\xi} = \sum_{\alpha=A,B} m^\alpha n^\alpha, \\
v_i &= \frac{1}{\rho}\int \xi_i \sum_{\alpha=A,B} m^\alpha F^\alpha d\boldsymbol{\xi} = \frac{1}{\rho}\sum_{\alpha=A,B} m^\alpha n^\alpha v_i^\alpha, \\
p &= knT = \frac{1}{3}\int (\xi_i - v_i)^2 \sum_{\alpha=A,B} m^\alpha F^\alpha d\boldsymbol{\xi} = \sum_{\alpha=A,B} [p^\alpha + m^\alpha n^\alpha (v_i^\alpha - v_i)^2/3], \\
p_{ij} &= \int (\xi_i - v_i)(\xi_j - v_j) \sum_{\alpha=A,B} m^\alpha F^\alpha d\boldsymbol{\xi} = \sum_{\alpha=A,B} [p_{ij}^\alpha + m^\alpha n^\alpha (v_i^\alpha - v_i)(v_j^\alpha - v_j)], \\
q_i &= (1/2)\int (\xi_i - v_i)(\xi_j - v_j)^2 \sum_{\alpha=A,B} m^\alpha F^\alpha d\boldsymbol{\xi} \\
&= \sum_{\alpha=A,B} [q_i^\alpha + p_{ij}^\alpha (v_j^\alpha - v_j) + (3/2)p^\alpha (v_i^\alpha - v_i) + (1/2)m^\alpha n^\alpha (v_i^\alpha - v_i)(v_j^\alpha - v_j)^2],
\end{aligned} \tag{2.13}$$

where $d\boldsymbol{\xi} = d\xi_1 d\xi_2 d\xi_3$, and the integration with respect to $\boldsymbol{\xi}$ in Eqs. (2.12) and (2.13) extends to the whole space of $\boldsymbol{\xi}$. In the present problem, the X_2 and X_3 components of the flow

velocities, those of the heat-flow vectors, and the nondiagonal components of the stress tensors vanish, i.e., $v_i^\alpha = v_i = q_i^\alpha = q_i = 0$ $(i = 2, 3)$ and $p_{ij}^\alpha = p_{ij} = 0$ $(i \neq j)$ (see the first paragraph of Sec. 2.3.B). It should be noted here that, in the literature, the *pressure*, *temperature*, *stress* tensor, and *heat-flow* vector of each component are often defined in a different way, i.e., by the third to fifth equations of Eq. (2.12) with v_i^α and v_j^α replaced by v_i and v_j. For this definition, the relations $p = p^A + p^B$ (Dalton's law), $p_{ij} = p_{ij}^A + p_{ij}^B$, and $q_i = q_i^A + q_i^B$ hold instead of the expressions in the last three equations of Eq. (2.13).

2.2.C Dimensionless form

We now introduce the following dimensionless variables.

$$x_1 = X_1/l_-, \qquad \zeta_i = \xi_i/(2kT_-/m^A)^{1/2}, \tag{2.14a}$$

$$\hat{F}^\alpha = F^\alpha(2kT_-/m^A)^{3/2}/n_-, \tag{2.14b}$$

where l_- is the mean free path of the molecules of the A-component when it is in an equilibrium state at rest with molecular number density n_- [Eq. (2.3b)], i.e.,

$$l_- = [\sqrt{2}\pi(d_m^A)^2 n_-]^{-1}. \tag{2.15}$$

(Note that l_- is independent of the temperature of the equilibrium state for hard-sphere molecules.) In what follows, the symbol $\boldsymbol{\zeta}$ is also used for ζ_i. Then the Boltzmann equation (2.5) is recast to the following dimensionless form:

$$\zeta_1 \frac{\partial \hat{F}^\alpha}{\partial x_1} = \sum_{\beta=A,B} C^{\beta\alpha} \left\{ \hat{G}^{\beta\alpha}[\hat{F}^\beta, \hat{F}^\alpha] - \hat{\nu}[\hat{F}^\beta]\hat{F}^\alpha \right\}, \qquad (\alpha = A, B), \tag{2.16}$$

where

$$\hat{G}^{\beta\alpha}[f, g] = \frac{1}{2\sqrt{2}\pi} \int f(x_1, \boldsymbol{\zeta}_*^{\beta\alpha}) g(x_1, \boldsymbol{\zeta}^{\beta\alpha}) |\boldsymbol{a} \cdot \hat{\boldsymbol{V}}| d\Omega(\boldsymbol{a}) d\boldsymbol{\zeta}_*, \tag{2.17}$$

$$\hat{\nu}[f] = \frac{1}{2\sqrt{2}\pi} \int f(x_1, \boldsymbol{\zeta}_*) |\boldsymbol{a} \cdot \hat{\boldsymbol{V}}| d\Omega(\boldsymbol{a}) d\boldsymbol{\zeta}_*, \tag{2.18}$$

$$\boldsymbol{\zeta}^{\beta\alpha} = \boldsymbol{\zeta} + \frac{\hat{\mu}^{\beta\alpha}}{\hat{m}^\alpha}(\boldsymbol{a} \cdot \hat{\boldsymbol{V}})\boldsymbol{a}, \quad \boldsymbol{\zeta}_*^{\beta\alpha} = \boldsymbol{\zeta}_* - \frac{\hat{\mu}^{\beta\alpha}}{\hat{m}^\beta}(\boldsymbol{a} \cdot \hat{\boldsymbol{V}})\boldsymbol{a}, \quad \hat{\boldsymbol{V}} = \boldsymbol{\zeta}_* - \boldsymbol{\zeta}, \tag{2.19}$$

$$C^{\beta\alpha} = (d_m^{\beta\alpha}/d_m^A)^2, \qquad \hat{\mu}^{\beta\alpha} = 2\hat{m}^\alpha\hat{m}^\beta/(\hat{m}^\alpha + \hat{m}^\beta), \qquad \hat{m}^\alpha = m^\alpha/m^A. \tag{2.20}$$

Here, $\boldsymbol{\zeta}_*$ is the integration variable for $\boldsymbol{\zeta}$, and $d\boldsymbol{\zeta}_* = d\zeta_{*1}d\zeta_{*2}d\zeta_{*3}$; the domain of integration is the whole space of $\boldsymbol{\zeta}_*$ and all directions of $\boldsymbol{a}$. The corresponding dimensionless forms of

boundary conditions (2.10) and (2.11) are, with $\alpha = A, B$,

$$\hat{F}^\alpha \to \left(\frac{\hat{m}^\alpha}{\pi}\right)^{3/2} \chi_-^\alpha \exp\left(-\hat{m}^\alpha \left[\left(\zeta_1 - M_- \sqrt{\frac{5}{6\sum_{\beta=A,B}\hat{m}^\beta \chi_-^\beta}}\right)^2 + \zeta_2^2 + \zeta_3^2\right]\right), \quad \text{for} \quad \zeta_1 > 0 \quad \text{as} \quad x_1 \to -\infty, \tag{2.21}$$

$$\hat{F}^\alpha \to \left(\frac{\hat{m}^\alpha}{\pi}\right)^{3/2} \chi_-^\alpha \frac{n_+^\alpha}{n_-^\alpha} \left(\frac{T_+}{T_-}\right)^{-3/2} \times \exp\left(-\hat{m}^\alpha \left(\frac{T_+}{T_-}\right)^{-1} \left[\left(\zeta_1 - \frac{U_+}{U_-} M_- \sqrt{\frac{5}{6\sum_{\beta=A,B}\hat{m}^\beta \chi_-^\beta}}\right)^2 + \zeta_2^2 + \zeta_3^2\right]\right), \quad \text{for} \quad \zeta_1 < 0 \quad \text{as} \quad x_1 \to \infty, \tag{2.22}$$

where n_+^α/n_-^α, U_+/U_-, and T_+/T_- are given by Eq. (2.1) and are determined by M_-.

Since $\hat{m}^A = 1$, $\hat{m}^B = m^B/m^A$, $C^{AA} = 1$, $C^{AB} = C^{BA} = [1 + (d_m^B/d_m^A)]^2/4$, and $C^{BB} = (d_m^B/d_m^A)^2$, and χ_-^A and χ_-^B are related as $\chi_-^A + \chi_-^B = 1$, it is seen that the boundary-value problem, Eqs. (2.16), (2.21), and (2.22), is characterized by the following four dimensionless parameters:

$$m^B/m^A, \qquad d_m^B/d_m^A, \qquad \chi_-^B, \qquad M_-. \tag{2.23}$$

We analyze the problem numerically for given values of these parameters.

2.3 Preliminary analysis

2.3.A Further transformation

We first transform Eq. (2.17). Let us decompose the relative velocity $\hat{\boldsymbol{V}}$ into the components perpendicular and parallel to $\boldsymbol{a}$, i.e.,

$$\hat{\boldsymbol{V}} = \mathbf{w} + \mathbf{z}, \qquad \mathbf{w} = \hat{\boldsymbol{V}} - (\boldsymbol{a}\cdot\hat{\boldsymbol{V}})\boldsymbol{a}, \qquad \mathbf{z} = (\boldsymbol{a}\cdot\hat{\boldsymbol{V}})\boldsymbol{a}. \tag{2.24}$$

Then, $\boldsymbol{\zeta}^{\beta\alpha}$ and $\boldsymbol{\zeta}_*^{\beta\alpha}$ are expressed as

$$\boldsymbol{\zeta}^{\beta\alpha} = \boldsymbol{\zeta} + \frac{\hat{\mu}^{\beta\alpha}}{\hat{m}^\alpha}\mathbf{z}, \qquad \boldsymbol{\zeta}_*^{\beta\alpha} = \boldsymbol{\zeta} + \mathbf{w} + \left(1 - \frac{\hat{\mu}^{\beta\alpha}}{\hat{m}^\beta}\right)\mathbf{z}. \tag{2.25}$$

If we change the integration variables from $(\boldsymbol{a}, \boldsymbol{\zeta}_*)$ to $(\mathbf{w}, \mathbf{z})$ noting that $\boldsymbol{a}$ and $-\boldsymbol{a}$ give the same $\mathbf{w}$ and $\mathbf{z}$, we obtain the following expression for $\hat{G}^{\beta\alpha}[f, g]$:

$$\hat{G}^{\beta\alpha}[f,g] = \frac{1}{\sqrt{2\pi}} \int f\left(\boldsymbol{\zeta} + \mathbf{w} + \left(1 - \frac{\hat{\mu}^{\beta\alpha}}{\hat{m}^\beta}\right)\mathbf{z}\right) g\left(\boldsymbol{\zeta} + \frac{\hat{\mu}^{\beta\alpha}}{\hat{m}^\alpha}\mathbf{z}\right) z^{-1} dS(\mathbf{w}) d\mathbf{z}, \tag{2.26}$$

where $z = |\mathbf{z}|$, $d\mathbf{z} = dz_1 dz_2 dz_3$, and $dS(\mathbf{w})$ is the surface element, around $\mathbf{w}$, of the plane perpendicular to $\mathbf{z}$; the domain of integration with respect to $\mathbf{w}$ is the whole plane perpendicular to $\mathbf{z}$, and that with respect to $\mathbf{z}$ is its whole space; the argument x_1 in f and g is omitted for simplicity.

On the other hand, the integration with respect to $\boldsymbol{a}$ in Eq. (2.18) can be carried out, and we have

$$\hat{\nu}[f] = \frac{1}{\sqrt{2}} \int |\boldsymbol{\zeta}_* - \boldsymbol{\zeta}| f(\boldsymbol{\zeta}_*) d\boldsymbol{\zeta}_*, \tag{2.27}$$

where the argument x_1 in f is also omitted.

2.3.B Similarity solution

In the present problem, we seek the solution in the following form:

$$\hat{F}^\alpha = \hat{F}^\alpha(x_1, \zeta_1, \zeta_r), \qquad \zeta_r = (\zeta_2^2 + \zeta_3^2)^{1/2}, \qquad (\alpha = A, B). \tag{2.28}$$

The compatibility of this form of $\hat{F}^\alpha$ with the Boltzmann equation (2.16) is shown by direct substitution. That is, the left-hand side (LHS) of Eq. (2.16) with Eq. (2.28) is obviously a function of x_1, ζ_1, and ζ_r; on the other hand, its right-hand side (RHS) with Eq. (2.28) is, as will be shown below, also a function of the same variables. [The latter fact is readily seen from the rotational invariance of $\hat{G}^{\beta\alpha}[f, g]$ and $\hat{\nu}[f]$. However, since we need the explicit functional form of the RHS of Eq. (2.16) with Eq. (2.28) for numerical analysis, we derive it below.] It is also obvious that Eq. (2.28) is compatible with boundary conditions (2.21) and (2.22). It follows immediately from Eq. (2.28) that $v_i^\alpha = v_i = q_i^\alpha = q_i = 0$ $(i = 2, 3)$ and $p_{ij}^\alpha = p_{ij} = 0$ $(i \neq j)$.

Now let $L(\zeta_1, \zeta_r)$ and $M(\zeta_1, \zeta_r)$ be arbitrary functions of ζ_1 and ζ_r (they may, of course, depend on x_1). We first derive, from Eq. (2.26), the explicit form of $\hat{G}^{\beta\alpha}[L, M]$. We express $\boldsymbol{\zeta}$ in cylindrical coordinates as

$$\zeta_1 = \zeta_1, \qquad \zeta_2 = \zeta_r \cos\psi, \qquad \zeta_3 = \zeta_r \sin\psi, \tag{2.29}$$

and $\mathbf{z}$ in spherical polar coordinates as

$$z_1 = z\cos\theta, \qquad z_2 = z\sin\theta\cos\epsilon, \qquad z_3 = z\sin\theta\sin\epsilon. \tag{2.30}$$

We further introduce two orthogonal unit vectors $\mathbf{e}'$ and $\mathbf{e}''$ on the plane perpendicular to $\mathbf{z}$, i.e.,

$$e'_1 = 0, \qquad e'_2 = -\sin\epsilon, \qquad e'_3 = \cos\epsilon, \tag{2.31a}$$

$$e''_1 = \sin\theta, \qquad e''_2 = -\cos\theta\cos\epsilon, \qquad e''_3 = -\cos\theta\sin\epsilon, \tag{2.31b}$$

and decompose $\mathbf{w}$ as

$$\mathbf{w} = w'\mathbf{e}' + w''\mathbf{e}''. \tag{2.32}$$

Then, noting that $dS(\mathbf{w}) = dw'dw''$ and $d\mathbf{z} = z^2\sin\theta dz d\theta d\epsilon$, we obtain the following expression for $\hat{G}^{\beta\alpha}[L, M]$:

$$\begin{aligned}
\hat{G}^{\beta\alpha}[L,M] &= \frac{1}{\sqrt{2}\pi}\int_0^\pi\int_{-\pi}^{\pi}\int_0^\infty\int_{-\infty}^{\infty}\int_{-\infty}^{\infty}\Delta_G^{\beta\alpha}(\zeta_1,\zeta_r,z,\theta,\cos(\epsilon-\psi),\sin(\epsilon-\psi),w',w'') \\
&\qquad\qquad \times dw'dw''dzd\epsilon d\theta \\
&= \frac{1}{\sqrt{2}\pi}\int_0^\pi\int_{-\pi}^{\pi}\int_0^\infty\int_{-\infty}^{\infty}\int_{-\infty}^{\infty}\Delta_G^{\beta\alpha}(\zeta_1,\zeta_r,z,\theta,\cos\bar{\epsilon},\sin\bar{\epsilon},w',w'') \\
&\qquad\qquad \times dw'dw''dzd\bar{\epsilon}d\theta \\
&= \frac{\sqrt{2}}{\pi}\int_0^\pi\int_{0}^{\pi}\int_0^\infty\int_{-\infty}^{\infty}\int_{-\infty}^{\infty}\Delta_G^{\beta\alpha}(\zeta_1,\zeta_r,z,\theta,\cos\bar{\epsilon},\sin\bar{\epsilon},w',w'') \\
&\qquad\qquad \times dw'dw''dzd\bar{\epsilon}d\theta,
\end{aligned} \tag{2.33}$$

where

$$\Delta_G^{\beta\alpha}(\zeta_1,\zeta_r,z,\theta,\cos\bar{\epsilon},\sin\bar{\epsilon},w',w'') = L(J_1,J_r)M(K_1,K_r)z\sin\theta, \tag{2.34}$$

and

$$J_1 = \zeta_1 + w''\sin\theta + (1-\hat{\mu}^{\beta\alpha}/\hat{m}^\beta)z\cos\theta, \tag{2.35a}$$

$$J_r = \{(w'-\zeta_r\sin\bar{\epsilon})^2 + [w''\cos\theta - \zeta_r\cos\bar{\epsilon} - (1-\hat{\mu}^{\beta\alpha}/\hat{m}^\beta)z\sin\theta]^2\}^{1/2}, \tag{2.35b}$$

$$K_1 = \zeta_1 + (\hat{\mu}^{\beta\alpha}/\hat{m}^\alpha)z\cos\theta, \tag{2.35c}$$

$$K_r = \{[(\hat{\mu}^{\beta\alpha}/\hat{m}^\alpha)z\sin\theta + \zeta_r\cos\bar{\epsilon}]^2 + (\zeta_r\sin\bar{\epsilon})^2\}^{1/2}. \tag{2.35d}$$

In the last equality of Eq. (2.33), the property

$$\Delta_G^{\beta\alpha}(\zeta_1,\zeta_r,z,\theta,\cos(-\bar{\epsilon}),\sin(-\bar{\epsilon}),-w',w'') = \Delta_G^{\beta\alpha}(\zeta_1,\zeta_r,z,\theta,\cos\bar{\epsilon},\sin\bar{\epsilon},w',w''), \tag{2.36}$$

has been used to reduce the range of integration with respect to $\bar{\epsilon}$ to $[0,\ \pi]$.

On the other hand, in Eq. (2.27), we express $\boldsymbol{\zeta}_*$ in cylindrical coordinates as

$$\zeta_{*1} = \zeta_{*1}, \qquad \zeta_{*2} = \zeta_{*r}\cos\phi, \qquad \zeta_{*3} = \zeta_{*r}\sin\phi, \tag{2.37}$$

and use Eq. (2.29) for $\boldsymbol{\zeta}$. Then, we obtain the following expression for $\hat{\nu}[L]$:

$$\begin{aligned}\hat{\nu}[L] &= \frac{1}{\sqrt{2}}\int_{-\infty}^{\infty}\int_{0}^{\infty}\int_{-\pi}^{\pi}\Delta_\nu(\zeta_1,\zeta_r,\zeta_{*1},\zeta_{*r},\cos(\phi-\psi))d\phi d\zeta_{*r}d\zeta_{*1} \\ &= \frac{1}{\sqrt{2}}\int_{-\infty}^{\infty}\int_{0}^{\infty}\int_{-\pi}^{\pi}\Delta_\nu(\zeta_1,\zeta_r,\zeta_{*1},\zeta_{*r},\cos\bar{\phi})d\bar{\phi}d\zeta_{*r}d\zeta_{*1},\end{aligned} \tag{2.38}$$

where

$$\Delta_\nu(\zeta_1,\zeta_r,\zeta_{*1},\zeta_{*r},\cos\bar{\phi}) = L(\zeta_{*1},\zeta_{*r})\hat{V}\zeta_{*r}, \tag{2.39a}$$

$$\hat{V} = [(\zeta_{*1}-\zeta_1)^2 + \zeta_{*r}^2 + \zeta_r^2 - 2\zeta_{*r}\zeta_r\cos\bar{\phi}]^{1/2}. \tag{2.39b}$$

From Eqs. (2.33) and (2.38), it is obvious that the RHS of Eq. (2.16) with Eq. (2.28) is a function of x_1, ζ_1, and ζ_r.

2.4 Numerical analysis

The method of analysis is the extension of the method developed by Ohwada[76] for a single component gas to the case of a binary mixture. The details will be given below.

2.4.A Finite-difference analysis

In this subsection we explain the finite-difference scheme and the solution procedure. In the actual computation, we consider a finite range of x_1, i.e., $-D \le x_1 \le D$, instead of the infinite range and impose the condition (2.21) at $x_1 = -D$ for $\zeta_1 > 0$ and (2.22) at $x_1 = D$ for $\zeta_1 < 0$. As for the molecular velocity, we only restrict ζ_1 to a finite range, i.e., $-Z_1^\alpha \le \zeta_1 \le Z_1^{\alpha\prime}$ for the α-component ($\alpha = A, B$) (as seen below, we do not need to restrict the range of ζ_r because of our solution method). The constants D, Z_1^α, and $Z_1^{\alpha\prime}$ are chosen in such a way that the deviation of the velocity distribution $\hat{F}^\alpha$ from the upstream Maxwellian (2.21) [or from the downstream Maxwellian (2.22)] is negligibly small at $x_1 \simeq -D$ (or at $x_1 \simeq D$) and that $\hat{F}^\alpha$ itself is negligibly small at $\zeta_1 \simeq -Z_1^\alpha$ and $\zeta_1 \simeq Z_1^{\alpha\prime}$. The choice is to be validated from the result of numerical computation. Now, let $x_1^{(i)}$ ($i = -N_D$, ..., 0, ..., N_D) be the lattice points in x_1 ($x_1^{(-N_D)} = -D$, $x_1^{(0)} = 0$, $x_1^{(N_D)} = D$), and let ($\zeta_1^{\alpha(j)}$, $\zeta_r^{\alpha(k)}$)

($j = -N_m^\alpha$, ..., 0, ..., N_p^α; $k = 0$, 1, ..., H^α) be the lattice points in the $\zeta_1\zeta_r$-plane for the α-component ($\zeta_1^{\alpha(-N_m^\alpha)} = -Z_1^\alpha$, $\zeta_1^{\alpha(0)} = 0$, $\zeta_1^{\alpha(N_p^\alpha)} = Z_1^{\alpha\prime}$; $\zeta_r^{\alpha(0)} = 0$; as will be seen in the next subsection, the lattice point $\zeta_r^{\alpha(0)}$ is not used in our practical computation). Then, we define $\hat{F}_i^{\alpha(n)}(\zeta_1, \zeta_r)$ and $\hat{F}_{ijk}^{\alpha(n)}$ as follows:

$$\hat{F}_i^{\alpha(n)}(\zeta_1, \zeta_r) = \hat{F}^\alpha(x_1^{(i)}, \zeta_1, \zeta_r) \quad \text{at the } n\text{th iteration step}, \tag{2.40a}$$

$$\hat{F}_{ijk}^{\alpha(n)} = \hat{F}_i^{\alpha(n)}(\zeta_1^{\alpha(j)}, \zeta_r^{\alpha(k)}). \tag{2.40b}$$

When confusion is expected, the commas are placed between subscripts as $\hat{F}_{i+1,j,k}^{\alpha(n)}$ in Eq. (2.41a) below. The finite-difference scheme that we adopt is essentially the same as that in Ref. 76, i.e.,

$$\zeta_1^{\alpha(j)}(\hat{F}_{i+1,j,k}^{\alpha(n+1)} - \hat{F}_{ijk}^{\alpha(n+1)})/(x_1^{(i+1)} - x_1^{(i)})$$
$$= \sum_{\beta=A,B} C^{\beta\alpha}(\hat{G}_{i+1,j,k}^{\beta\alpha(n)} - \hat{\nu}_{i+1,j,k}^{\beta\alpha(n)}\hat{F}_{i+1,j,k}^{\alpha(n+1)} + \hat{G}_{ijk}^{\beta\alpha(n)} - \hat{\nu}_{ijk}^{\beta\alpha(n)}\hat{F}_{ijk}^{\alpha(n+1)})/2, \quad (j > 0), \tag{2.41a}$$

$$\zeta_1^{\alpha(j)}(\hat{F}_{i-1,j,k}^{\alpha(n+1)} - \hat{F}_{ijk}^{\alpha(n+1)})/(x_1^{(i-1)} - x_1^{(i)})$$
$$= \sum_{\beta=A,B} C^{\beta\alpha}(\hat{G}_{i-1,j,k}^{\beta\alpha(n)} - \hat{\nu}_{i-1,j,k}^{\beta\alpha(n)}\hat{F}_{i-1,j,k}^{\alpha(n+1)} + \hat{G}_{ijk}^{\beta\alpha(n)} - \hat{\nu}_{ijk}^{\beta\alpha(n)}\hat{F}_{ijk}^{\alpha(n+1)})/2, \quad (j < 0), \tag{2.41b}$$

$$0 = \sum_{\beta=A,B} C^{\beta\alpha}(\hat{G}_{ijk}^{\beta\alpha(n)} - \hat{\nu}_{ijk}^{\beta\alpha(n)}\hat{F}_{ijk}^{\alpha(n+1)}), \quad (j = 0), \tag{2.41c}$$

where

$$\hat{G}_{ijk}^{\beta\alpha(n)} = \hat{G}^{\beta\alpha}[\hat{F}_i^{\beta(n)}(\zeta_1, \zeta_r), \hat{F}_i^{\alpha(n)}(\zeta_1, \zeta_r)] \quad \text{at } (\zeta_1, \zeta_r) = (\zeta_1^{\alpha(j)}, \zeta_r^{\alpha(k)}), \tag{2.42a}$$

$$\hat{\nu}_{ijk}^{\beta\alpha(n)} = \hat{\nu}[\hat{F}_i^{\beta(n)}(\zeta_1, \zeta_r)] \quad \text{at } (\zeta_1, \zeta_r) = (\zeta_1^{\alpha(j)}, \zeta_r^{\alpha(k)}). \tag{2.42b}$$

The most complicated part in this scheme is the evaluation of $\hat{G}_{ijk}^{\beta\alpha(n)}$ and $\hat{\nu}_{ijk}^{\beta\alpha(n)}$, which will be explained in the following subsections. With this method for the evaluation, the process of computation for the above finite-difference scheme is obvious. We first choose appropriate initial distributions $\hat{F}_{ijk}^{\alpha(0)}$. Now, suppose that $\hat{F}_{ijk}^{\alpha(n)}$ are known.

(i) Compute $\hat{G}_{ijk}^{\beta\alpha(n)}$ and $\hat{\nu}_{ijk}^{\beta\alpha(n)}$ using $\hat{F}_{ijk}^{\alpha(n)}$.

(ii) For $j > 0$, compute $\hat{F}_{ijk}^{\alpha(n+1)}$ successively from $i = -N_D+1$ to $i = N_D$ from Eq. (2.41a) using $\hat{G}_{ijk}^{\beta\alpha(n)}$, $\hat{\nu}_{ijk}^{\beta\alpha(n)}$ and the boundary condition at $x_1 = -D$.

(iii) For $j < 0$, compute $\hat{F}_{ijk}^{\alpha(n+1)}$ successively from $i = N_D-1$ to $i = -N_D$ from Eq. (2.41b) using $\hat{G}_{ijk}^{\beta\alpha(n)}$, $\hat{\nu}_{ijk}^{\beta\alpha(n)}$ and the boundary condition at $x_1 = D$.

(iv) For $j = 0$, compute $\hat{F}_{i0k}^{\alpha(n+1)}$ for all i from Eq. (2.41c) using $\hat{G}_{i0k}^{\beta\alpha(n)}$ and $\hat{\nu}_{i0k}^{\beta\alpha(n)}$.

Repeat the steps (i)–(iv) for $n = 0$, 1, ... until $\hat{F}_{ijk}^{\alpha(n)}$ converges.

2.4.B Numerical computation of collision integrals

In order to complete the above finite-difference scheme, we need to express $\hat{G}_{ijk}^{l\beta\alpha(n)}$ and $\hat{\nu}_{ijk}^{\beta\alpha(n)}$ in terms of $\hat{F}_{ijk}^{\alpha(n)}$. For this purpose, we first express $\hat{F}_i^{\alpha(n)}(\zeta_1, \zeta_r)$ in terms of $\hat{F}_{ijk}^{\alpha(n)}$. It is done by the following three steps. First, we expand $\hat{F}_i^{\alpha(n)}(\zeta_1, \zeta_r)$ with respect to ζ_1 using a set of basis functions $\Psi_j^\alpha(\zeta_1)$, i.e.,

$$\hat{F}_i^{\alpha(n)}(\zeta_1, \zeta_r) = \sum_{j=-N_m^\alpha}^{N_p^\alpha} \hat{F}_i^{\alpha(n)}(\zeta_1^{\alpha(j)}, \zeta_r)\Psi_j^\alpha(\zeta_1), \tag{2.43}$$

where $\Psi_j^\alpha(\zeta_1)$ is assumed to have the following property: $\Psi_j^\alpha(\zeta_1) = 1$ at $\zeta_1 = \zeta_1^{\alpha(j)}$, and $\Psi_j^\alpha(\zeta_1) = 0$ at $\zeta_1 = \zeta_1^{\alpha(l)}$ $(l \neq j)$. In the practical computation, we use Ψ_j^α that is nonzero only in a neighborhood (e.g., some lattice intervals) of $\zeta_1 = \zeta_1^{\alpha(j)}$. The explicit choice of Ψ_j^α will be made later. [Hereafter, we assume Eq. (2.43) for the whole range of ζ_1; therefore, the practical range of ζ_1 becomes slightly wider than $-Z_1^\alpha \leq \zeta_1 \leq Z_1^{\alpha\prime}$.] Second, expecting that $\hat{F}_i^{\alpha(n)}$ is a smooth and rapidly decreasing function of $\sqrt{\hat{m}^\alpha}\zeta_r$, we assume the following form of $\hat{F}_i^{\alpha(n)}(\zeta_1^{\alpha(j)}, \zeta_r)$:

$$\hat{F}_i^{\alpha(n)}(\zeta_1^{\alpha(j)}, \zeta_r) = \exp\Big(-\frac{\hat{m}^\alpha\zeta_r^2}{2}\Big)\sum_{m=0}^{H^\alpha-1} a_{ijm}^{\alpha(n)} L_m(\hat{m}^\alpha\zeta_r^2), \tag{2.44}$$

where $L_m(y)$ is the Laguerre polynomial[99] of mth order, which is defined by

$$L_m(y) = \sum_{s=0}^{m} \frac{(-1)^s}{s!}\binom{m}{s} y^s, \tag{2.45}$$

and satisfy the relation

$$\int_0^\infty L_m(y)L_n(y)\exp(-y)dy = \delta_{mn}. \tag{2.46}$$

The system of functions $\exp(-y/2)L_m(y)$ $(m = 0, 1, ...)$ forms a complete orthonormal system in $L^2(0, \infty)$. Therefore, Eq. (2.44) means that, assuming $\hat{F}_i^{\alpha(n)}(\zeta_1^{\alpha(j)}, \zeta_r)$ to be a rapidly decreasing function of $\hat{m}^\alpha\zeta_r^2$, we expand it in terms of the orthonormal system and truncate it at the H^αth term. If we consider Eq. (2.44) at the lattice points $\zeta_r = \zeta_r^{\alpha(k)}$ $(k = 1, ..., H^\alpha)$, we have

$$\hat{F}_{ijk}^{\alpha(n)} = \exp\Big(-\frac{\hat{m}^\alpha(\zeta_r^{\alpha(k)})^2}{2}\Big)\sum_{m=0}^{H^\alpha-1} a_{ijm}^{\alpha(n)} L_m(\hat{m}^\alpha(\zeta_r^{\alpha(k)})^2). \tag{2.47}$$

The coefficients $a_{ijm}^{\alpha(n)}$ ($m = 0, ..., H^\alpha - 1$) in Eq. (2.44) are expressed in terms of $\hat{F}_{ijk}^{\alpha(n)}$ ($k = 1, ..., H^\alpha$) by solving the system of linear algebraic equations (2.47). [Equation (2.44) with $a_{ijm}^{\alpha(n)}$ thus determined is equivalent to approximating $\exp(\hat{m}^\alpha \zeta_r^2/2)\hat{F}_i^{\alpha(n)}(\zeta_1^{\alpha(j)}, \zeta_r)$ by the $H^\alpha - 1$ degree polynomial of $\hat{m}^\alpha \zeta_r^2$ that takes the values $\exp(\hat{m}^\alpha(\zeta_r^{\alpha(k)})^2/2)\hat{F}_{ijk}^{\alpha(n)}$ at $\zeta_r = \zeta_r^{\alpha(k)}$ ($k = 1, ..., H^\alpha$) (Lagrange interpolation).] Equation (2.44), arranged in the form of power series of $\hat{m}^\alpha \zeta_r^2$, can be written as

$$\hat{F}_i^{\alpha(n)}(\zeta_1^{\alpha(j)}, \zeta_r) = \exp\Big(-\frac{\hat{m}^\alpha \zeta_r^2}{2}\Big) \sum_{m=0}^{H^\alpha - 1} A_{ijm}^{\alpha(n)} (\hat{m}^\alpha \zeta_r^2)^m, \tag{2.48}$$

where $A_{ijm}^{\alpha(n)}$ are the constants depending explicitly on $\hat{F}_{ijk}^{\alpha(n)}$ and the lattice points $\zeta_r^{\alpha(k)}$ ($k = 1, ..., H^\alpha$) (Explicit expression of $A_{ijm}^{\alpha(n)}$ will be given later for a special choice of $\zeta_r^{\alpha(k)}$). Finally, by substituting Eq. (2.48) into Eq. (2.43), we have the following expression of $\hat{F}_i^{\alpha(n)}(\zeta_1, \zeta_r)$ in terms of $\hat{F}_{ijk}^{\alpha(n)}$:

$$\hat{F}_i^{\alpha(n)}(\zeta_1, \zeta_r) = \exp\Big(-\frac{\hat{m}^\alpha \zeta_r^2}{2}\Big) \sum_{j=-N_m^\alpha}^{N_p^\alpha} \sum_{m=0}^{H^\alpha - 1} A_{ijm}^{\alpha(n)} \Psi_j^\alpha(\zeta_1)(\hat{m}^\alpha \zeta_r^2)^m. \tag{2.49}$$

If we substitute Eq. (2.49) into Eq. (2.42), we obtain the desired expressions of $\hat{G}_{ijk}^{\beta\alpha(n)}$ and $\hat{\nu}_{ijk}^{\beta\alpha(n)}$, i.e.,

$$\hat{G}_{ijk}^{\beta\alpha(n)} = \sum_{p=-N_m^\beta}^{N_p^\beta} \sum_{q=-N_m^\alpha}^{N_p^\alpha} \sum_{a=0}^{H^\beta - 1} \sum_{b=0}^{H^\alpha - 1} \Omega_{pqab}^{\beta\alpha jk} A_{ipa}^{\beta(n)} A_{iqb}^{\alpha(n)}, \tag{2.50a}$$

$$\hat{\nu}_{ijk}^{\beta\alpha(n)} = \sum_{p=-N_m^\beta}^{N_p^\beta} \sum_{a=0}^{H^\beta - 1} \Lambda_{pa}^{\beta\alpha jk} A_{ipa}^{\beta(n)}, \tag{2.50b}$$

where

$$\Omega_{pqab}^{\beta\alpha jk} = \hat{G}^{\beta\alpha}[\Psi_p^\beta(\zeta_1)(\hat{m}^\beta \zeta_r^2)^a E_r^\beta, \Psi_q^\alpha(\zeta_1)(\hat{m}^\alpha \zeta_r^2)^b E_r^\alpha] \quad \text{at } (\zeta_1, \zeta_r) = (\zeta_1^{\alpha(j)}, \zeta_r^{\alpha(k)}), \tag{2.51a}$$

$$\Lambda_{pa}^{\beta\alpha jk} = \hat{\nu}[\Psi_p^\beta(\zeta_1)(\hat{m}^\beta \zeta_r^2)^a E_r^\beta] \quad \text{at } (\zeta_1, \zeta_r) = (\zeta_1^{\alpha(j)}, \zeta_r^{\alpha(k)}), \tag{2.51b}$$

$$E_r^\alpha = \exp(-\hat{m}^\alpha \zeta_r^2/2). \tag{2.51c}$$

The $\Omega_{pqab}^{\beta\alpha jk}$ and $\Lambda_{pa}^{\beta\alpha jk}$ are the universal constants in the sense that they do not depend on i and n. Therefore, we can compute them beforehand once we have chosen the lattice points in the $\zeta_1\zeta_r$-plane and the explicit form of $\Psi_j^\alpha(\zeta_1)$ (note that they depend also on m^B/m^A, but not on d_m^B/d_m^A). We call $\Omega_{pqab}^{\beta\alpha jk}$ and $\Lambda_{pa}^{\beta\alpha jk}$ the *numerical kernels* of the collision integrals.

In this way, the computation of the collision integrals has been reduced to the matrix products of the numerical kernels and $A_{ijk}^{\alpha(n)}$ that are determined by $\hat{F}_{ijk}^{\alpha(n)}$ and by the lattice points $\zeta_r^{\alpha(k)}$. A convenient choice of $\zeta_r^{\alpha(k)}$ is,

$$\zeta_r^{\alpha(k)} = \sqrt{y_k/\hat{m}^\alpha}, \qquad (k = 1, \ ..., \ H), \tag{2.52}$$

where $H^\alpha = H$ is assumed for simplicity, and y_k stands for the zeros ($y_k < y_l$ for $k < l$) of the Laguerre polynomial $L_H(y)$ of order H. Then, we obtain the following simple expression of the solution $a_{ijm}^{\alpha(n)}$ of the system of algebraic equations (2.47):

$$a_{ijm}^{\alpha(n)} = \sum_{k=1}^{H} w_{mk} \hat{F}_{ijk}^{\alpha(n)}, \tag{2.53a}$$

$$w_{mk} = \frac{L_m(y_k) \exp(y_k/2)}{c_{H-1,H-1} L_{H-1}(y_k) \prod_{s=1(\neq k)}^{H} (y_k - y_s)}, \tag{2.53b}$$

where c_{mn} is the coefficient of y^m in $L_n(y)$ [see Appendix A for the derivation of Eq. (2.53)]. Equation (2.53a) leads to the concise expression of the coefficients $A_{ijm}^{\alpha(n)}$ in Eq. (2.49) in terms of $\hat{F}_{ijk}^{\alpha(n)}$ and y_k (Appendix A), i.e.,

$$A_{ijm}^{\alpha(n)} = \sum_{k=1}^{H} \sum_{l=0}^{H-1} M_{ml} w_{lk} \hat{F}_{ijk}^{\alpha(n)}, \tag{2.54a}$$

$$M_{ml} = \begin{cases} 0 & (m > l), \\ c_{ml} & (0 \le m \le l). \end{cases} \tag{2.54b}$$

2.4.C Numerical kernels of collision integrals

1 Basis functions

The number of the elements of the numerical kernels $\Omega_{pqab}^{\beta\alpha jk}$ is still too large for precise numerical computations because of its six-fold indices (j, k, p, q, a, b). However, by using a uniform lattice system for ζ_1 that is common to both components, i.e.,

$$\zeta_1^{\alpha(j)} = \zeta_1^{(j)} = jh, \qquad (j = -N_m, ..., 0, ..., N_p), \tag{2.55}$$

(here $N_m^\alpha = N_m$ and $N_p^\alpha = N_p$ are assumed for simplicity) and by exploiting the basic properties of $\hat{G}^{\beta\alpha}$ and $\hat{\nu}$, we can reduce the number of the independent elements of $\Omega_{pqab}^{\beta\alpha jk}$ and $\Lambda_{pa}^{\beta\alpha jk}$ significantly, as we will see below. Since $\hat{F}^\alpha$ is expected to be a rapidly decaying function of $\sqrt{\hat{m}^\alpha}\zeta_1$, it is reasonable to use different lattice systems for individual gas components, such

as $\zeta_1^{\alpha(j)} = jh/\sqrt{\hat{m}^\alpha}$, rather than Eq. (2.55). But in this case, such reduction of the number of the independent elements is not possible. We can perform much more efficient computation with the lattice system (2.55).

To define the explicit form of the basis functions $\Psi_j^\alpha(\zeta_1)$ in Eq. (2.43), we introduce the following $\widetilde{\Psi}_j(\zeta_1)$:

$$\widetilde{\Psi}_{2\ell}(\zeta_1) = \begin{cases} [\zeta_1 - (2\ell-1)h]\,[\zeta_1 - (2\ell-2)h]\,/2h^2, & [(2\ell-2)h \le \zeta_1 \le 2\ell h], \\ [\zeta_1 - (2\ell+1)h]\,[\zeta_1 - (2\ell+2)h]\,/2h^2, & [2\ell h < \zeta_1 \le (2\ell+2)h], \\ 0, & (\text{otherwise}), \end{cases} \tag{2.56a}$$

$$\widetilde{\Psi}_{2\ell+1}(\zeta_1) = \begin{cases} -(\zeta_1 - 2\ell h)\,[\zeta_1 - (2\ell+2)h]\,/h^2, & [2\ell h \le \zeta_1 \le (2\ell+2)h], \\ 0, & (\text{otherwise}). \end{cases} \tag{2.56b}$$

Then, in the computation of $\Omega_{pqab}^{\beta\alpha jk}$ and $\Lambda_{pa}^{\beta\alpha jk}$, we use two different sets of basis functions depending on the parity of j that are common to both components, i.e.,

$$\Psi_p^\alpha(\zeta_1) = \Psi_p(\zeta_1) = \widetilde{\Psi}_p(\zeta_1), \qquad (p = 0, \pm1, \pm2, ...), \qquad \text{for } j = 2\ell, \tag{2.57a}$$

$$\Psi_p^\alpha(\zeta_1) = \Psi_p(\zeta_1) = \widetilde{\Psi}_{p-1}(\zeta_1 - h), \qquad (p = 0, \pm1, \pm2, ...), \qquad \text{for } j = 2\ell+1. \tag{2.57b}$$

By this choice of the basis functions, Eq. (2.43) means that $\hat{F}_i^{\alpha(n)}(\zeta_1, \zeta_r)$, as the function of ζ_1, is approximated by a piecewise quadratic function of ζ_1 that takes the value $\hat{F}_i^{\alpha(n)}(\zeta_1^{(j)}, \zeta_r)$ at the lattice point $\zeta_1 = \zeta_1^{(j)}$ $(j = -N_m, ..., 0, ..., N_p)$. The piecewise quadratic function is quadratic in the interval $2\ell h \le \zeta_1 \le 2(\ell+1)h$ for Eq. (2.57a) and in $(2\ell-1)h \le \zeta_1 \le (2\ell+1)h$ for Eq. (2.57b). [These statements are not true in a small neighborhood of the outermost lattice point $\zeta_1^{(-N_m)}$ or $\zeta_1^{(N_p)}$, where the value of $\hat{F}_i^{\alpha(n)}(\zeta_1, \zeta_r)$ is negligibly small.] The use of the two sets of basis functions is just for convenience that the lattice point $\zeta_1^{(j)}$ under consideration in the integrals in Eq. (2.51) is always at a node [$\zeta_1^{(2\ell)}$ for Eq. (2.57a) and $\zeta_1^{(2\ell+1)}$ for Eq. (2.57b)] of the piecewise quadratic function. The $\widetilde{\Psi}_p(\zeta_1)$ defined above has the property

$$\widetilde{\Psi}_p(\zeta_1 + \zeta_1^{(2\ell)}) = \widetilde{\Psi}_p(\zeta_1 + 2\ell h) = \widetilde{\Psi}_{p-2\ell}(\zeta_1), \tag{2.58a}$$

$$\widetilde{\Psi}_p(-\zeta_1) = \widetilde{\Psi}_{-p}(\zeta_1). \tag{2.58b}$$

On the other hand, $\hat{G}^{\beta\alpha}$ and $\hat{\nu}$ satisfy the following relations.

$$\hat{G}^{\beta\alpha}[f(\boldsymbol{\zeta}), g(\boldsymbol{\zeta})](\boldsymbol{\zeta}) = \hat{G}^{\beta\alpha}[f(\boldsymbol{\zeta}+\boldsymbol{a}), g(\boldsymbol{\zeta}+\boldsymbol{a})](\boldsymbol{\zeta}-\boldsymbol{a}), \tag{2.59a}$$

$$\hat{\nu}[f(\boldsymbol{\zeta})](\boldsymbol{\zeta}) = \hat{\nu}[f(\boldsymbol{\zeta}+\boldsymbol{a})](\boldsymbol{\zeta}-\boldsymbol{a}), \tag{2.59b}$$

$$\hat{G}^{\beta\alpha}[f(\zeta_1,\zeta_r), g(\zeta_1,\zeta_r)](0,\zeta_r) = \hat{G}^{\beta\alpha}[f(-\zeta_1,\zeta_r), g(-\zeta_1,\zeta_r)](0,\zeta_r), \tag{2.59c}$$

$$\hat{\nu}[f(\zeta_1,\zeta_r)](0,\zeta_r) = \hat{\nu}[f(-\zeta_1,\zeta_r)](0,\zeta_r), \tag{2.59d}$$

$$\hat{G}^{\alpha\alpha}[f(\boldsymbol{\zeta}), g(\boldsymbol{\zeta})] = \hat{G}^{\alpha\alpha}[g(\boldsymbol{\zeta}), f(\boldsymbol{\zeta})], \tag{2.59e}$$

$$\hat{G}^{\alpha\alpha}[f_1(\zeta_1)g_1(\zeta_r), f_2(\zeta_1)g_2(\zeta_r)] = \hat{G}^{\alpha\alpha}[f_1(\zeta_1)g_2(\zeta_r), f_2(\zeta_1)g_1(\zeta_r)], \tag{2.59f}$$

where f, g, etc. are arbitrary functions of the independent variables specified in the equations, and the independent variables of $\hat{G}^{\beta\alpha}$ and $\hat{\nu}$ in Eqs. (2.59a)–(2.59d) are shown in the respective last parentheses. Equations (2.59a) and (2.59b) follow from Eqs. (2.17) and (2.18), and Eqs. (2.59c) and (2.59d) follow from Eqs. (2.33) and (2.38). Equations (2.59e) and (2.59f) are essentially the same as the corresponding relation for a single-component gas, the derivation of which is given in Ref. 76.

It follows from Eqs. (2.58a), (2.59a), and (2.59b) that

$$\Omega^{\beta\alpha jk}_{pqab} = \Omega^{\beta\alpha 0k}_{p-j,q-j,a,b}, \qquad \Lambda^{\beta\alpha jk}_{pa} = \Lambda^{\beta\alpha 0k}_{p-j,a}, \tag{2.60}$$

from Eqs. (2.58b), (2.59c), and (2.59d) that

$$\Omega^{\beta\alpha 0k}_{pqab} = \Omega^{\beta\alpha 0k}_{-p,-q,a,b}, \qquad \Lambda^{\beta\alpha 0k}_{pa} = \Lambda^{\beta\alpha 0k}_{-p,a}, \tag{2.61}$$

and from Eqs. (2.59e) and (2.59f) that

$$\Omega^{\alpha\alpha 0k}_{pqab} = \Omega^{\alpha\alpha 0k}_{qpba} = \Omega^{\alpha\alpha 0k}_{pqba}. \tag{2.62}$$

Equations (2.60) and (2.61) reduce the number of independent elements of $\Omega^{\beta\alpha jk}_{pqab}$ from $O(N^6)$ to $O(N^5)$ and that of $\Lambda^{\beta\alpha jk}_{pa}$ from $O(N^4)$ to $O(N^3)$, where N is the representative number of the lattice points of each molecular velocity component [i.e., N is of the order of N_m+N_p+1 and of H].

2 Numerical kernels

From Eqs. (2.33), (2.51a), and (2.57a), we obtain the following expression of $\Omega^{\beta\alpha 0k}_{pqab}$:

$$\Omega^{\beta\alpha 0k}_{pqab} = \frac{\sqrt{2}}{\pi}\int_0^\pi\int_0^\pi\int_0^\infty\int_{-\infty}^\infty\int_{-\infty}^\infty \widetilde{\Psi}_p(J_1)\widetilde{\Psi}_q(K_1)(\sqrt{\hat{m}^\beta}J_r^{(k)})^{2a}(\sqrt{\hat{m}^\alpha}K_r^{(k)})^{2b} \times \exp\left(-\frac{(\sqrt{\hat{m}^\beta}J_r^{(k)})^2+(\sqrt{\hat{m}^\alpha}K_r^{(k)})^2}{2}\right) z\sin\theta dw'dw''dzd\bar{\epsilon}d\theta, \quad (2.63)$$

where

$$J_1 = w''\sin\theta + (1-\hat{\mu}^{\beta\alpha}/\hat{m}^\beta)z\cos\theta, \quad (2.64a)$$

$$J_r^{(k)} = \{(w'-\zeta_r^{\alpha(k)}\sin\bar{\epsilon})^2 + [w''\cos\theta - \zeta_r^{\alpha(k)}\cos\bar{\epsilon} - (1-\hat{\mu}^{\beta\alpha}/\hat{m}^\beta)z\sin\theta]^2\}^{1/2}, \quad (2.64b)$$

$$K_1 = (\hat{\mu}^{\beta\alpha}/\hat{m}^\alpha)z\cos\theta, \quad (2.64c)$$

$$K_r^{(k)} = \{[(\hat{\mu}^{\beta\alpha}/\hat{m}^\alpha)z\sin\theta + \zeta_r^{\alpha(k)}\cos\bar{\epsilon}]^2 + (\zeta_r^{\alpha(k)}\sin\bar{\epsilon})^2\}^{1/2}. \quad (2.64d)$$

Because of the property (2.61), we only need $\Omega^{\beta\alpha 0k}_{pqab}$ for $q>0$ and for $q=0$, $p\geq 0$. For these p and q, Eq. (2.63) can be rewritten in the following form:

$$\Omega^{\beta\alpha 0k}_{pqab} = \frac{\sqrt{2}}{\pi}\int_0^{\pi/2}\int_0^\pi \Gamma^k_{pqab}(\theta,\bar{\epsilon})d\bar{\epsilon}d\theta, \qquad (q>0), \quad (2.65a)$$

$$\Omega^{\beta\alpha 0k}_{p0ab} = \frac{\sqrt{2}}{\pi}\int_0^{\pi/2}\int_0^\pi [\Gamma^k_{p0ab}(\theta,\bar{\epsilon}) + \Gamma^k_{-p,0,a,b}(\theta,\bar{\epsilon})]d\bar{\epsilon}d\theta, \qquad (p\geq 0), \quad (2.65b)$$

where

$$\Gamma^k_{pqab}(\theta,\bar{\epsilon}) = \sin\theta\int_0^\infty z\widetilde{\Psi}_q(K_1)(\sqrt{\hat{m}^\alpha}K_r^{(k)})^{2b}\exp\left(-\frac{(\sqrt{\hat{m}^\alpha}K_r^{(k)})^2}{2}\right)\Theta^k_{pa}(z,\theta,\bar{\epsilon})dz, \quad (2.66a)$$

$$\Theta^k_{pa}(z,\theta,\bar{\epsilon}) = \int_{-\infty}^\infty\int_{-\infty}^\infty \widetilde{\Psi}_p(J_1)(\sqrt{\hat{m}^\beta}J_r^{(k)})^{2a}\exp\left(-\frac{(\sqrt{\hat{m}^\beta}J_r^{(k)})^2}{2}\right)dw'dw''. \quad (2.66b)$$

In Eq. (2.65a) we have omitted the part $[\pi/2,\ \pi]$ of the integration with respect to θ because $\widetilde{\Psi}_q$ is identically zero for the negative argument when $q>0$. In Eq. (2.65b), we have reduced the integral with respect to θ in Eq. (2.63) to that over $[0,\ \pi/2]$. This can be done by splitting the integral into that over $[0,\ \pi/2]$ and that over $[\pi/2,\ \pi]$, changing the variables as $w''=-w''$ and $\theta=\pi-\theta$ in the latter, and taking into account the property $\widetilde{\Psi}_p(-\zeta_1)=\widetilde{\Psi}_{-p}(\zeta_1)$. As shown in Appendix B, Eq. (2.66b) can be integrated analytically. Therefore, the final expression of $\Omega^{\beta\alpha 0k}_{pqab}$ contains triple integral with respect to z, $\bar{\epsilon}$, and θ. It is computed numerically by the Gauss-Legendre formula.[100] (In the actual computation,

we carry out the numerical integration using slightly different variables, i.e., $\bar{z}$, $\bar{\epsilon}$, and θ, as shown in Appendix C.) When $\alpha = \beta$, Θ_{pa}^{k} does not depend on z (Appendix B), and thus the integration with respect to z in Eq. (2.66a) can be performed analytically (see Appendix C). Hence, the final expression of $\Omega_{pqab}^{\alpha\alpha 0k}$ contains double integral with respect to $\bar{\epsilon}$ and θ, which is computed numerically by the Gauss-Legendre formula. In the case of a single-component gas, the numerical kernel for the gain term is essentially the same as $\Omega_{pqab}^{\alpha\alpha 0k}$ (Ref. 76). Therefore, only the double integral (with respect to $\bar{\epsilon}$ and θ) should be calculated numerically to generate the numerical kernel. In the case of a binary mixture, one more integration (with respect to z) should be carried out numerically.

On the other hand, the integration with respect to $\bar{\phi}$ in Eq. (2.38) can be carried out and leads to the following expression for $\hat{\nu}[L]$:

$$\hat{\nu}[L] = 2\sqrt{2}\int_{-\infty}^{\infty}\int_{0}^{\infty}[(\zeta_{*1}-\zeta_1)^2+(\zeta_{*r}+\zeta_r)^2]^{1/2}\mathcal{E}_{II}\Big(\frac{4\zeta_{*r}\zeta_r}{(\zeta_{*1}-\zeta_1)^2+(\zeta_{*r}+\zeta_r)^2}\Big) \times\zeta_{*r}L(\zeta_{*1},\zeta_{*r})d\zeta_{*r}d\zeta_{*1}, \quad (2.67)$$

where $\mathcal{E}_{II}$ is the complete elliptic integral of the second kind, i.e.,

$$\mathcal{E}_{II}(x) = \int_0^{\pi/2}(1-x\sin^2 t)^{1/2}dt, \qquad (0\le x\le 1). \quad (2.68)$$

From Eqs. (2.51b), (2.57a), and (2.67), the numerical kernel $\Lambda_{pa}^{\beta\alpha 0k}$ is expressed by

$$\Lambda_{pa}^{\beta\alpha 0k} = 2\sqrt{2}\int_{-\infty}^{\infty}\int_{0}^{\infty}[\zeta_{*1}^2+(\zeta_{*r}+\zeta_r^{\alpha(k)})^2]^{1/2}\mathcal{E}_{II}\left(\frac{4\zeta_{*r}\zeta_r^{\alpha(k)}}{\zeta_{*1}^2+(\zeta_{*r}+\zeta_r^{\alpha(k)})^2}\right) \times\zeta_{*r}(\hat{m}^\beta\zeta_{*r}^2)^a\exp\Big(-\frac{\hat{m}^\beta\zeta_{*r}^2}{2}\Big)\widetilde{\Psi}_p(\zeta_{*1})d\zeta_{*r}d\zeta_{*1}. \quad (2.69)$$

The two-fold integration with respect to ζ_{*1} and ζ_{*r} in $\Lambda_{pa}^{\beta\alpha 0k}$ is carried out numerically by the Gauss-Legendre formula.

2.5 Results of numerical analysis

In this section, we show the results of numerical analysis, choosing the point at which $n(X_1) = (n_- + n_+)/2$ to be the origin $X_1 = 0$ of the X_1 coordinate.

2.5.A Macroscopic quantities

To show the profiles of the molecular number densities n^α and n, the flow velocities (in the X_1 direction) v_1^α and v_1, and the temperatures T^α and T, we introduce the following

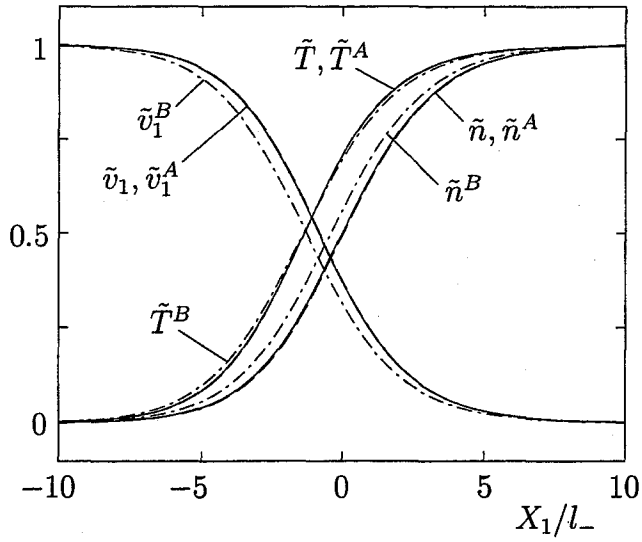

(a) $\chi_-^B = 0.1$

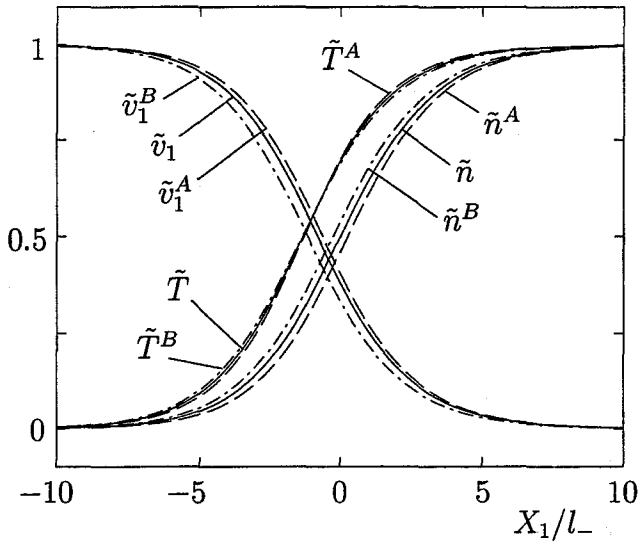

(b) $\chi_-^B = 0.5$

Figure 2.1: Profiles of molecular number densities, flow velocities, and temperatures for $M_- = 1.5$, $m^B/m^A = 0.5$, and $d_m^B/d_m^A = 1$. (a) $\chi_-^B = 0.1$, (b) $\chi_-^B = 0.5$, and (c) $\chi_-^B = 0.9$. For this M_-, the downstream values are $n_+^\alpha = 1.714 n_-^\alpha$, $U_+ = 0.5833 U_-$, $T_+ = 1.495 T_-$, and $M_+ = 0.7157$. Here, the solid lines indicate $\tilde{n}$, $\tilde{v}_1$, and $\tilde{T}$ for the total mixture, the dashed lines $\tilde{n}^A$, $\tilde{v}_1^A$, and $\tilde{T}^A$ for the A–component, and the dot–dash lines $\tilde{n}^B$, $\tilde{v}_1^B$, and $\tilde{T}^B$ for the B–component [see Eq. (2.70)].

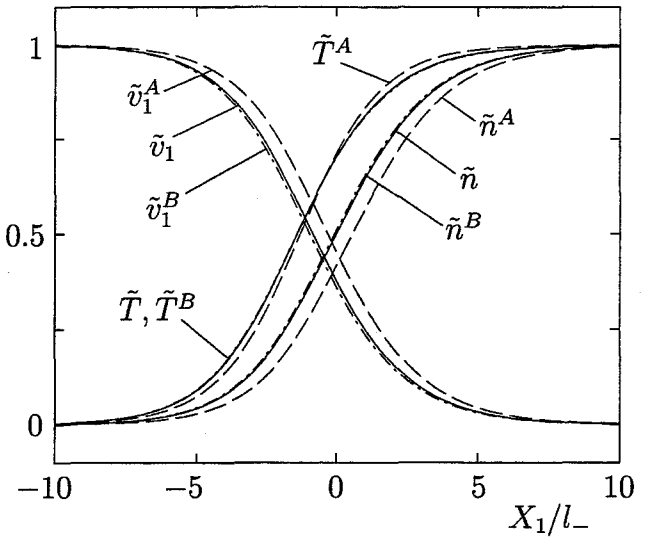

(c) $\chi_-^B = 0.9$

Figure 2.1: (continued from the previous page)

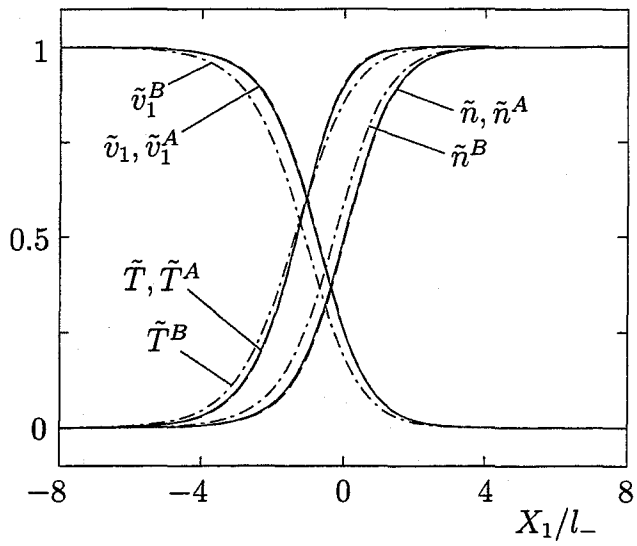

(a) $\chi_-^B = 0.1$

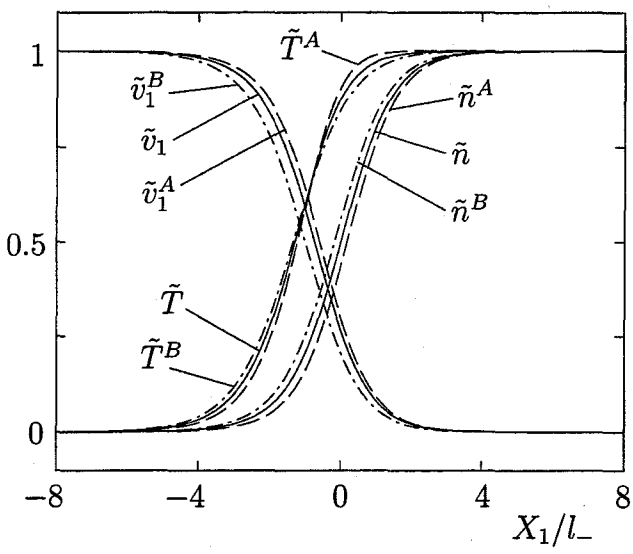

(b) $\chi_-^B = 0.5$

Figure 2.2: Profiles of molecular number densities, flow velocities, and temperatures for $M_- = 3$, $m^B/m^A = 0.5$, and $d_m^B/d_m^A = 1$. (a) $\chi_-^B = 0.1$, (b) $\chi_-^B = 0.5$, and (c) $\chi_-^B = 0.9$. For this M_-, the downstream values are $n_+^\alpha = 3n_-^\alpha$, $U_+ = U_-/3$, $T_+ = 3.667T_-$, and $M_+ = 0.5222$. See the caption of Fig. 2.1.

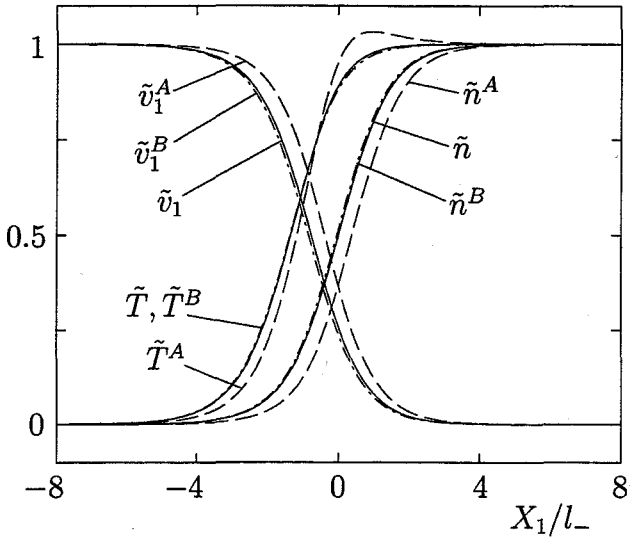

(c) $\chi_-^B = 0.9$

Figure 2.2: (continued from the previous page)

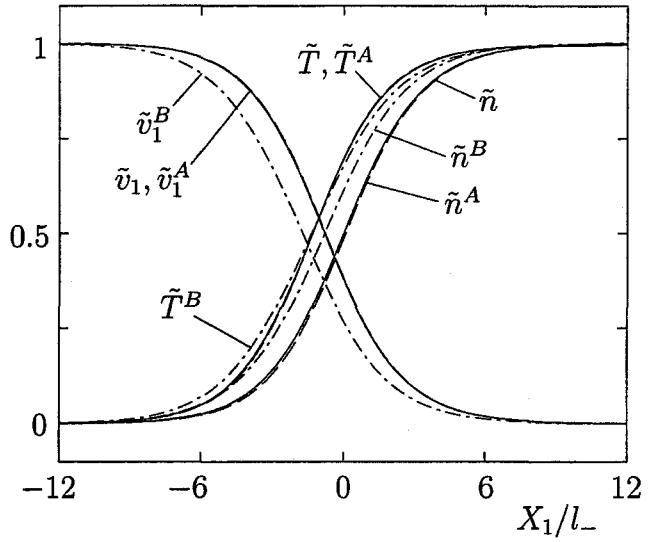

(a) $\chi_-^B = 0.1$

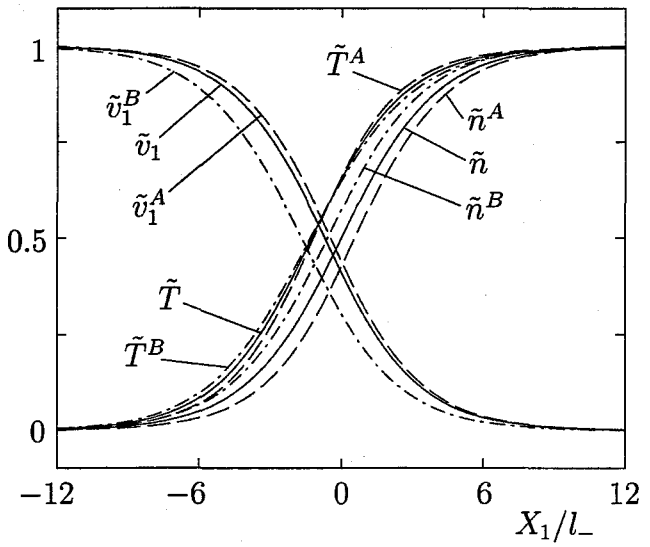

(b) $\chi_-^B = 0.5$

Figure 2.3: Profiles of molecular number densities, flow velocities, and temperatures for $M_- = 1.5$, $m^B/m^A = 0.25$, and $d_m^B/d_m^A = 1$. (a) $\chi_-^B = 0.1$, (b) $\chi_-^B = 0.5$, and (c) $\chi_-^B = 0.9$. For this M_-, the downstream values are $n_+^\alpha = 1.714 n_-^\alpha$, $U_+ = 0.5833 U_-$, $T_+ = 1.495 T_-$, and $M_+ = 0.7157$. See the caption of Fig. 2.1.

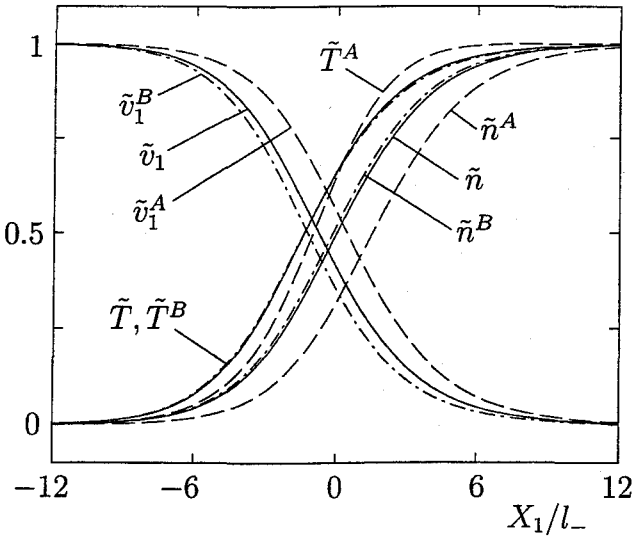

(c) $\chi_-^B = 0.9$

Figure 2.3: (continued from the previous page)

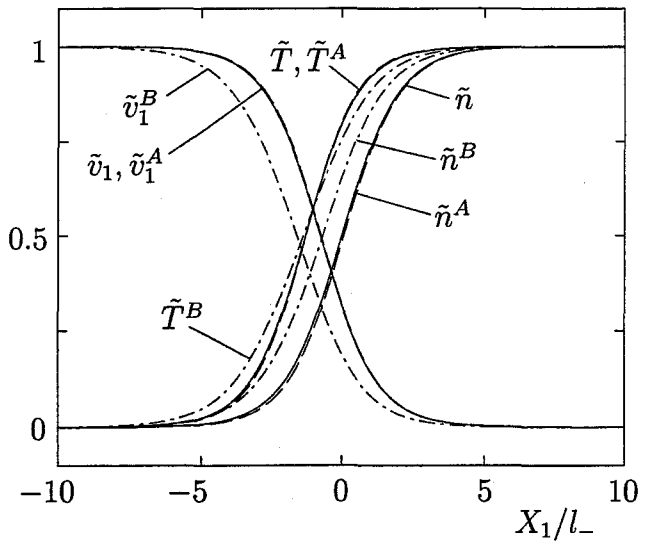

(a) $\chi_-^B = 0.1$

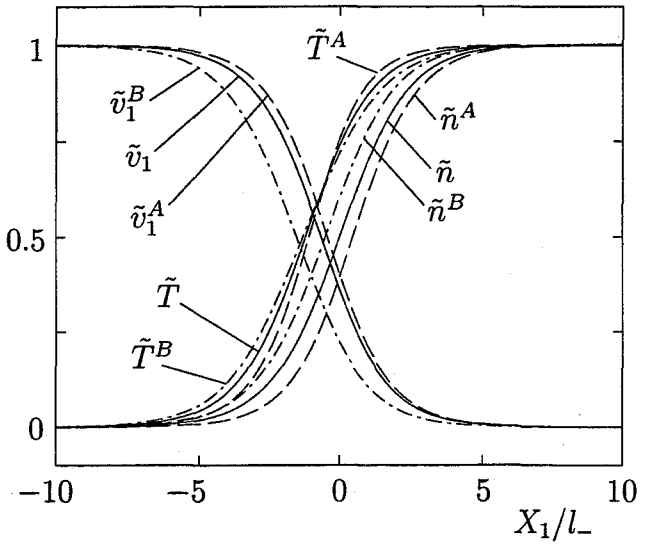

(b) $\chi_-^B = 0.5$

Figure 2.4: Profiles of molecular number densities, flow velocities, and temperatures for $M_- = 2$, $m^B/m^A = 0.25$, and $d_m^B/d_m^A = 1$. (a) $\chi_-^B = 0.1$, (b) $\chi_-^B = 0.5$, and (c) $\chi_-^B = 0.9$. For this M_-, the downstream values are $n_+^\alpha = 2.286 n_-^\alpha$, $U_+ = 0.4375 U_-$, $T_+ = 2.078 T_-$, and $M_+ = 0.6070$. See the caption of Fig. 2.1.

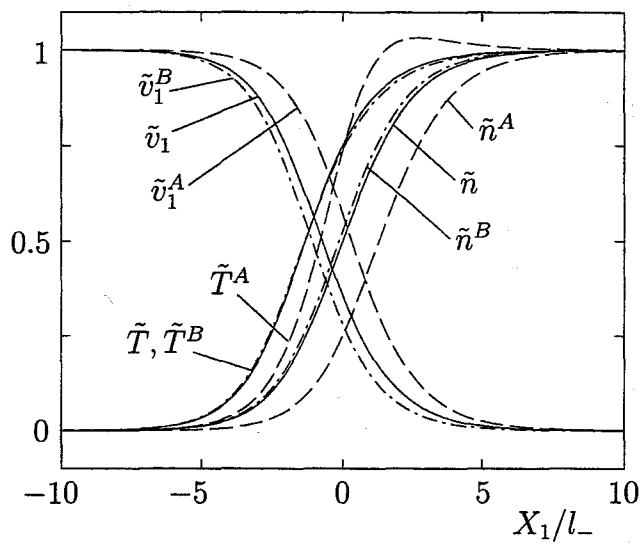

(c) $\chi_-^B = 0.9$

Figure 2.4: (continued from the previous page)

Table 2.1: The distributions of the molecular number density n, flow velocity v_1, and temperature T of the total mixture for $M_- = 1.5$, $m^B/m^A = 0.5$, and $d_m^B/d_m^A = 1$ (cf. Fig. 2.1).

	n/n_-			$v_1/(2kT_-/m^A)^{1/2}$			T/T_-		
X_1/l_-	$\chi_-^B = 0.1$	$\chi_-^B = 0.5$	$\chi_-^B = 0.9$	$\chi_-^B = 0.1$	$\chi_-^B = 0.5$	$\chi_-^B = 0.9$	$\chi_-^B = 0.1$	$\chi_-^B = 0.5$	$\chi_-^B = 0.9$
$-\infty$	1.000	1.000	1.000	1.405	1.581	1.846	1.000	1.000	1.000
-12	1.000	1.000	1.000	1.405	1.581	1.846	1.000	1.000	1.000
-9	1.002	1.003	1.002	1.402	1.577	1.842	1.003	1.004	1.003
-7	1.008	1.010	1.008	1.395	1.567	1.831	1.011	1.014	1.013
-5	1.028	1.033	1.030	1.367	1.534	1.793	1.042	1.046	1.045
-4	1.053	1.059	1.056	1.336	1.498	1.751	1.075	1.080	1.079
-3	1.094	1.102	1.098	1.285	1.442	1.685	1.127	1.131	1.131
-2	1.160	1.167	1.164	1.213	1.364	1.592	1.198	1.199	1.200
-1	1.250	1.255	1.253	1.126	1.269	1.479	1.277	1.274	1.277
0	1.357	1.357	1.357	1.037	1.173	1.366	1.349	1.343	1.347
1	1.462	1.458	1.459	0.962	1.090	1.270	1.404	1.398	1.402
2	1.549	1.543	1.545	0.908	1.029	1.198	1.441	1.436	1.439
3	1.612	1.606	1.607	0.872	0.987	1.151	1.464	1.460	1.462
4.5	1.668	1.663	1.664	0.843	0.952	1.111	1.481	1.479	1.480
6	1.694	1.691	1.692	0.830	0.935	1.092	1.489	1.488	1.489
9	1.711	1.710	1.710	0.821	0.925	1.080	1.493	1.493	1.494
12	1.715	1.714	1.714	0.820	0.923	1.078	1.494	1.494	1.494
∞	1.714	1.714	1.714	0.820	0.922	1.077	1.495	1.495	1.495

Table 2.2: The distributions of the molecular number density n, flow velocity v_1, and temperature T of the total mixture for $M_- = 3$, $m^B/m^A = 0.5$, and $d_m^B/d_m^A = 1$ (cf. Fig. 2.2).

	n/n_-			$v_1/(2kT_-/m^A)^{1/2}$			T/T_-		
X_1/l_-	$\chi_-^B = 0.1$	$\chi_-^B = 0.5$	$\chi_-^B = 0.9$	$\chi_-^B = 0.1$	$\chi_-^B = 0.5$	$\chi_-^B = 0.9$	$\chi_-^B = 0.1$	$\chi_-^B = 0.5$	$\chi_-^B = 0.9$
$-\infty$	1.000	1.000	1.000	2.810	3.162	3.693	1.000	1.000	1.000
-6	1.001	1.001	1.001	2.807	3.158	3.688	1.008	1.009	1.009
-5	1.004	1.004	1.004	2.800	3.150	3.679	1.027	1.028	1.028
-4	1.012	1.013	1.013	2.778	3.125	3.649	1.084	1.087	1.088
-3	1.039	1.042	1.040	2.708	3.048	3.556	1.261	1.262	1.269
-2	1.127	1.134	1.131	2.501	2.821	3.281	1.748	1.732	1.758
-1.5	1.229	1.238	1.234	2.298	2.599	3.016	2.168	2.135	2.174
-1	1.400	1.409	1.406	2.019	2.294	2.654	2.659	2.607	2.656
-0.5	1.662	1.669	1.667	1.700	1.941	2.243	3.101	3.040	3.088
0	2.000	2.000	2.000	1.412	1.614	1.869	3.397	3.342	3.380
0.5	2.344	2.338	2.338	1.203	1.373	1.595	3.552	3.511	3.536
1	2.617	2.610	2.609	1.076	1.223	1.425	3.621	3.595	3.610
1.5	2.794	2.788	2.786	1.007	1.140	1.331	3.650	3.634	3.643
2	2.893	2.890	2.888	0.972	1.097	1.282	3.662	3.652	3.657
3	2.973	2.972	2.971	0.945	1.065	1.244	3.667	3.664	3.665
4	2.993	2.993	2.992	0.939	1.057	1.234	3.667	3.666	3.666
5	2.998	2.998	2.998	0.937	1.055	1.232	3.666	3.666	3.666
∞	3.000	3.000	3.000	0.937	1.054	1.231	3.667	3.667	3.667

Table 2.3: The distributions of the molecular number density n, flow velocity v_1, and temperature T of the total mixture for $M_- = 1.5$, $m^B/m^A = 0.25$, and $d_m^B/d_m^A = 1$ (cf. Fig. 2.3).

	n/n_-			$v_1/(2kT_-/m^A)^{1/2}$			T/T_-		
X_1/l_-	$\chi_-^B = 0.1$	$\chi_-^B = 0.5$	$\chi_-^B = 0.9$	$\chi_-^B = 0.1$	$\chi_-^B = 0.5$	$\chi_-^B = 0.9$	$\chi_-^B = 0.1$	$\chi_-^B = 0.5$	$\chi_-^B = 0.9$
$-\infty$	1.000	1.000	1.000	1.424	1.732	2.402	1.000	1.000	1.000
-12	1.000	1.002	1.001	1.423	1.730	2.400	1.000	1.002	1.001
-10	1.001	1.005	1.003	1.422	1.726	2.396	1.002	1.006	1.004
-8	1.005	1.013	1.010	1.417	1.714	2.382	1.007	1.016	1.013
-6	1.017	1.036	1.030	1.401	1.685	2.342	1.024	1.042	1.039
-4.5	1.043	1.071	1.064	1.369	1.638	2.274	1.059	1.081	1.081
-3	1.100	1.133	1.129	1.300	1.558	2.157	1.129	1.146	1.150
-2	1.165	1.195	1.193	1.229	1.484	2.050	1.197	1.203	1.209
-1	1.253	1.271	1.271	1.143	1.397	1.930	1.273	1.265	1.271
0	1.357	1.357	1.357	1.054	1.307	1.810	1.344	1.324	1.328
1	1.460	1.444	1.441	0.979	1.224	1.702	1.399	1.375	1.376
2.5	1.581	1.554	1.546	0.903	1.130	1.579	1.450	1.430	1.427
4	1.651	1.628	1.618	0.863	1.072	1.501	1.475	1.461	1.457
6	1.693	1.680	1.671	0.841	1.035	1.445	1.488	1.481	1.478
8	1.708	1.702	1.696	0.834	1.019	1.420	1.492	1.489	1.487
10	1.713	1.710	1.707	0.831	1.013	1.409	1.493	1.492	1.491
12	1.715	1.714	1.712	0.831	1.011	1.404	1.493	1.493	1.493
∞	1.714	1.714	1.714	0.831	1.010	1.401	1.495	1.495	1.495

Table 2.4: The distributions of the molecular number density n, flow velocity v_1, and temperature T of the total mixture for $M_- = 2$, $m^B/m^A = 0.25$, and $d_m^B/d_m^A = 1$ (cf. Fig. 2.4).

	n/n_-			$v_1/(2kT_-/m^A)^{1/2}$			T/T_-		
X_1/l_-	$\chi_-^B = 0.1$	$\chi_-^B = 0.5$	$\chi_-^B = 0.9$	$\chi_-^B = 0.1$	$\chi_-^B = 0.5$	$\chi_-^B = 0.9$	$\chi_-^B = 0.1$	$\chi_-^B = 0.5$	$\chi_-^B = 0.9$
$-\infty$	1.000	1.000	1.000	1.898	2.309	3.203	1.000	1.000	1.000
-8	1.001	1.002	1.001	1.897	2.306	3.200	1.001	1.004	1.002
-6	1.004	1.010	1.006	1.892	2.293	3.187	1.010	1.021	1.014
-4	1.026	1.050	1.037	1.857	2.232	3.107	1.065	1.098	1.087
-3	1.065	1.105	1.088	1.794	2.148	2.984	1.159	1.198	1.195
-2	1.157	1.211	1.195	1.658	1.992	2.749	1.347	1.366	1.381
-1.5	1.238	1.291	1.280	1.552	1.882	2.587	1.479	1.474	1.496
-1	1.348	1.392	1.386	1.426	1.753	2.404	1.620	1.588	1.613
-0.5	1.486	1.511	1.510	1.292	1.614	2.218	1.752	1.700	1.720
0	1.643	1.643	1.643	1.167	1.478	2.042	1.860	1.798	1.811
0.5	1.799	1.776	1.773	1.063	1.357	1.889	1.938	1.878	1.882
1	1.938	1.899	1.890	0.985	1.258	1.764	1.991	1.940	1.937
2	2.129	2.088	2.068	0.894	1.127	1.592	2.046	2.015	2.006
3	2.222	2.194	2.174	0.855	1.062	1.498	2.066	2.050	2.042
4	2.261	2.246	2.230	0.840	1.033	1.449	2.073	2.065	2.060
6	2.283	2.279	2.273	0.832	1.014	1.413	2.077	2.075	2.073
8	2.286	2.285	2.283	0.831	1.011	1.404	2.077	2.077	2.076
∞	2.286	2.286	2.286	0.831	1.010	1.401	2.078	2.078	2.078

quantities:

$$\tilde{n}^\alpha(X_1) = \frac{n^\alpha - n_-^\alpha}{n_+^\alpha - n_-^\alpha}, \qquad \tilde{n}(X_1) = \frac{n - n_-}{n_+ - n_-}, \tag{2.70a}$$

$$\tilde{v}_1^\alpha(X_1) = \frac{v_1^\alpha - U_+}{U_- - U_+}, \qquad \tilde{v}_1(X_1) = \frac{v_1 - U_+}{U_- - U_+}, \tag{2.70b}$$

$$\tilde{T}^\alpha(X_1) = \frac{T^\alpha - T_-}{T_+ - T_-}, \qquad \tilde{T}(X_1) = \frac{T - T_-}{T_+ - T_-}, \tag{2.70c}$$

where $\alpha = A, B$. The distributions of these variables are shown in Figs. 2.1–2.4: Fig. 2.1 is for $M_- = 1.5$, $m^B/m^A = 0.5$, and $d_m^B/d_m^A = 1$; Fig. 2.2 for $M_- = 3$, $m^B/m^A = 0.5$, and $d_m^B/d_m^A = 1$; Fig. 2.3 for $M_- = 1.5$, $m^B/m^A = 0.25$, and $d_m^B/d_m^A = 1$; and Fig. 2.4 for $M_- = 2$, $m^B/m^A = 0.25$, and $d_m^B/d_m^A = 1$. The downstream values n_+^α, U_+, T_+, and M_+ are given in the respective captions. The values of $n(X_1)$, $v_1(X_1)$, and $T(X_1)$ of the total mixture, which are obtained from the values at the lattice points by interpolation, are also shown in Tables 2.1–2.4 for the cases corresponding to Figs. 2.1–2.4. The macroscopic variables of the light component (B–component) start to deviate from their upstream uniform values earlier than the corresponding variables of the heavy component (A–component). Then, the number density n^B and flow velocity v_1^B of the light component reach their downstream uniform values n_+^B and U_+ earlier. However, the temperature of the heavy component T^A rises more steeply and exceeds that of the light component T^B at a point inside the shock. Then, the former approaches the downstream equilibrium temperature monotonically or once becomes higher than the downstream temperature and then decreases to it [Figs. 2.2(c) and 2.4(c)]. These features appear more clearly when the mass ratio m^B/m^A is small (Figs. 2.3 and 2.4).

The aforementioned nonmonotonic distribution of the temperature T^A of the heavy component manifests itself when the concentration of the light component χ_-^B is large and the shock wave is not weak. This phenomenon has already been shown by the computations in the early stages[92,96] and has been known as the temperature overshoot.[36,97] As mentioned at the end of Sec. 2.2.B, however, the following T_*^α, which is different from our T^α, is often adopted as the temperature of the individual components in the literature:

$$T_*^\alpha = (3kn^\alpha)^{-1} \int m^\alpha (\xi_i - v_1 \delta_{i1})^2 F^\alpha d\boldsymbol{\xi}. \tag{2.71}$$

The comparison of T_*^α with T^α is given in Fig. 2.5, where $\tilde{T}_*^\alpha$ is defined by

$$\tilde{T}_*^\alpha = (T_*^\alpha - T_-)/(T_+ - T_-). \tag{2.72}$$

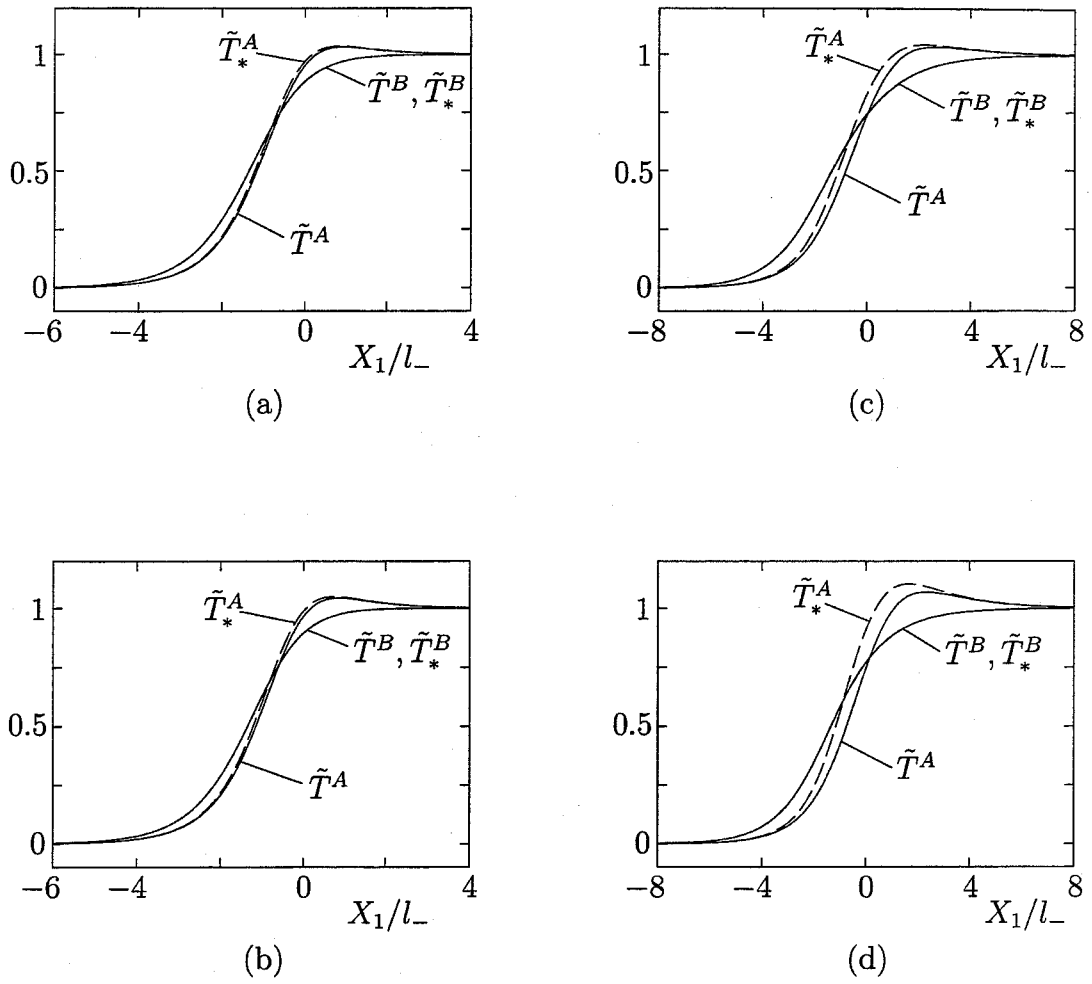

Figure 2.5: Profiles of T^α and T_*^α ($\alpha = A, B$) for $d_m^B/d_m^A = 1$. (a) $M_- = 3$, $m^B/m^A = 0.5$, $\chi_-^B = 0.9$, (b) $M_- = 3$, $m^B/m^A = 0.5$, $\chi_-^B = 0.95$, (c) $M_- = 2$, $m^B/m^A = 0.25$, $\chi_-^B = 0.9$, and (d) $M_- = 2$, $m^B/m^A = 0.25$, $\chi_-^B = 0.95$. Here, the solid line indicates $\tilde{T}^A$ and $\tilde{T}^B$ [see Eq. (2.70c)], and the dashed line $\tilde{T}_*^A$ and $\tilde{T}_*^B$ [see Eq. (2.72)].

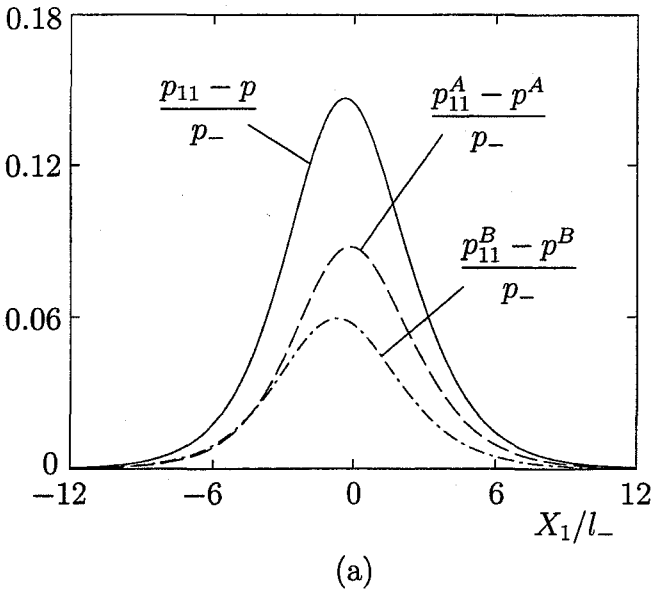

(a)

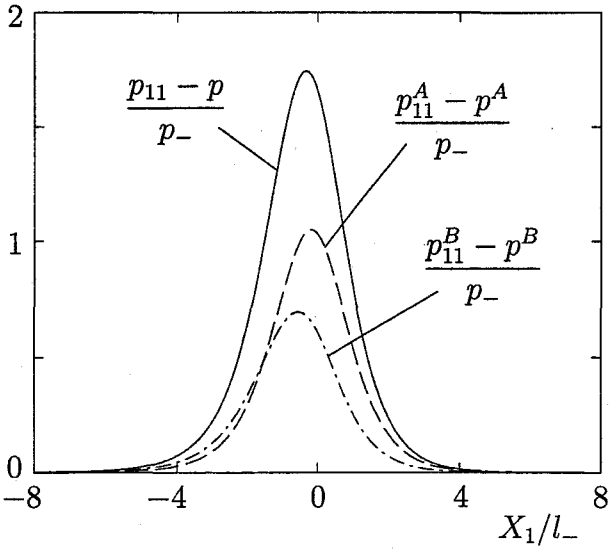

(b)

Figure 2.6: Distribution of the components p_{11}^α and p_{11} of the stress tensors for $\chi_-^B = 0.5$ and $d_m^B/d_m^A = 1$. (a) $M_- = 1.5$, $m^B/m^A = 0.5$, (b) $M_- = 3$, $m^B/m^A = 0.5$, (c) $M_- = 1.5$, $m^B/m^A = 0.25$, and (d) $M_- = 2$, $m^B/m^A = 0.25$. Here, the solid line indicates $(p_{11}-p)/p_-$, the dashed line $(p_{11}^A - p^A)/p_-$, and the dot–dash line $(p_{11}^B - p^B)/p_-$, where $p_- = kn_-T_-$.

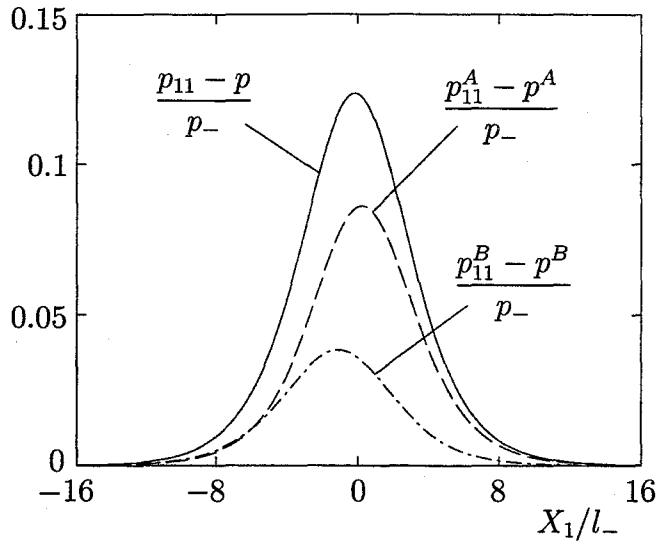

(c)

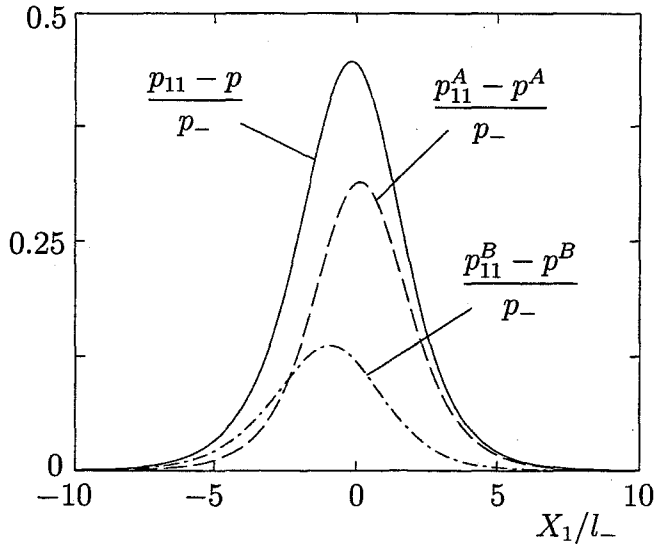

(d)

Figure 2.6: (continued from the previous page)

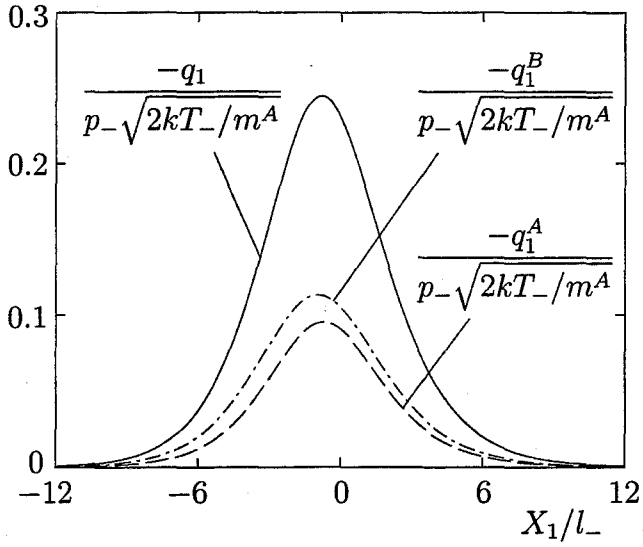

(a)

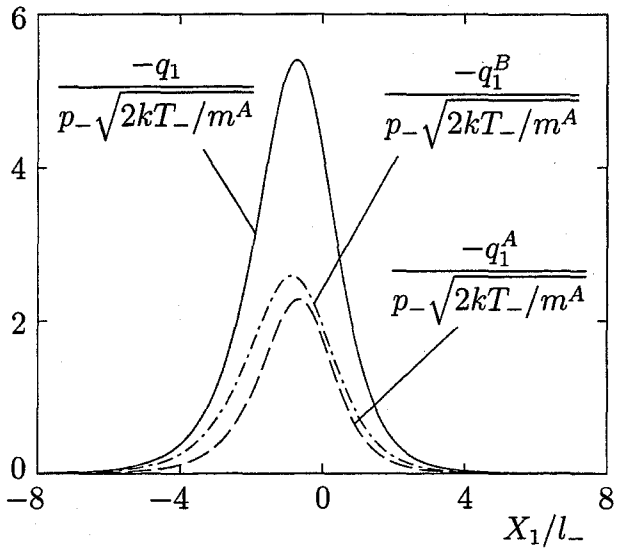

(b)

Figure 2.7: Distribution of the components q_1^α and q_1 of the heat-flow vectors for $\chi_-^B = 0.5$ and $d_m^B/d_m^A = 1$. (a) $M_- = 1.5$, $m^B/m^A = 0.5$, (b) $M_- = 3$, $m^B/m^A = 0.5$, (c) $M_- = 1.5$, $m^B/m^A = 0.25$, and (d) $M_- = 2$, $m^B/m^A = 0.25$. Here, the solid line indicates $-q_1/p_-(2kT_-/m^A)^{1/2}$, the dashed line $-q_1^A/p_-(2kT_-/m^A)^{1/2}$, and the dot–dash line $-q_1^B/p_-(2kT_-/m^A)^{1/2}$, where $p_- = kn_-T_-$.

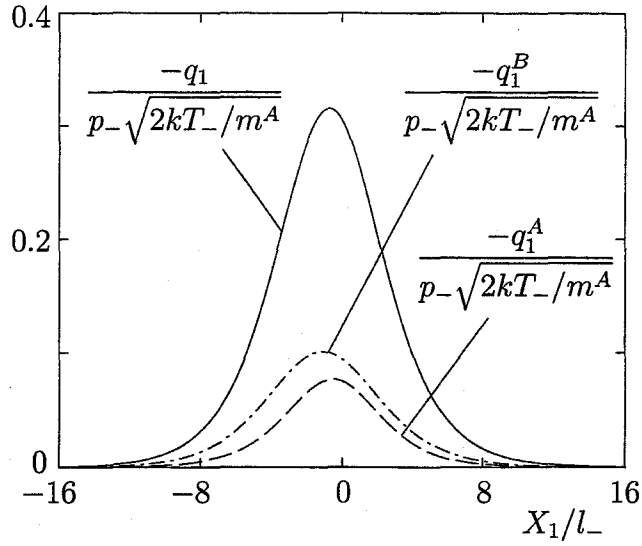

(c)

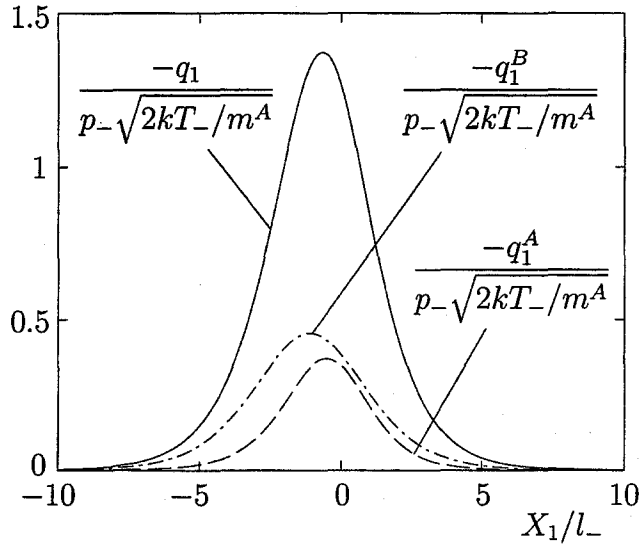

(d)

Figure 2.7: (continued from the previous page)

As is seen from the figure, the overshoot is observed more clearly for T_*^A.

Finally, we show the distributions of $p_{11}^\alpha - p^\alpha$ and $p_{11} - p$ in Fig. 2.6 and those of q_1^α and q_1 in Fig. 2.7.

2.5.B Velocity distribution functions

Next we show the behavior of the velocity distribution functions. Figures 2.8–2.11 show the nondimensional velocity distribution functions $\hat{F}^\alpha(x_1, \zeta_1, \zeta_r)$ $[= (2kT_-/m^A)^{3/2} n_-^{-1} F^\alpha(X_1, \xi_1, \xi_r);\ \xi_r = (\xi_2^2 + \xi_3^2)^{1/2}]$ $(\alpha = A, B)$ as functions of ζ_1 $[= (2kT_-/m^A)^{-1/2}\xi_1]$ and ζ_r $[= (2kT_-/m^A)^{-1/2}\xi_r]$ at several points in the gas for $\chi_-^B = 0.5$ and $d_m^B/d_m^A = 1$; Figs. 2.8 and 2.9 are for $M_- = 3$ and $m^B/m^A = 0.5$, and Figs. 2.10 and 2.11 are for $M_- = 2$ and $m^B/m^A = 0.25$. Here, in consistency with the figures and tables in Sec. 2.5.A, the positions in the gas are indicated by using the dimensional coordinate X_1. The equilibrium distributions at upstream infinity and those at downstream infinity are also shown in the figures. Compared with the upstream Maxwellians, the downstream Maxwellians, the centers of which are shifted (from U_- to U_+ in the dimensional ξ_i space), have lower heights and larger extents because of the increase of the temperature at downstream infinity. The figures clearly demonstrate the transition of the velocity distribution functions from the upstream to the downstream Maxwellians. In Figs. 2.8 and 2.9, corresponding to the peaks of the upstream and downstream Maxwellians, two small lumps are observed both in $\hat{F}^A$ and $\hat{F}^B$ in the transition region [Figs. 2.8(c)–2.8(e) and 2.9(c)–2.9(e)]. As is seen from Eqs. (2.21) and (2.22) and from Figs. 2.8–2.11, smaller mass ratio m^B/m^A makes the height of $\hat{F}^B$ lower and its extent larger for a fixed χ_-^B.

In Figs. 2.12–2.15, we show $\hat{F}^A$ and $\hat{F}^B$ at $\zeta_r = 0.15$ as functions of ζ_1 for several points in the gas. Figs. 2.12–2.15 correspond to the cases of Figs. 2.1–2.4, respectively, but the results for $\chi_-^B = 0.95$ are also included in the former figures.

2.5.C Comparison with the DSMC computation

We have also carried out the computation of the problem by means of the standard DSMC method by Bird[36] for hard-sphere molecules in several cases. We here give some comparisons of the DSMC result with our present computation. Figure 2.16 shows the profiles of the macroscopic variables corresponding to Figs. 2.2(b) and 2.4(b), i.e., $M_- = 3$, $\chi_-^B = 0.5$,

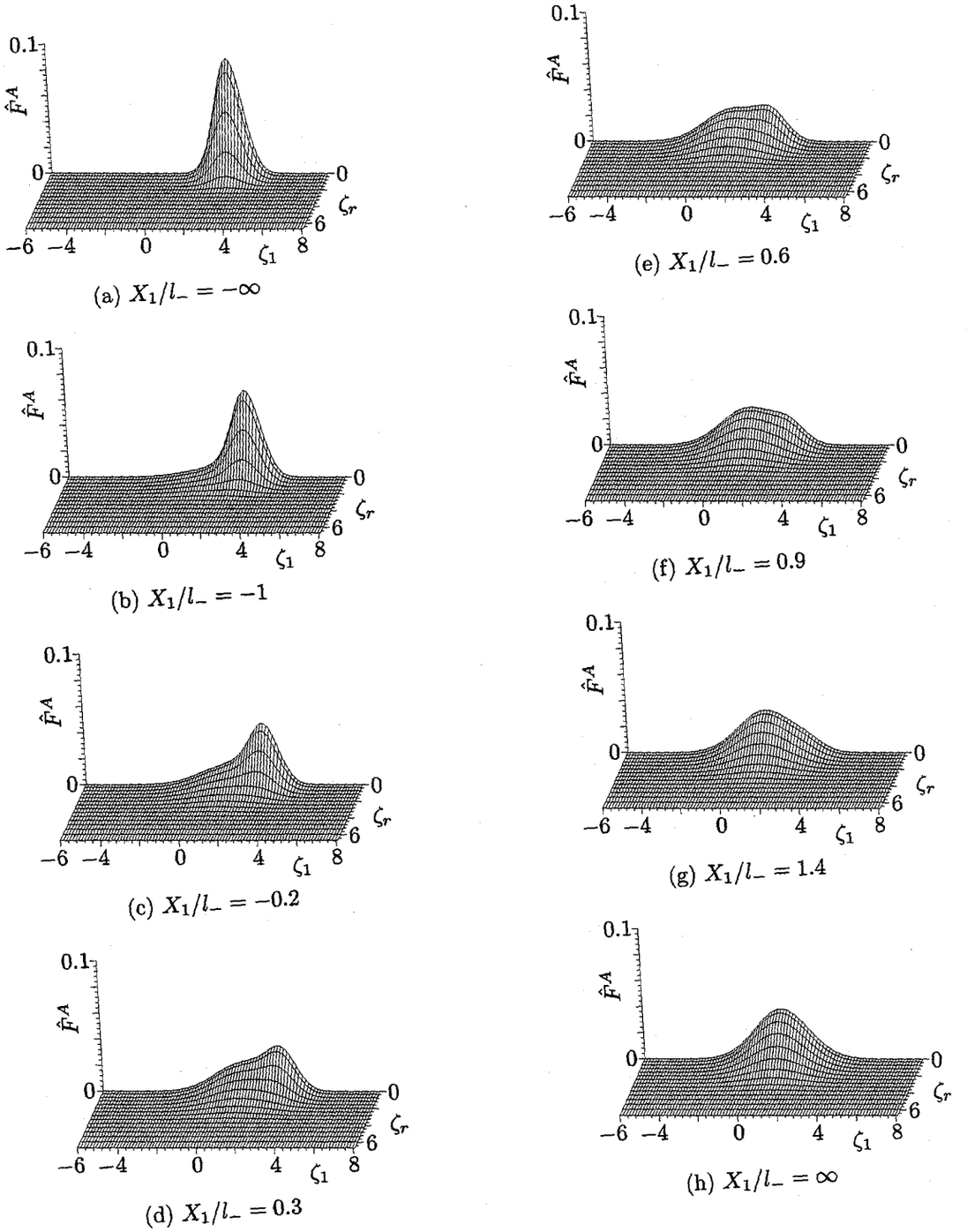

(a) $X_1/l_- = -\infty$

(b) $X_1/l_- = -1$

(c) $X_1/l_- = -0.2$

(d) $X_1/l_- = 0.3$

(e) $X_1/l_- = 0.6$

(f) $X_1/l_- = 0.9$

(g) $X_1/l_- = 1.4$

(h) $X_1/l_- = \infty$

Figure 2.8: Dimensionless velocity distribution function $\hat{F}^A$ at eight points in the gas for $M_- = 3$, $\chi_-^B = 0.5$, $m^B/m^A = 0.5$, and $d_m^B/d_m^A = 1$ [cf. Fig. 2.2(b)]. (a) $X_1/l_- = -\infty$, (b) $X_1/l_- = -1$, (c) $X_1/l_- = -0.2$, (d) $X_1/l_- = 0.3$, (e) $X_1/l_- = 0.6$, (f) $X_1/l_- = 0.9$, (g) $X_1/l_- = 1.4$, and (h) $X_1/l_- = \infty$.

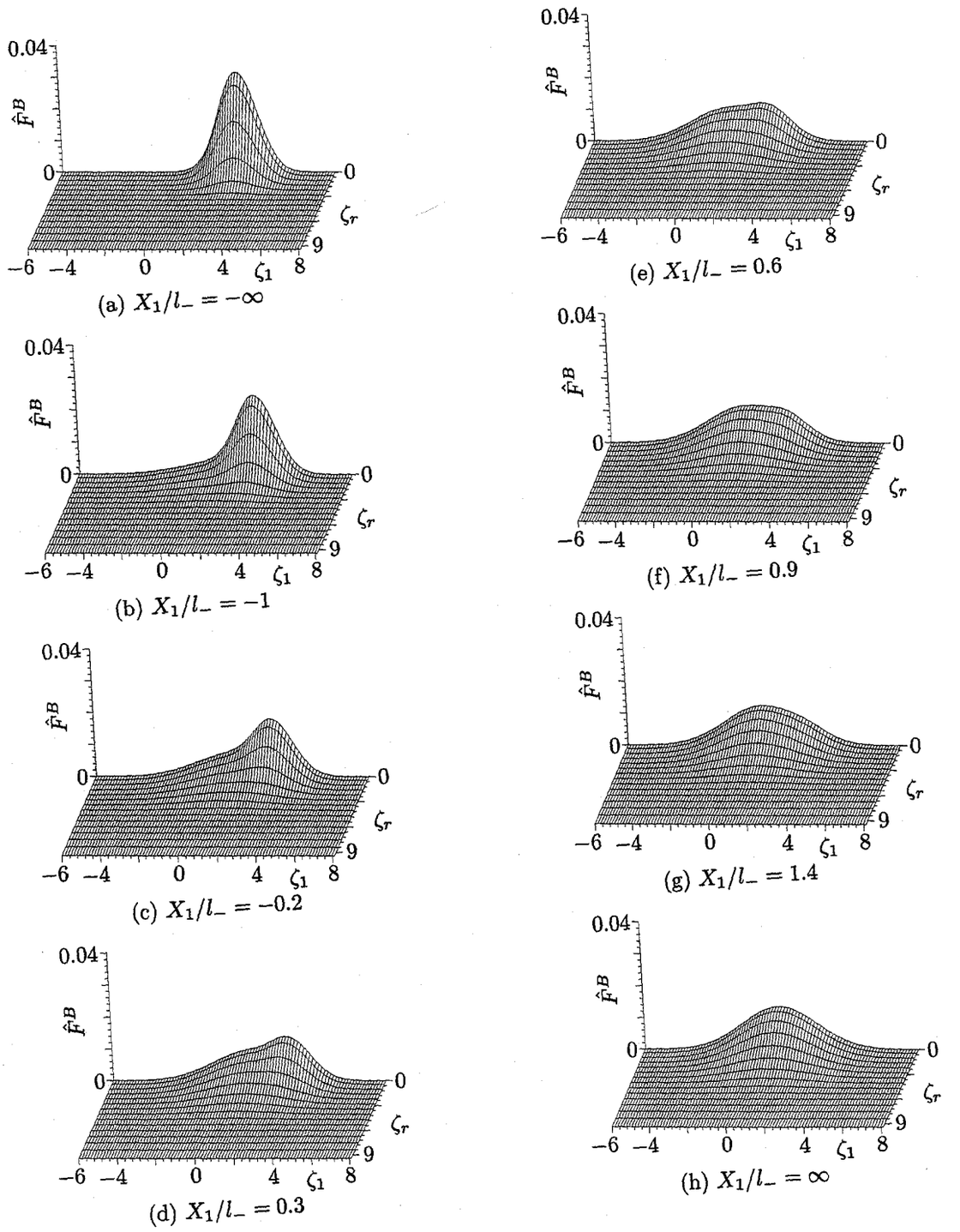

Figure 2.9: Dimensionless velocity distribution function $\hat{F}^B$ at eight points in the gas for $M_- = 3$, $\chi_-^B = 0.5$, $m^B/m^A = 0.5$, and $d_m^B/d_m^A = 1$ [cf. Fig. 2.2(b)]. (a) $X_1/l_- = -\infty$, (b) $X_1/l_- = -1$, (c) $X_1/l_- = -0.2$, (d) $X_1/l_- = 0.3$, (e) $X_1/l_- = 0.6$, (f) $X_1/l_- = 0.9$, (g) $X_1/l_- = 1.4$, and (h) $X_1/l_- = \infty$.

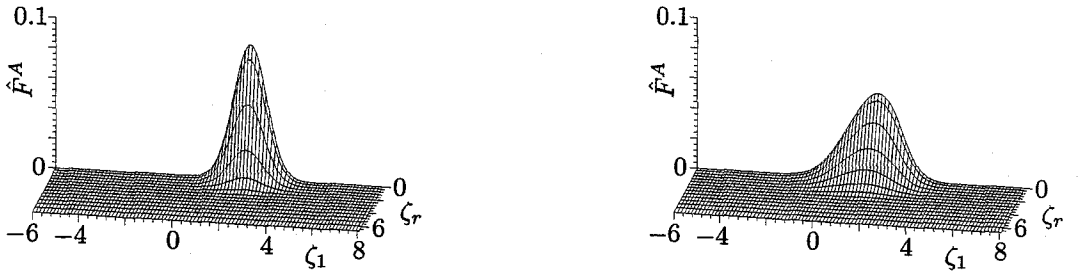

(a) $X_1/l_- = -\infty$

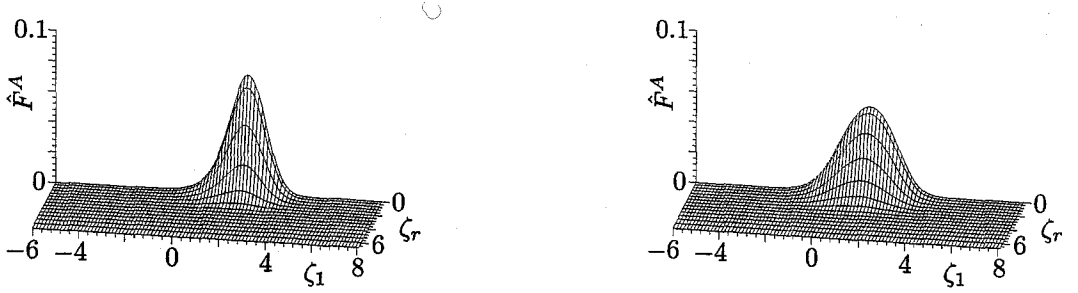

(b) $X_1/l_- = -2$

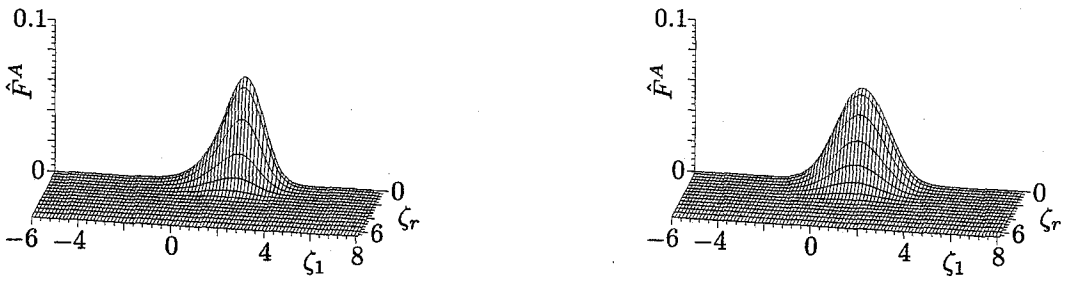

(c) $X_1/l_- = -1$

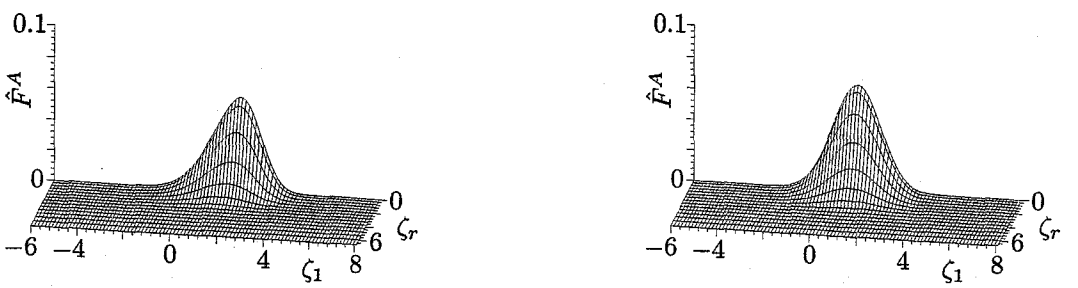

(d) $X_1/l_- = -0.2$

(e) $X_1/l_- = 0.4$

(f) $X_1/l_- = 1$

(g) $X_1/l_- = 2$

(h) $X_1/l_- = \infty$

Figure 2.10: Dimensionless velocity distribution function $\hat{F}^A$ at eight points in the gas for $M_- = 2$, $\chi_-^B = 0.5$, $m^B/m^A = 0.25$, and $d_m^B/d_m^A = 1$ [cf. Fig. 2.4(b)]. (a) $X_1/l_- = -\infty$, (b) $X_1/l_- = -2$, (c) $X_1/l_- = -1$, (d) $X_1/l_- = -0.2$, (e) $X_1/l_- = 0.4$, (f) $X_1/l_- = 1$, (g) $X_1/l_- = 2$, and (h) $X_1/l_- = \infty$.

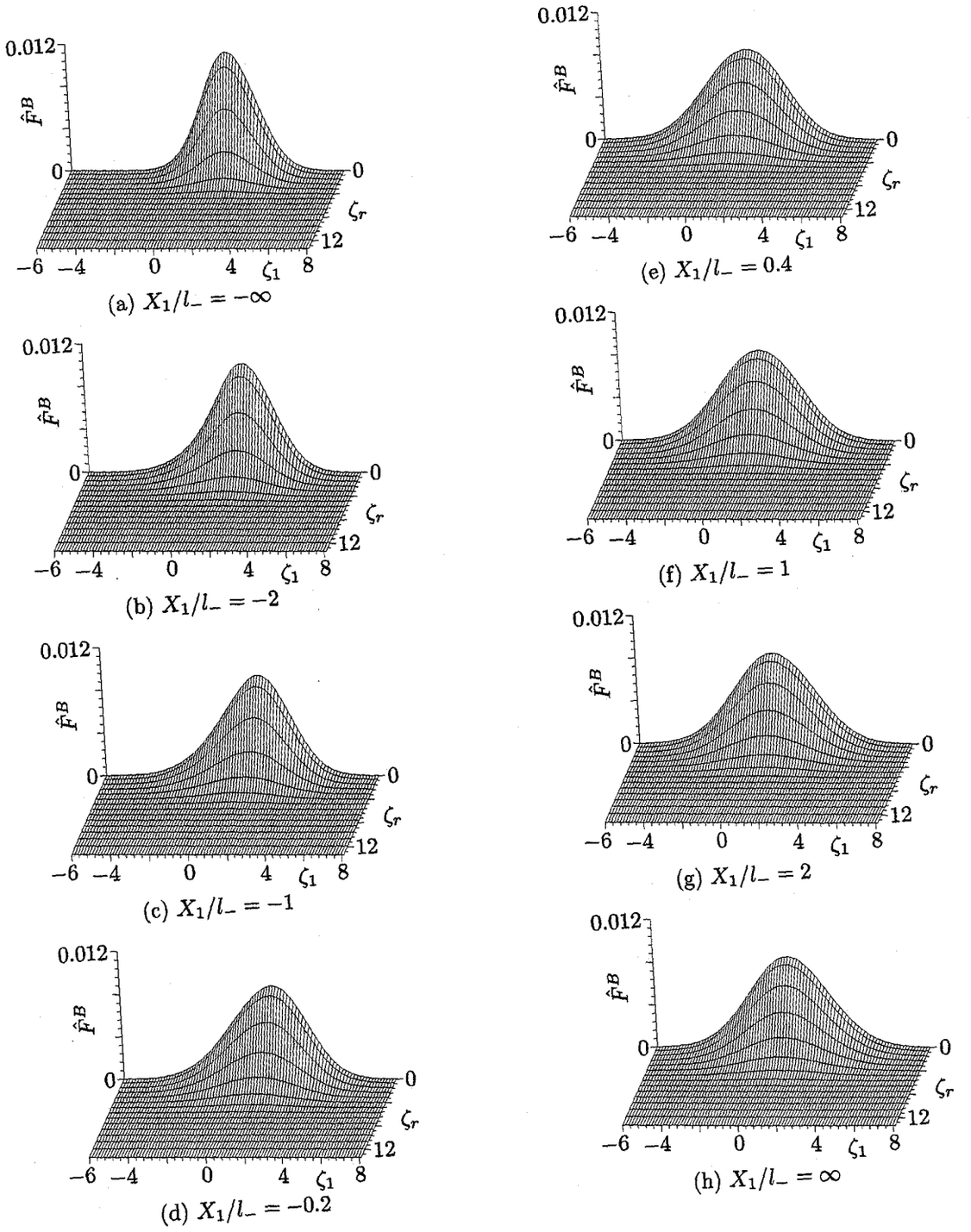

Figure 2.11: Dimensionless velocity distribution function $\hat{F}^B$ at eight points in the gas for $M_- = 2$, $\chi_-^B = 0.5$, $m^B/m^A = 0.25$, and $d_m^B/d_m^A = 1$ [cf. Fig. 2.4(b)]. (a) $X_1/l_- = -\infty$, (b) $X_1/l_- = -2$, (c) $X_1/l_- = -1$, (d) $X_1/l_- = -0.2$, (e) $X_1/l_- = 0.4$, (f) $X_1/l_- = 1$, (g) $X_1/l_- = 2$, and (h) $X_1/l_- = \infty$.

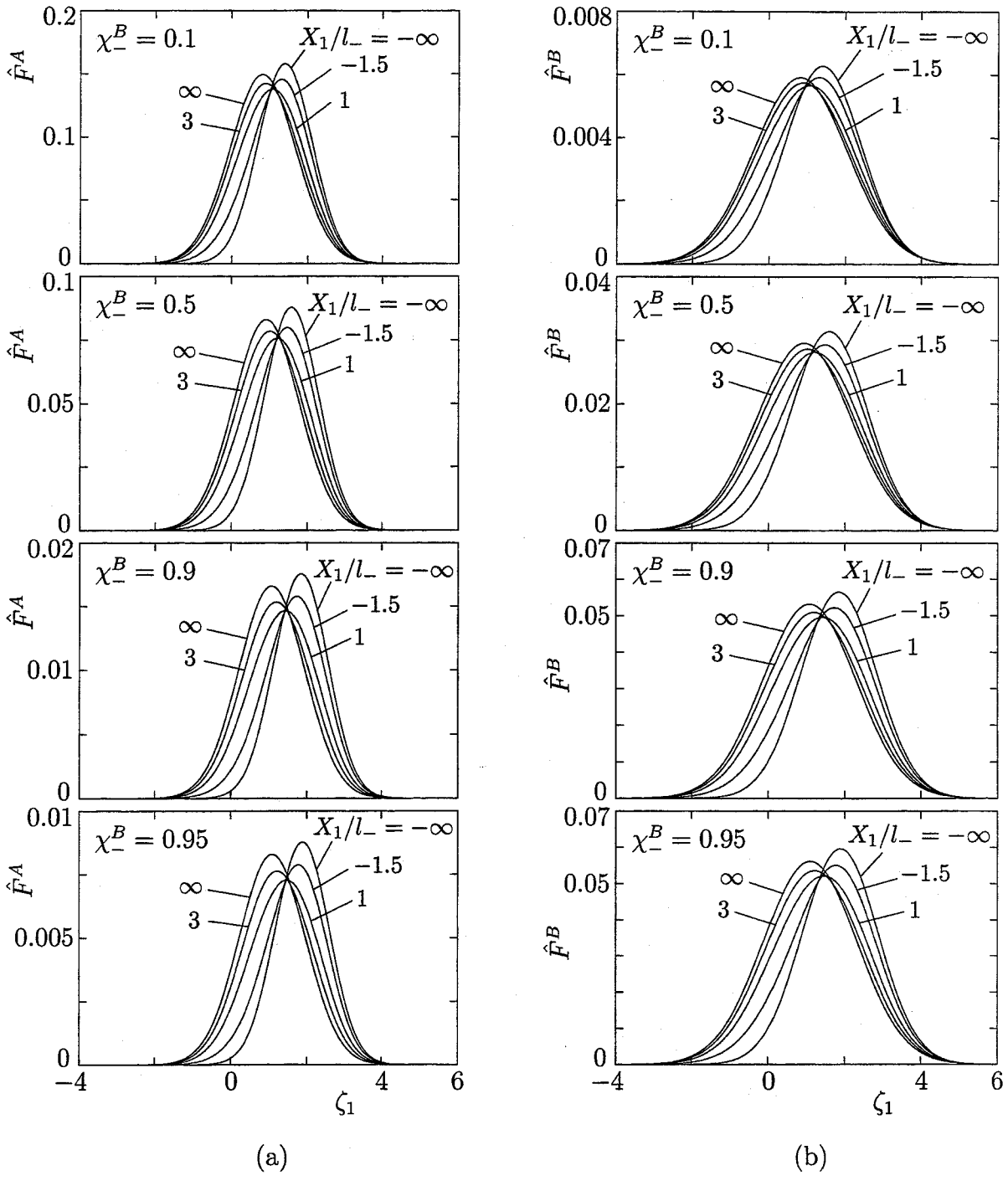

Figure 2.12: Dimensionless velocity distribution functions $\hat{F}^A$ and $\hat{F}^B$ at $\zeta_r = 0.15$ for $M_- = 1.5$, $m^B/m^A = 0.5$, and $d_m^B/d_m^A = 1$. (a) $\hat{F}^A$, (b) $\hat{F}^B$. The $\hat{F}^A$ and $\hat{F}^B$ at several points in the gas are shown for $\chi_-^B = 0.1$, $\chi_-^B = 0.5$, $\chi_-^B = 0.9$, and $\chi_-^B = 0.95$.

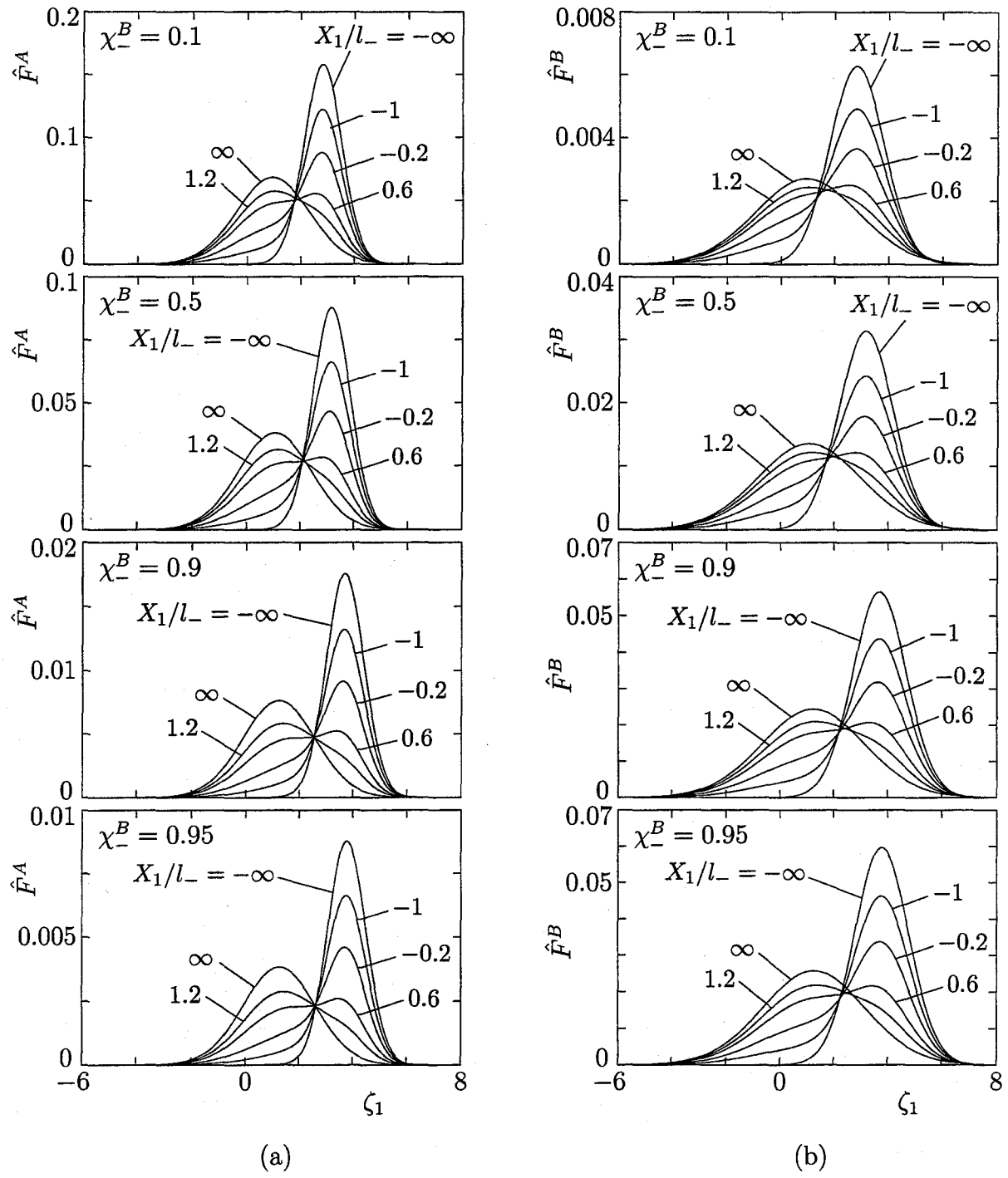

Figure 2.13: Dimensionless velocity distribution functions $\hat{F}^A$ and $\hat{F}^B$ at $\zeta_r = 0.15$ for $M_- = 3$, $m^B/m^A = 0.5$, and $d_m^B/d_m^A = 1$. (a) $\hat{F}^A$, (b) $\hat{F}^B$. See the caption of Fig. 2.12.

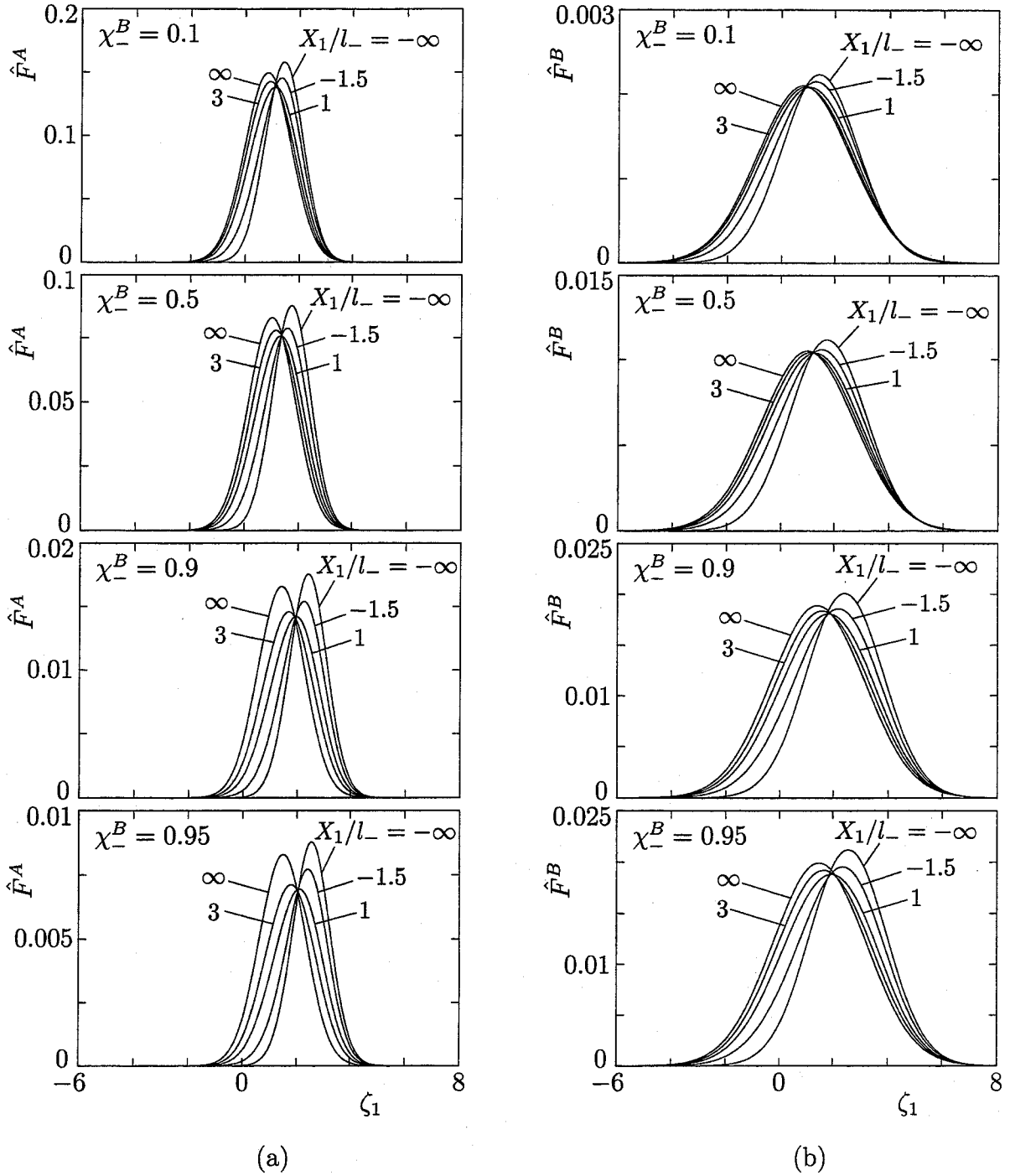

Figure 2.14: Dimensionless velocity distribution functions $\hat{F}^A$ and $\hat{F}^B$ at $\zeta_r = 0.15$ for $M_- = 1.5$, $m^B/m^A = 0.25$, and $d_m^B/d_m^A = 1$. (a) $\hat{F}^A$, (b) $\hat{F}^B$. See the caption of Fig. 2.12.

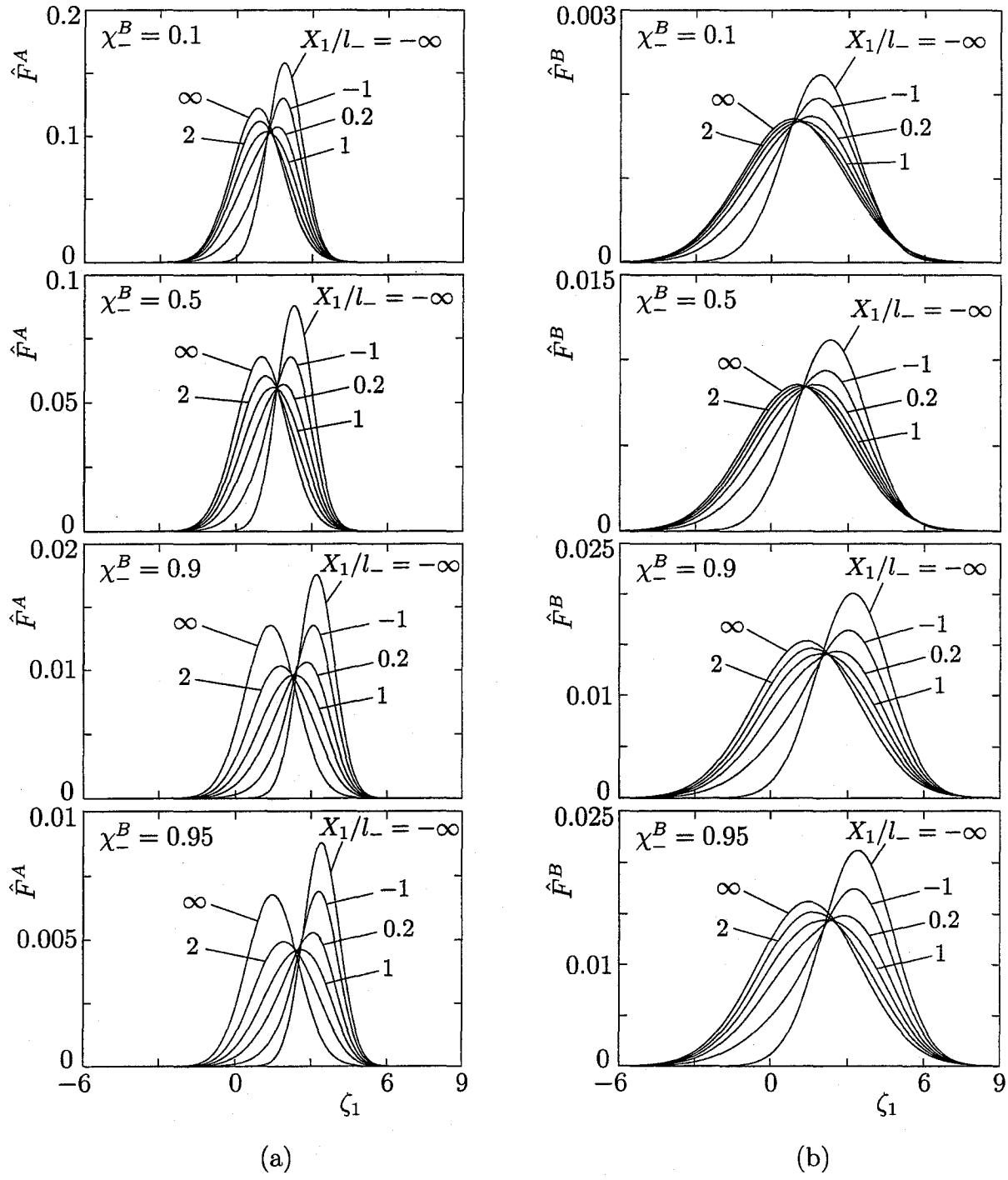

Figure 2.15: Dimensionless velocity distribution functions $\hat{F}^A$ and $\hat{F}^B$ at $\zeta_r = 0.15$ for $M_- = 2$, $m^B/m^A = 0.25$, and $d_m^B/d_m^A = 1$. (a) $\hat{F}^A$, (b) $\hat{F}^B$. See the caption of Fig. 2.12.

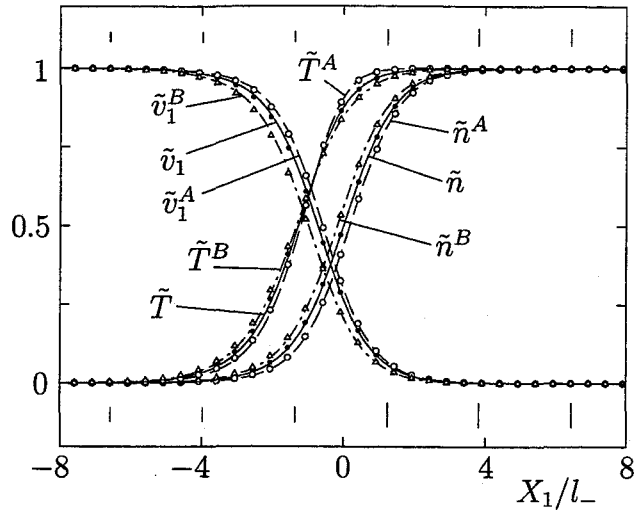

(a)

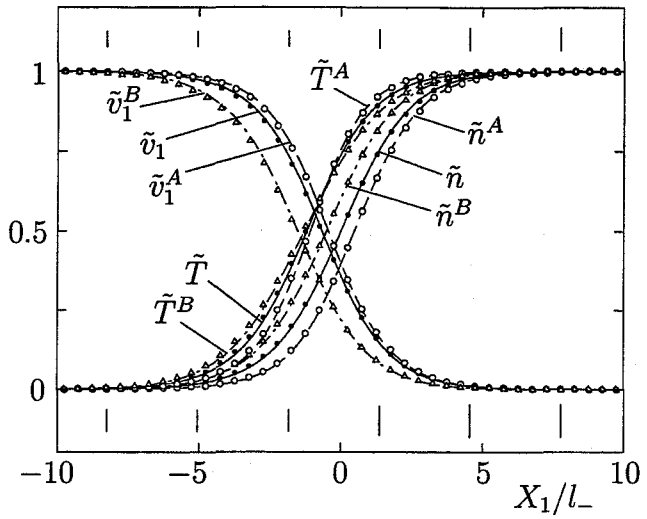

(b)

Figure 2.16: Comparison with the DSMC results: Profiles of molecular number densities, flow velocities, and temperatures. (a) $M_- = 3$, $\chi_-^B = 0.5$, $m^B/m^A = 0.5$, and $d_m^B/d_m^A = 1$ [see Fig. 2.2(b)], (b) $M_- = 2$, $\chi_-^B = 0.5$, $m^B/m^A = 0.25$, and $d_m^B/d_m^A = 1$ [see Fig. 2.4(b)]. The results obtained by the DSMC method are shown by the symbols • ($\tilde{n}$, $\tilde{v}_1$, and $\tilde{T}$), ∘ ($\tilde{n}^A$, $\tilde{v}_1^A$, and $\tilde{T}^A$), and △ ($\tilde{n}^B$, $\tilde{v}_1^B$, and $\tilde{T}^B$). The results by the present finite-difference method are shown by the solid line ($\tilde{n}$, $\tilde{v}_1$, and $\tilde{T}$), dashed line ($\tilde{n}^A$, $\tilde{v}_1^A$, and $\tilde{T}^A$), and dot–dash line ($\tilde{n}^B$, $\tilde{v}_1^B$, and $\tilde{T}^B$). The short vertical bar above the profiles indicates the standard deviation of the samples for $\tilde{n}$ at the corresponding point, and that below the profiles the larger value of the standard deviation for $\tilde{n}^A$ and that for $\tilde{n}^B$.

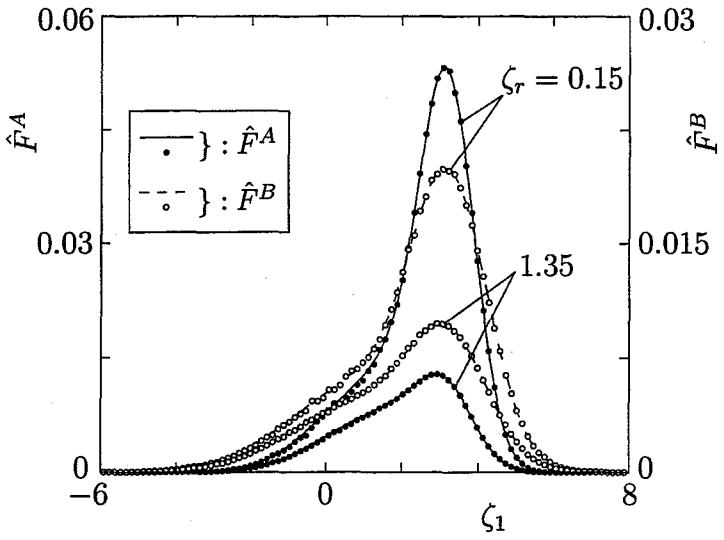

(a) $X_1/l_- = -0.45$

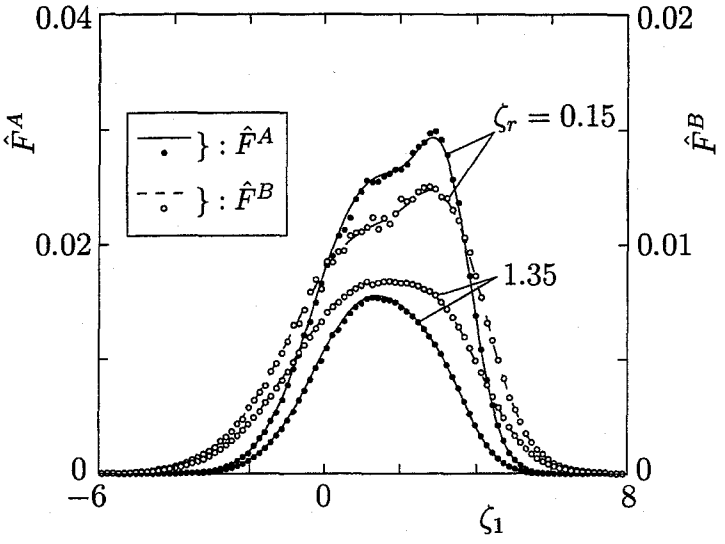

(b) $X_1/l_- = 0.55$

Figure 2.17: Comparison with the DSMC results: Dimensionless velocity distribution functions $\hat{F}^A$ and $\hat{F}^B$ at $\zeta_r = 0.15$ and 1.35 for $M_- = 3$, $\chi_-^B = 0.5$, $m^B/m^A = 0.5$, and $d_m^B/d_m^A = 1$. (a) $X_1/l_- = -0.45$, (b) $X_1/l_- = 0.55$, (c) $X_1/l_- = 1.05$. The results obtained by the DSMC method are shown by • ($\hat{F}^A$) and ∘ ($\hat{F}^B$). The results by the present finite-difference method by solid line ($\hat{F}^A$) and dashed line ($\hat{F}^B$).

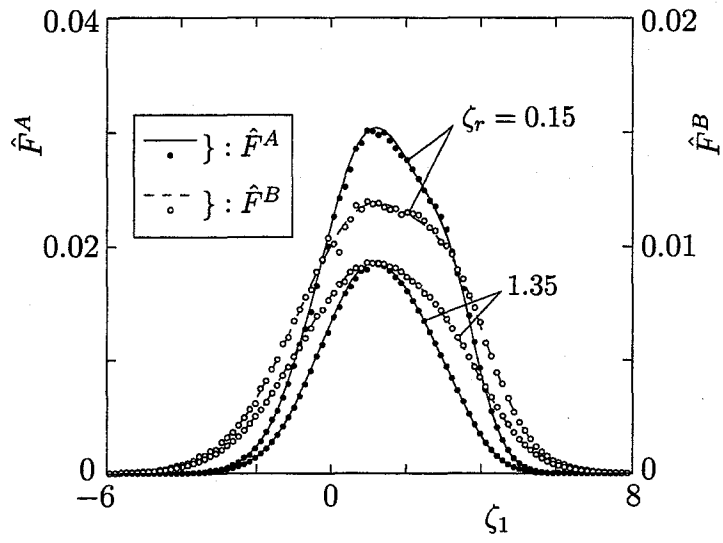

(c) $X_1/l_- = 1.05$

Figure 2.17: (continued from the previous page)

$m^B/m^A = 0.5$, and $d_m^B/d_m^A = 1$ [Fig. 2.16(a)], and $M_- = 2$, $\chi_-^B = 0.5$, $m^B/m^A = 0.25$, and $d_m^B/d_m^A = 1$ [Fig. 2.16(b)]. In the figures, the DSMC results are shown by the symbols •, ○, and △, whereas the results of our present computation by the solid, dashed, and dot-dash lines as in Figs. 2.1–2.4. On the other hand, Fig. 2.17 shows the comparison of the velocity distribution function for the case of Fig. 2.16(a). To be more specific, the dimensionless velocity distribution functions $\hat{F}^A$ and $\hat{F}^B$ at $\zeta_r = 0.15$ and 1.35 are shown as the functions of ζ_1 for three points in the gas. The DSMC results show good agreement with those of the present computation for the velocity distribution function as well as for the macroscopic variables. The data about the present DSMC computation are as follows: 400 cells of a uniform size with length of $0.1l_-$ are used, and the average number of simulation particles per cell is about 250 for each component in Fig. 2.16(a) and about 200 for each component in Fig. 2.16(b); the time step is $0.01t_-$, where $t_- = l_-(2kT_-/m^A)^{-1/2}$; after the steady state has been established, the time average of 10,000 samples with sampling interval $0.5t_-$ is taken, and the average is shown in Figs. 2.16 and 2.17. The short vertical bar above the profiles in Fig. 2.16 indicates the standard deviation of the 10,000 samples for $\tilde{n}$ at the corresponding point, and that below the profiles indicate the larger value of the standard deviation for $\tilde{n}^A$ and that for $\tilde{n}^B$.

2.6 Data for computation and its accuracy

In this section, we use the original X_1 (or x_1) coordinate system, not the rearranged system used in Sec. 2.5, unless the contrary is stated.

Table 2.5: Lattice systems in the molecular velocity space.

	N_m	N_p	h	H	$\zeta_1^{(-N_m)}$	$\zeta_1^{(N_p)}$	$\zeta_r^{\alpha(1)}$ or $\zeta_r^{(1)}$	$\zeta_r^{\alpha(H)}$ or $\zeta_r^{(H)}$
(M1)	26	34	0.25	14	−6.5	8.5	0.3158	6.6608
(M2)	44	56	0.15	14	−6.6	8.4	0.3158	6.6608
(M3)	60	73	0.15	14	−9.0	10.95	$0.3158/\sqrt{\hat{m}^\alpha}$	$6.6608/\sqrt{\hat{m}^\alpha}$
(M4)	66	81	0.15	14	−9.9	12.15	$0.3158/\sqrt{\hat{m}^\alpha}$	$6.6608/\sqrt{\hat{m}^\alpha}$
(M5)	44	56	0.15	18	−6.6	8.4	0.2796	7.6870
(M6)	60	73	0.15	18	−9.0	10.95	0.2796	7.6870
(M7)	44	56	0.15	14	−6.6	8.4	$0.3158/\sqrt{\hat{m}^\alpha}$	$6.6608/\sqrt{\hat{m}^\alpha}$
(M8)	60	73	0.15	14	−9.0	10.95	$0.3158/\sqrt{\hat{m}^\alpha}$	$6.6608/\sqrt{\hat{m}^\alpha}$

2.6.A Lattice systems

We first summarize the lattice systems that are used in the actual computation. For the molecular velocity space, the four lattice systems ($\overline{\text{M1}}$), ($\overline{\text{M2}}$), (M3), and (M4) given in Table 2.5 are used [see Eqs. (2.52) and (2.55)]. The reason why the bar is put on M1 and M2 is that, in ($\overline{\text{M1}}$) and ($\overline{\text{M2}}$) systems, ζ_r–lattice points slightly different from those explained in Sec. 2.4.B [cf. Eq. (2.52)] are used. That is, we assume the form

$$\hat{F}_i^{\alpha(n)}(\zeta_1^{\alpha(j)}, \zeta_r) = \exp\Big(-\frac{\zeta_r^2}{2}\Big) \sum_{m=0}^{H-1} a_{ijm}^{\alpha(n)} L_m(\zeta_r^2), \tag{2.73}$$

instead of Eq. (2.44) and use

$$\zeta_r^{\alpha(k)} = \zeta_r^{(k)} = \sqrt{y_k}, \qquad (k = 1,\ ...,\ H), \tag{2.74}$$

instead of Eq. (2.52). As a result, the forms of numerical kernels $\Omega_{pqab}^{\beta\alpha 0k}$ and $\Lambda_{pa}^{\beta\alpha 0k}$ undergo slight changes (In fact, $\Omega_{pqab}^{AA0k} = \Omega_{pqab}^{BB0k}$ holds and $\Lambda_{pa}^{\beta\alpha 0k}$ becomes independent of the labels α and β, which are the advantage of this choice). Since the changes are rather straightforward, we omit them here. This choice works when the molecular masses m^A and m^B are not very different ($0.5 \lesssim m^B/m^A$ when $m^B < m^A$). The edges of the domain in ζ_1, i.e., $\zeta_1^{(-N_m)}$ and $\zeta_1^{(N_p)}$, and the first and last lattice points in ζ_r, i.e., $\zeta_r^{\alpha(1)}$ and $\zeta_r^{\alpha(H)}$ (or $\zeta_r^{(1)}$ and $\zeta_r^{(H)}$), for the systems ($\overline{\text{M1}}$), ($\overline{\text{M2}}$), (M3), and (M4) are also shown in Table 2.5. The computer memory required for the numerical kernels corresponding to these four systems is: ($\overline{\text{M1}}$): 263MB, ($\overline{\text{M2}}$): 720MB, and (M3): 1.4GB, and (M4): 1.7GB.

The lattice system for the space coordinate x_1 is defined by

$$x_1^{(i)} = f_\delta \bar{x}_1^{(i)}, \qquad (i = -N_D, ..., 0, ..., N_D), \tag{2.75}$$

where

$$f_\delta = \frac{\sqrt{\frac{m^B}{m^A}}\chi_-^A + \chi_-^B}{\sqrt{\frac{m^B}{m^A}}(\chi_-^A)^2 + 2\Big(\frac{d_m^{BA}}{d_m^A}\Big)^2\sqrt{\frac{m^B+m^A}{2m^A}}\chi_-^A\chi_-^B + \Big(\frac{d_m^B}{d_m^A}\Big)^2(\chi_-^B)^2}, \tag{2.76a}$$

$$\bar{x}_1^{(i)} = \frac{50d'}{N_D}i + \left[\text{erf}(3.5) - \text{erf}\left(3.5 \times \frac{N_D - i}{N_D}\right)\right](D' - 50d'), \qquad (i = 0, ..., N_D - 1), \tag{2.76b}$$

$$\bar{x}_1^{(N_D)} = D', \tag{2.76c}$$

$$\bar{x}_1^{(-i)} = -\bar{x}_1^{(i)}, \tag{2.76d}$$

and $\mathrm{erf}(x)$ is the error function defined by Eq. (B11) (Appendix B). Equation (2.75) means that the X_1 coordinate is rescaled by $f_\delta l_-$ and then the lattice points are set in the rescaled coordinate $X_1/f_\delta l_-$. This is because in the $X_1/f_\delta l_-$ coordinate, the shock thickness is less sensitive to the change in the parameters m^B/m^A, d_m^B/d_m^A, and χ_-^B than in the X_1/l_- (or x_1) coordinate. However, f_δ is almost unity ($0.973 < f_\delta < 1$) for the values of the parameters chosen in our computation. We use the following two systems for the computation:

(S1): $D' = 10\sqrt{\pi}$ $(= 17.7245)$, $N_D = 25$, $d' = 0.05\sqrt{\pi}$ $(= 0.088623)$,

(S2): $D' = 10\sqrt{\pi}$, $N_D = 50$, $d' = 0.05\sqrt{\pi}$.

The lattice interval is minimum at $x_1 = 0$ $[x_1^{(1)} - x_1^{(0)} = 0.1773 f_\delta$ for (S1) and $0.08863 f_\delta$ for (S2)] and increases, with the increase of $|x_1|$, to the maximum value at the edge of the domain, $|x_1| = 17.7245 f_\delta$ $[x_1^{(N_D)} - x_1^{(N_D-1)} = 2.264 f_\delta$ for (S1) and $1.137 f_\delta$ for (S2)].

The data for ($M_- = 1.5$, $m^B/m^A = 0.5$) in Sec. 2.5 are based on the ($\overline{\mathrm{M2}}$; S2) system, those for ($M_- = 3$, $m^B/m^A = 0.5$) are based on the (M3; S2) system, and those for $m^B/m^A = 0.25$ are based on the (M4; S2) system. The ($\overline{\mathrm{M1}}$) and (S1) systems are used for accuracy test. The computing time for one iteration [the steps (i)–(iv) in Sec. 2.2.A] in a parallel computation using ten CPU's on a VPP800 computer (see the last paragraph of Sec. 2.7) is as follows: 9 sec for ($\overline{\mathrm{M1}}$; S2) system; 46 sec for ($\overline{\mathrm{M2}}$; S2) system; 99 sec for (M3; S2) system; and 142 sec for (M4; S2) system.

2.6.B Criterion for convergence

In order to save the number of iterations, we use the following initial distributions $\hat{F}_{ijk}^{\alpha(0)}$. For $\chi_-^B = 0.5$, we first compute the corresponding numerical solution of the model Boltzmann equation proposed by Garzó *et al.*[62] by a finite-difference method and use the solution as $\hat{F}_{ijk}^{\alpha(0)}$. Then we carry out the iteration process described in Sec. 2.4.A to obtain the desired solution for $\chi_-^B = 0.5$. For other values of χ_-^B, we use $\hat{F}_{ijk}^{\alpha(0)}$ obtained by suitable modification of the solution (of the Boltzmann equation) for $\chi_-^B = 0.5$.

In the actual computation, however, even after the profiles of the macroscopic variables seem to have converged, the profiles move by a small but almost constant value in each iteration. This is due to the fact that the Rankine–Hugoniot relation, Eq. (2.1), is not satisfied exactly because of the computational error. Therefore, we set the following criterion for the convergence. Let us denote by $\hat{n}^{(m)}(x_1)$ the dimensionless number density $n(X_1)/n_-$

of the total mixture corresponding to the solution $\hat{F}_{ijk}^{\alpha(m)}$ at the mth step of iteration, and let us denote by S_m the x_1 coordinate at which $\hat{n}^{(m)}(x_1)$ takes the value $(1+n_+/n_-)/2$ [i.e., $n(\text{at } m\text{th iteration}) = (n_- + n_+)/2$ at $x_1 = S_m$]. That is, $x_1 = S_m$ is the *center* of the shock wave at the mth iteration. Now we introduce the shift of the *center* in 20 steps, i.e.,

$$(\Delta S)_{20l} = S_{20l} - S_{20(l-1)}, \qquad (l = 1, 2, ...). \tag{2.77}$$

Then, we examine the change of the profile of the number density relative to the *center* in the 20 steps, i.e., we introduce the following quantity:

$$(\Delta\hat{n})_{20l} = \max_i \Big\{ |\hat{n}^{(20l)}(x_1^{(i)} + (\Delta S)_{20l}) - \hat{n}^{(20(l-1))}(x_1^{(i)})| \\ \text{at } i = 0,\ \pm 5,\ \pm 10 \ldots \quad (|i| < N_D) \Big\}. \tag{2.78}$$

Here, the values $\hat{n}^{(20l)}(x_1^{(i)} + (\Delta S)_{20l})$ are computed by means of interpolation. When the condition $(\Delta\hat{n})_{20l} < 10^{-5}$ is satisfied, we stop the iteration judging that the solution has converged. Then, we regard the result of the last iteration as the desired steady solution. The necessary iteration steps n_*, the shift of the *center* $(\Delta S)_{n_*}$ in the final 20 steps, and the difference $|(\Delta S)_{n_*} - (\Delta S)_{n_*-20}|$ between the shift in the final 20 steps and that in the preceding 20 steps in the cases of Figs. 2.1(b), 2.2(b), 2.3(b), and 2.4(b) are as follows:

$n_* = 280,\ (\Delta S)_{n_*} = 2.80 \times 10^{-3},\ |(\Delta S)_{n_*} - (\Delta S)_{n_*-20}| = 4.83 \times 10^{-5}$ for Fig. 2.1(b);

$n_* = 320,\ (\Delta S)_{n_*} = 7.34 \times 10^{-4},\ |(\Delta S)_{n_*} - (\Delta S)_{n_*-20}| = 1.90 \times 10^{-6}$ for Fig. 2.2(b);

$n_* = 360,\ (\Delta S)_{n_*} = 8.50 \times 10^{-3},\ |(\Delta S)_{n_*} - (\Delta S)_{n_*-20}| = 7.36 \times 10^{-5}$ for Fig. 2.3(b);

$n_* = 480,\ (\Delta S)_{n_*} = 2.70 \times 10^{-3},\ |(\Delta S)_{n_*} - (\Delta S)_{n_*-20}| = 1.45 \times 10^{-5}$ for Fig. 2.4(b).

The initial distributions $\hat{F}_{ijk}^{\alpha(0)}$ are arranged in such a way that the *center* of the shock at the final stage of iteration stays in the vicinity of the origin of the original coordinate system. As a result, if we denote by $x_1 = S_{n_*}$ the position of the *center* at the final stage, $|S_{n_*}|$ is less than 0.6 for all the cases in Sec. 2.5.

2.6.C Accuracy of computation

The accuracy of computation can be estimated by comparing the macroscopic quantities for the different lattice systems. Let $\sigma(\mathrm{M}, \mathrm{S})$ represent n, v_1, and T obtained by the use of lattice systems (M, S) (M= $\overline{\mathrm{M1}}$, $\overline{\mathrm{M2}}$, and M3, and S=S1 and S2). We introduce the

maximum difference of the two results based on two different lattice systems (M, S) and (M′, S′) by

$$\mathsf{D}(\mathrm{M}',\mathrm{S}';\mathrm{M},\mathrm{S}) = \max_{\sigma=n,v_1,T}\left(\max_{X_1}\frac{|\sigma(\mathrm{M}',\mathrm{S}')-\sigma(\mathrm{M},\mathrm{S})|}{\sigma(\mathrm{M},\mathrm{S})}\right), \tag{2.79}$$

where $|\sigma(\mathrm{M}',\mathrm{S}')-\sigma(\mathrm{M},\mathrm{S})|/\sigma(\mathrm{M},\mathrm{S})$ is evaluated at about 2,000 uniformly distributed points in the rearranged X_1 coordinate system (see the first sentence of Sec. 2.5) by means of interpolation, and the maximum with respect to X_1 is taken over these points. The values of D for some test computations for $m^B/m^A = 0.5$, $d_m^B/d_m^A = 1$, and $M_- = 1.5$ or 2 are given as follows.

$$\mathsf{D}(\overline{\mathrm{M1}},\mathrm{S2};\overline{\mathrm{M2}},\mathrm{S2}) = \begin{cases} 8.09\times10^{-4}, & (M_- = 1.5,\ \chi_-^B = 0.95),\\ 1.97\times10^{-3}, & (M_- = 2,\ \chi_-^B = 0.1),\\ 1.23\times10^{-3}, & (M_- = 2,\ \chi_-^B = 0.5),\\ 6.57\times10^{-4}, & (M_- = 2,\ \chi_-^B = 0.9),\\ 5.78\times10^{-4}, & (M_- = 2,\ \chi_-^B = 0.95), \end{cases}$$

$$\mathsf{D}(\overline{\mathrm{M1}},\mathrm{S2};\mathrm{M3},\mathrm{S2}) = 1.30\times10^{-3}, \qquad (M_- = 2,\ \chi_-^B = 0.5),$$

$$\mathsf{D}(\overline{\mathrm{M2}},\mathrm{S2};\mathrm{M3},\mathrm{S2}) = 4.17\times10^{-4}, \qquad (M_- = 2,\ \chi_-^B = 0.5),$$

$$\mathsf{D}(\overline{\mathrm{M2}},\mathrm{S1};\overline{\mathrm{M2}},\mathrm{S2}) = 1.46\times10^{-3}, \qquad (M_- = 2,\ \chi_-^B = 0.5).$$

Another measure of accuracy is given by the conservation laws. That is, by integrating Eq. (2.5) ($\alpha = A, B$), $\sum_{\alpha=A,B}[m^\alpha\xi_1 \times$ Eq. (2.5)], and $\sum_{\alpha=A,B}[m^\alpha\xi_j^2 \times$ Eq. (2.5)] over the whole space of ξ_i respectively and by taking into account the fact that the gas is in the equilibrium distribution (2.10) (for all ξ_1) at upstream infinity, we have

$$J_M^\alpha = \int \xi_1 F^\alpha d\boldsymbol{\xi} = n_-^\alpha U_-, \tag{2.80a}$$

$$J_P = \int \sum_{\alpha=A,B} m^\alpha \xi_1^2 F^\alpha d\boldsymbol{\xi} = kn_-T_- + \rho_- U_-^2, \tag{2.80b}$$

$$J_E = \frac{1}{2}\int \sum_{\alpha=A,B} m^\alpha \xi_1 \xi_j^2 F^\alpha d\boldsymbol{\xi} = \frac{1}{2}U_-(5kn_-T_- + \rho_- U_-^2), \tag{2.80c}$$

where $\rho_- = \sum_{\alpha=A,B} m^\alpha n_-^\alpha$. Here, J_M^α, J_P, and J_E are, respectively, the flux in the X_1 direction of the particle of the α-component, that of the X_1 component of the total momentum, and that of the total energy. The J_M^α, J_P, and J_E do not depend on X_1 theoretically. But, in the actual computation, the values of these fluxes deviate slightly from the RHS's of Eq. (2.80) and vary with X_1 because of the computational error. This deviation provides a measure of accuracy of the computation. Let us denote by $(J_M^\alpha)_c$, $(J_P)_c$, and $(J_E)_c$ the

fluxes J_M^α, J_P, and J_E obtained by the numerical computation and by $(J_M^\alpha)_e$, $(J_P)_e$, and $(J_E)_e$ their exact values [i.e., RHS's of Eq. (2.80)]. Then, we introduce the following relative difference:

$$\mathsf{E} = \max_{J=J_M^\alpha, J_P, J_E} \left(\max_{X_1} |[(J)_c - (J)_e]/(J)_e| \right), \tag{2.81}$$

where the maximum with respect to X_1 is taken over the original lattice points. For the results shown in Sec. 2.5, we give the estimate of E here. For $m^B/m^A = 0.5$ and $d_m^B/d_m^A = 1$ (cf. Figs. 2.1, 2.2, 2.12, and 2.13),

$$\mathsf{E} \le \begin{cases} 4.55 \times 10^{-4}, & (M_- = 1.5,\ \chi_-^B = 0.1), \\ 1.77 \times 10^{-4}, & (M_- = 1.5,\ \chi_-^B = 0.5,\ 0.9,\ 0.95), \\ 2.12 \times 10^{-4}, & (M_- = 3,\ \chi_-^B = 0.1,\ 0.5), \\ 3.51 \times 10^{-4}, & (M_- = 3,\ \chi_-^B = 0.9,\ 0.95), \end{cases}$$

and for $m^B/m^A = 0.25$ and $d_m^B/d_m^A = 1$ (cf. Figs. 2.3, 2.4, 2.14, and 2.15),

$$\mathsf{E} \le \begin{cases} 5.71 \times 10^{-4}, & (M_- = 1.5,\ \chi_-^B = 0.1,\ 0.5), \\ 3.72 \times 10^{-4}, & (M_- = 1.5,\ \chi_-^B = 0.9,\ 0.95), \\ 3.19 \times 10^{-4}, & (M_- = 2,\ \chi_-^B = 0.1,\ 0.5,\ 0.9,\ 0.95). \end{cases}$$

Next, we give some information about the values of the velocity distribution functions at (or near) the edges of the range of computation in X_1 and ξ_1 for the results given in Sec. 2.5. For convenience, we use the nondimensional form in the following discussions. Let $\hat{F}_-^\alpha(\zeta_1, \zeta_r)$ and $\hat{F}_+^\alpha(\zeta_1, \zeta_r)$ denote the upstream Maxwellian [Eq. (2.21) for all ζ_1] and the downstream one [Eq. (2.22) for all ζ_1], respectively. Then, the maxima of $\hat{F}_-^\alpha$ and $\hat{F}_+^\alpha$ are, respectively, $(\hat{F}_-^\alpha)_{\max} = \pi^{-3/2}(\hat{m}^\alpha)^{3/2}\chi_-^\alpha$ and $(\hat{F}_+^\alpha)_{\max} = \pi^{-3/2}(\hat{m}^\alpha)^{3/2}\chi_-^\alpha(n_+^\alpha/n_-^\alpha)(T_+/T_-)^{-3/2}$. At the edge of the computational range in ζ_1, i.e., at $\zeta_1 = \zeta_1^{(-N_m)}$ and $\zeta_1^{(N_p)}$ (cf. Table 2.5), the value of $\hat{F}^\alpha$ are

$$\hat{F}^A/(\hat{F}_-^A)_{\max} \le \begin{cases} 1.95 \times 10^{-12}, & (M_- = 1.5,\ 3,\ m^B/m^A = 0.5), \\ 4.35 \times 10^{-19}, & (M_- = 1.5,\ 2,\ m^B/m^A = 0.25), \end{cases}$$

$$\hat{F}^B/(\hat{F}_-^B)_{\max} \le \begin{cases} 1.62 \times 10^{-8}, & (M_- = 1.5,\ m^B/m^A = 0.5,\ 0.25), \\ 1.10 \times 10^{-6}, & (M_- = 3,\ m^B/m^A = 0.5), \\ 8.08 \times 10^{-7}, & (M_- = 2,\ m^B/m^A = 0.25). \end{cases}$$

It is noted that the range in ζ_r is not truncated in our computation. On the other hand, the computational range in x_1 is $|x_1| \le D$ $(= 17.7245 f_\delta)$ (cf. Sec. 2.6.A). Let us introduce the following maximum difference between $\hat{F}^\alpha$ and $\hat{F}_+^\alpha$ and that between $\hat{F}^\alpha$ and $\hat{F}_-^\alpha$:

$$[\Delta\hat{F}^\alpha]_\pm = \max_{\zeta_1, \zeta_r} |\hat{F}^\alpha - \hat{F}_\pm^\alpha|/(\hat{F}_\pm^\alpha)_{\max}. \tag{2.82}$$

For $-D \le x_1 < -14.5 f_\delta$,

$$[\Delta \hat{F}^\alpha]_- \le \begin{cases} 3.31 \times 10^{-5}, & (M_- = 1.5,\ 3,\ m^B/m^A = 0.5), \\ 2.60 \times 10^{-4}, & (M_- = 1.5,\ m^B/m^A = 0.25), \\ 2.69 \times 10^{-5}, & (M_- = 2,\ m^B/m^A = 0.25), \end{cases}$$

and for $14.5 f_\delta < x_1 \le D$,

$$[\Delta \hat{F}^\alpha]_+ \le \begin{cases} 1.88 \times 10^{-3}, & (M_- = 1.5,\ 3,\ m^B/m^A = 0.5), \\ 2.67 \times 10^{-3}, & (M_- = 1.5,\ 2,\ m^B/m^A = 0.25), \end{cases}$$

where x_1 is the original coordinate system.

Since the size of the present computation is quite large, we cannot perform the accuracy test in a more systematic way. However, concerning the accuracy of the collision integrals, we can obtain a measure of accuracy by computing the gain and loss terms numerically for Maxwellian distributions and comparing the result with the exact values. If we insert $\hat{F}^\alpha_-$ and $\hat{F}^\alpha_+$ in the RHS of Eq. (2.16), each collision term $\hat{G}^{\beta\alpha}[\hat{F}^\beta_\pm, \hat{F}^\alpha_\pm] - \hat{\nu}[\hat{F}^\beta_\pm]\hat{F}^\alpha_\pm$ vanishes, and therefore, we have

$$\hat{G}^{\beta\alpha}[\hat{F}^\beta_\pm, \hat{F}^\alpha_\pm] = \hat{\nu}[\hat{F}^\beta_\pm]\hat{F}^\alpha_\pm = \mathsf{F}^{\beta\alpha}_\pm(\zeta_1, \zeta_r). \tag{2.83}$$

The middle term $\hat{\nu}[\hat{F}^\beta_\pm]\hat{F}^\alpha_\pm$ can be calculated exactly and gives the exact $\mathsf{F}^{\beta\alpha}_\pm(\zeta_1, \zeta_r)$. On the other hand, the numerical values corresponding to the first and second terms, say $\hat{G}^{\beta\alpha}_{\pm jk}$ and $\hat{\nu}^{\beta\alpha}_{\pm jk}\hat{F}^\alpha_{\pm jk}$ $[\hat{F}^\alpha_{\pm jk} = \hat{F}^\alpha_\pm(\zeta_1^{(j)}, \zeta_r^{\alpha(k)})]$, can be computed from Eqs. (2.50a) and (2.50b) and Eq. (2.54a) with $\hat{F}^{\alpha(n)}_{ijk} = \hat{F}^\alpha_{\pm jk}$. We compare $\hat{G}^{\beta\alpha}_{\pm jk}$ and $\hat{\nu}^{\beta\alpha}_{\pm jk}\hat{F}^\alpha_{\pm jk}$ with $\mathsf{F}^{\beta\alpha}_\pm(\zeta_1, \zeta_r)$ to get an estimate of the accuracy. In this check, if we compare the values only for a fixed ζ_r–lattice point $\zeta_r^{\alpha(k)}$, we need to construct the numerical kernels $\Omega^{\beta\alpha 0k}_{pqab}$ and $\Lambda^{\beta\alpha 0k}_{pa}$ only for the $\zeta_r^{\alpha(k)}$, so that a more variety of the lattice systems for the $\zeta_1\zeta_r$-plane can be checked. We consider the lattice systems ($\overline{\text{M5}}$), ($\overline{\text{M6}}$), (M7), and (M8) in Table 2.5 in addition to ($\overline{\text{M1}}$), ($\overline{\text{M2}}$), (M3), and (M4). The bar on (M5), etc., has the same meaning as in ($\overline{\text{M1}}$) and ($\overline{\text{M2}}$). Let us introduce the following maximum difference relative to the maximum value of $\mathsf{F}^{\beta\alpha}_\pm$:

$$\mathsf{G}^{\beta\alpha}_\pm = \max_j |\hat{G}^{\beta\alpha}_{\pm jk} - \mathsf{F}^{\beta\alpha}_\pm(\zeta_1^{(j)}, \zeta_r^{\alpha(k)})| / \max_{\zeta_1} \mathsf{F}^{\beta\alpha}_\pm, \tag{2.84a}$$

$$\mathsf{L}^{\beta\alpha}_\pm = \max_j |\hat{\nu}^{\beta\alpha}_{\pm jk}\hat{F}^\alpha_{\pm jk} - \mathsf{F}^{\beta\alpha}_\pm(\zeta_1^{(j)}, \zeta_r^{\alpha(k)})| / \max_{\zeta_1} \mathsf{F}^{\beta\alpha}_\pm. \tag{2.84b}$$

In the case of $d^B_m/d^A_m = 1$ and $\chi^B_- = 0.1$, 0.5, 0.9, and 0.95, the $\mathsf{G}^{\beta\alpha}_\pm$ and $\mathsf{L}^{\beta\alpha}_\pm$ for $\zeta_r^{\alpha(k)} = \zeta_r^{\alpha(1)}$ [or $\zeta_r^{\alpha(k)} = \zeta_r^{(1)}$] (cf. Table 2.5) are estimated as follows:

$$\mathsf{G}^{\beta\alpha}_\pm \le 3.23 \times 10^{-4}, \qquad \mathsf{L}^{\beta\alpha}_\pm \le 4.61 \times 10^{-5}, \qquad [\text{for } (\overline{\text{M1}})],$$

$$\mathsf{G}^{\beta\alpha}_\pm \le 3.98 \times 10^{-5}, \qquad \mathsf{L}^{\beta\alpha}_\pm \le 6.31 \times 10^{-6}, \qquad [\text{for } (\overline{\text{M2}}),\ (\overline{\text{M5}}), \text{and } (\overline{\text{M6}})],$$

for $M_- = 1.5$ and $m^B/m^A = 0.5$;

$$\mathsf{G}_{\pm}^{\beta\alpha} \leq 3.93 \times 10^{-5}, \qquad \mathsf{L}_{\pm}^{\beta\alpha} \leq 5.28 \times 10^{-6}, \qquad \text{[for (M3)]},$$
$$\mathsf{G}_{\pm}^{\beta\alpha} \leq 1.33 \times 10^{-4}, \qquad \mathsf{L}_{\pm}^{\beta\alpha} \leq 2.81 \times 10^{-4}, \qquad \text{[for (M7)]},$$

for $M_- = 3$ and $m^B/m^A = 0.5$; and

$$\mathsf{G}_{\pm}^{\beta\alpha} \leq 3.93 \times 10^{-5}, \qquad \mathsf{L}_{\pm}^{\beta\alpha} \leq 5.28 \times 10^{-6}, \qquad \text{[for (M4) and (M8)]},$$

for $M_- = 1.5$ and 2 and $m^B/m^A = 0.25$.

2.7 Concluding remarks

In this chapter, we have investigated the structure of a normal shock wave for a binary gas mixture on the basis of the Boltzmann equation for hard-sphere molecules. Extending the numerical kernel method developed in Ref. 76 for a single component gas to the case of a binary mixture, we have constructed an accurate method to compute the collision integrals (Secs. 2.4.B and 2.4.C). Then, we have analyzed the problem by an accurate finite-difference method in which the numerical kernel method is incorporated (Sec. 2.4.A). As a result, the transition from the upstream to the downstream state was clarified for the velocity distribution functions as well as for the macroscopic variables (Sec. 2.5). The accuracy of the computation was also examined carefully (Sec. 2.6.C). The numerical kernels constructed in this chapter can be applied to any problems in which the velocity distribution functions are of the form of Eq. (2.28).

In the present method, the collision integrals are approximated by using the values of the velocity distribution functions at the discrete lattice points in the molecular velocity space. One of the important mathematical questions relevant to this type of method is whether or not the approximated collision integrals converge to the real collision integrals of the Boltzmann equation when the lattice interval in the molecular velocity space tends to zero. For a single-component gas, a positive answer was given recently for some different types of discretization of the collision integral.[101–103] In all of them, the discretization is made in such a way that the mass, momentum, and energy are conserved exactly in each collision. In this point, these conservative methods (or discrete velocity models) are different from the methods of Ref. 76 and the present study, in which the conservation laws are not

satisfied artificially but are satisfied approximately within the error of computation. In the latter methods, therefore, the conservation laws can be used as a measure of accuracy (see Sec. 2.6.C).

The present computation was carried out on Fujitsu VPP800/63 computer at the Data Processing Center, Kyoto University, Fujitsu VPP800/12 computer at the Institute of Space and Astronautical Science, and VT-Alpha 533 and 600 Workstations at the Section of Dynamics in Aeronautics and Astronautics, Department of Aeronautics and Astronautics, Kyoto University.

Chapter 3

Heat transfer in a binary gas mixture between two parallel plates [104]

3.1 Introduction

The problem of heat transfer and temperature distribution in a rarefied gas between two parallel plates with different temperatures is one of the classical problems in rarefied gas dynamics, and a large number of theoretical and experimental works have been devoted to this problem, especially in the case of single-component gases (see, e.g., Refs. 105–107,85 and the references cited in Refs. 107,85). Early theoretical works covering a wide range of the Knudsen number were mainly based upon either moment and variational methods, containing arbitrary assumptions on the form of the velocity distribution function, or numerical analysis using model Boltzmann equations. Only in 1989, Ohwada *et al.*[107] reported an accurate numerical solution of the linearized Boltzmann equation for a hard-sphere gas in the case of a small temperature difference between the plates. Their solution method was a finite-difference method, in which the collision integral was computed efficiently as well as accurately by the numerical kernel method developed by Sone *et al.*[77] Subsequently, Ohwada extended the method to the collision integral of the full Boltzmann equation in his shock-structure analysis[76] and then applied it to the heat-transfer problem for a nonsmall temperature difference between the plates.[85,86]

As for the case of binary gas mixtures, the accumulation of the results is not satisfactory, though some analyses (by means of a moment method) as well as experiments were performed in 1970's.[108,109] In this chapter, therefore, we investigate the heat-transfer problem for a binary mixture of hard-sphere gases on the basis of the full Boltzmann equation for a large temperature difference, aiming to provide an accurate numerical solution that can be regarded as a standard for the problem. In Chap. 2, we have extended Ohwada's numerical kernel method for the nonlinear collision integral to the case of binary mixtures in the study of shock wave structure.[70] The same method is employed in the present analysis.

3.2 Problem

Consider a rarefied mixture of two gases, say components A and B, in the domain $0 \leq X_1 \leq D$ between two parallel plane walls at rest, where X_i is a rectangular coordinate system in space. Let the wall at $X_1 = 0$ be kept at temperature T_I and that at $X_1 = D$ at temperature T_{II}. Investigate the steady behavior of the mixture (temperature distribution, heat flow, etc.) on the basis of kinetic theory under the following assumptions:

(i) The molecules of each component are hard spheres, and the interaction between two gaseous molecules is the complete elastic collision.

(ii) The molecules of each component are reflected according to the diffuse reflection condition on the walls.

3.3 Basic equation

Let $\boldsymbol{\xi} = (\xi_1, \xi_2, \xi_3)$ be the molecular velocity and $F^\alpha(X_1, \boldsymbol{\xi})$ the velocity distribution function of the molecules of α-component ($\alpha = A, B$). The Boltzmann equation in the present problem is written as

$$\xi_1 \frac{\partial F^\alpha}{\partial X_1} = \sum_{\beta=A,B} J^{\beta\alpha}(F^\beta, F^\alpha), \qquad (\alpha = A, B), \tag{3.1}$$

$$J^{\beta\alpha}(f, g) = [(d_m^{\beta\alpha})^2/2] \int [f(\boldsymbol{\xi}_*^{\beta\alpha}) g(\boldsymbol{\xi}^{\beta\alpha}) - f(\boldsymbol{\xi}_*) g(\boldsymbol{\xi})] |\mathbf{e} \cdot \boldsymbol{V}| d\Omega d\boldsymbol{\xi}_*, \tag{3.2}$$

$$\boldsymbol{\xi}^{\beta\alpha} = \boldsymbol{\xi} + \frac{\mu^{\beta\alpha}}{m^\alpha}(\mathbf{e} \cdot \boldsymbol{V})\mathbf{e}, \quad \boldsymbol{\xi}_*^{\beta\alpha} = \boldsymbol{\xi}_* - \frac{\mu^{\beta\alpha}}{m^\beta}(\mathbf{e} \cdot \boldsymbol{V})\mathbf{e}, \quad \boldsymbol{V} = \boldsymbol{\xi}_* - \boldsymbol{\xi}, \tag{3.3}$$

$$d_m^{\beta\alpha} = (d_m^\alpha + d_m^\beta)/2, \qquad \mu^{\beta\alpha} = 2m^\alpha m^\beta/(m^\alpha + m^\beta). \tag{3.4}$$

Here, m^α and d_m^α are the mass and diameter of a molecule of α-component; $\boldsymbol{\xi}_*$ is the integration variable for $\boldsymbol{\xi}$, $\mathbf{e}$ is a unit vector, $d\boldsymbol{\xi}_* = d\xi_{*1} d\xi_{*2} d\xi_{*3}$, and $d\Omega$ is the solid-angle element around $\mathbf{e}$; the domain of integration is the whole space of $\boldsymbol{\xi}_*$ and all directions of $\mathbf{e}$.

The boundary condition on the walls ($X_1 = 0$ and D) is expressed as follows: For $\boldsymbol{\xi} \cdot \boldsymbol{n} > 0$,

$$\begin{aligned} F^\alpha(X_1, \boldsymbol{\xi}) &= \sigma_w^\alpha \Big(\frac{m^\alpha}{2\pi k T_w}\Big)^{3/2} \exp\Big(-\frac{m^\alpha |\boldsymbol{\xi}|^2}{2kT_w}\Big), \\ \sigma_w^\alpha &= -\Big(\frac{2\pi m^\alpha}{kT_w}\Big)^{1/2} \int_{\boldsymbol{\xi}_* \cdot \boldsymbol{n} < 0} \boldsymbol{\xi}_* \cdot \boldsymbol{n} F^\alpha(X_1, \boldsymbol{\xi}_*) d\boldsymbol{\xi}_*, \end{aligned} \tag{3.5}$$

where

$$
\begin{aligned}
&T_w = T_I, \quad \boldsymbol{n} = (1,0,0), \quad \text{at } X_1 = 0, \\
&\text{and} \qquad T_w = T_{II}, \quad \boldsymbol{n} = (-1,0,0), \quad \text{at } X_1 = D,
\end{aligned}
\tag{3.6}
$$

and k is the Boltzmann constant.

If we rewrite the equation and boundary condition in a dimensionless form, we find that the problem is characterized by the following five parameters: m^B/m^A, d_m^B/d_m^A, T_{II}/T_I, n_{av}^B/n_{av}^A, and Kn. Here, n_{av}^α is the average molecular number density of α–component in the domain $0 \le X_1 \le D$, and Kn$= l_0/D$ is the Knudsen number, where $l_0 = [\sqrt{2}\pi(d_m^A)^2 n_{av}]^{-1}$ is the mean free path of the molecules of A–component when it is in the equilibrium state at rest with number density $n_{av} = n_{av}^A + n_{av}^B$.

3.4 Numerical analysis

We first note that in the present problem we can seek the solution in the form $F^\alpha(X_1, \xi_1, \eta)$, where $\eta = (\xi_2^2 + \xi_3^2)^{1/2}$. We analyze Eqs. (3.1)–(3.6) numerically by means of an iterative finite-difference method. The key issue in the analysis is an accurate and efficient computation of the complicated collision integral $J^{\beta\alpha}$ using the discrete values F_{ijl}^α of F^α at the grid points $(X_1^{(i)}, \xi_1^{\alpha(j)}, \eta^{\alpha(l)})$ in the (X_1, ξ_1, η) space. For this purpose, we expand F^α at $X_1 = X_1^{(i)}$ as

$$
\begin{aligned}
F^\alpha(X_1^{(i)}, \xi_1, \eta) &= \exp\Big(-\frac{(\bar{\eta}^\alpha)^2}{2}\Big) \sum_{j,l} a_{jl}^{\alpha(i)} \Psi_j^\alpha(\bar{\xi}_1^\alpha) L_l((\bar{\eta}^\alpha)^2), \\
\bar{\xi}_1^\alpha &= \xi_1 (2kT_I/m^\alpha)^{-1/2}, \quad \bar{\eta}^\alpha = \eta(2kT_I/m^\alpha)^{-1/2},
\end{aligned}
\tag{3.7}
$$

where $\Psi_j^\alpha(\bar{\xi}_1^\alpha)$ is a localized basis function that is sectionally quadratic, takes unity at $\bar{\xi}_1^\alpha = \xi_1^{\alpha(j)}(2kT_I/m^\alpha)^{-1/2}$, and is nonzero only in its neighborhood; $L_l(y)$ is the Laguerre polynomial in y of order l. The coefficients $a_{jl}^{\alpha(i)}$ are determined in such a way that Eq. (3.7) coincides with F_{ijl}^α at the grid point $(\xi_1^{\alpha(j)}, \eta^{\alpha(l)})$. If we substitute Eq. (3.7) into the collision integral $J^{\beta\alpha}(F^\beta, F^\alpha)$, it is expressed as a linear combination of the collision integrals for the functions of the form $(\bar{\eta}^\alpha)^{2m}\Psi_n^\alpha$. The latter collision integrals are independent of F_{ijl}^α and therefore can be computed beforehand (numerical collision kernel). Once the numerical kernel is prepared, the computation of the collision integral in each iteration step is reduced to simple products and sums of matrices. In this way, high efficiency in the computation of the collision integral is attained (Ref. 76 and Chap. 2).

3.5 Result of analysis

The computation was carried out for $T_{II}/T_I = 2$, $(m^B/m^A,\ d_m^B/d_m^A) = (0.25, 0.5)$ and $(0.5, 1)$, $n_{av}^B/n_{av}^A = 0.1$, 1, and 10, and Kn= 0.1, 1, and 10. To show the result, we denote by n^α the molecular number density of α–component ($\alpha = A, B$) and by T and $q_i = (q_1, 0, 0)$ the temperature and the heat flow of the total mixture, respectively [i.e., $n^\alpha = \int F^\alpha d\boldsymbol{\xi}$, $(3knT,\ 2q_1) = \int (1,\ \xi_1)|\boldsymbol{\xi}|^2(m^A F^A + m^B F^B) d\boldsymbol{\xi}$, where $n = n^A + n^B$ and $d\boldsymbol{\xi} = d\xi_1 d\xi_2 d\xi_3$]. Note that the flow velocity of each component vanishes identically and the heat flow q_1 is independent of X_1 in the present problem because of the conservation of mass and that of energy.

The values of q_1 in all the cases are shown in Table 3.1, where $p_0 = kn_{av}T_I$ is a reference pressure. The numerical result of q_1 varies slightly with X_1 because of numerical error. Its average, say q_{1av}, over $0 \le X_1 \le D$ is shown as q_1 in the table. The maximum variation of q_1 over $0 \le X_1 \le D$ relative to q_{1av}: $\Delta = \max |q_1 - q_{1av}|/|q_{1av}|$, which gives a good measure of accuracy of the computation, is shown in percentage in Table 3.1. Figures 3.1–3.3 show the profiles of the number densities n^A and n^B and of the temperature T for the case of $m^B/m^A = 0.5$, $d_m^B/d_m^A = 1$: Fig. 3.1 is for $n_{av}^B/n_{av}^A = 0.1$, Fig. 3.2 for $n_{av}^B/n_{av}^A = 1$, and Fig. 3.3 for $n_{av}^B/n_{av}^A = 10$. On the other hand, the corresponding figures for the case of $m^B/m^A = 0.25$, $d_m^B/d_m^A = 0.5$ are shown in Figs. 3.4–3.6: Fig. 3.4 is for $n_{av}^B/n_{av}^A = 0.1$, Fig. 3.5 for $n_{av}^B/n_{av}^A = 1$, and Fig. 3.6 for $n_{av}^B/n_{av}^A = 10$. The smaller molecules (the molecules of B–component) have a larger mean free path. Since Kn is based on the average number

Table 3.1: Heat flow $q_i = (q_1,\ 0,\ 0)$ of the total mixture for $T_{II}/T_I = 2$. Here, $p_0 = kn_{av}T_I$ is the reference pressure.

		$m^B/m^A = 0.5,\ d_m^B/d_m^A = 1$		$m^B/m^A = 0.25,\ d_m^B/d_m^A = 0.5$	
n_{av}^B/n_{av}^A	Kn	$q_1/[p_0(2kT_I/m^A)^{1/2}]$	Δ (%)	$q_1/[p_0(2kT_I/m^A)^{1/2}]$	Δ (%)
0.1	0.1	−0.184	0.45	−0.207	0.72
0.1	1	−0.509	0.19	−0.547	0.19
0.1	10	−0.656	0.049	−0.693	0.047
1	0.1	−0.209	0.34	−0.370	0.67
1	1	−0.589	0.15	−0.814	0.13
1	10	−0.763	0.047	−0.966	0.036
10	0.1	−0.245	0.34	−0.659	0.19
10	1	−0.677	0.10	−1.124	0.075
10	10	−0.871	0.038	−1.244	0.014

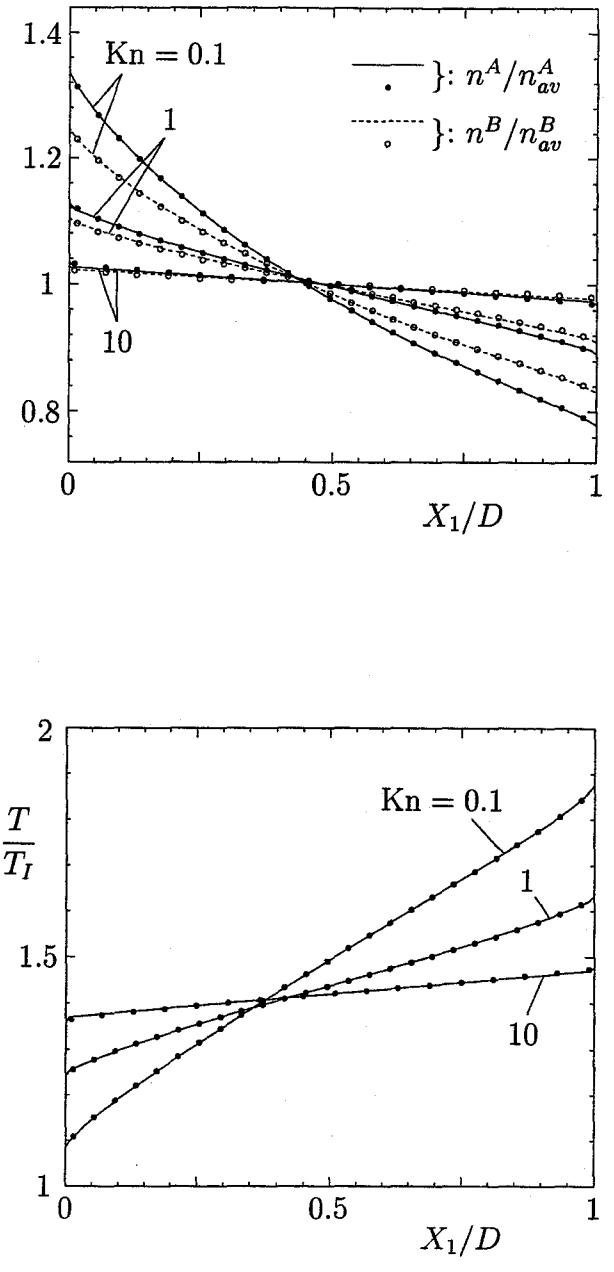

Figure 3.1: Profiles of the number densities n^A and n^B and of the temperature of the total mixture T for $m^B/m^A = 0.5$, $d^B_m/d^A_m = 1$, and $n^B_{av}/n^A_{av} = 0.1$. Here, — and --- indicate the result by the finite-difference method, and • and ∘ that by the DSMC method.

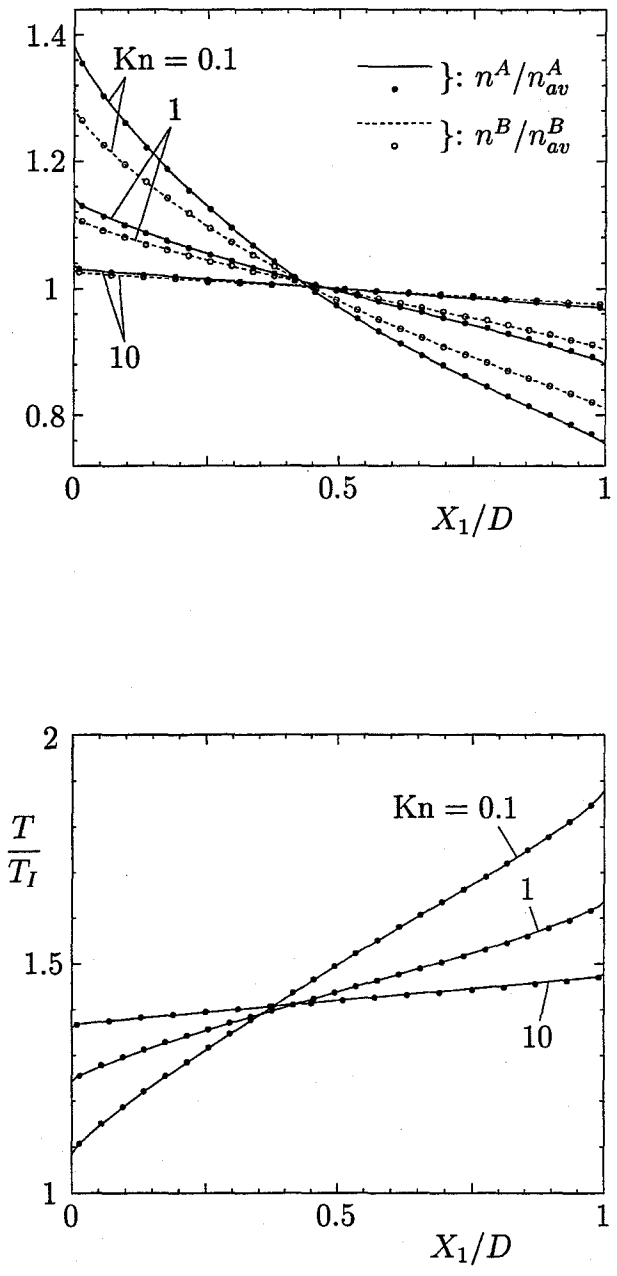

Figure 3.2: Profiles of the number densities n^A and n^B and of the temperature of the total mixture T for $m^B/m^A = 0.5$, $d^B_m/d^A_m = 1$, and $n^B_{av}/n^A_{av} = 1$. See the caption of Fig. 3.1.

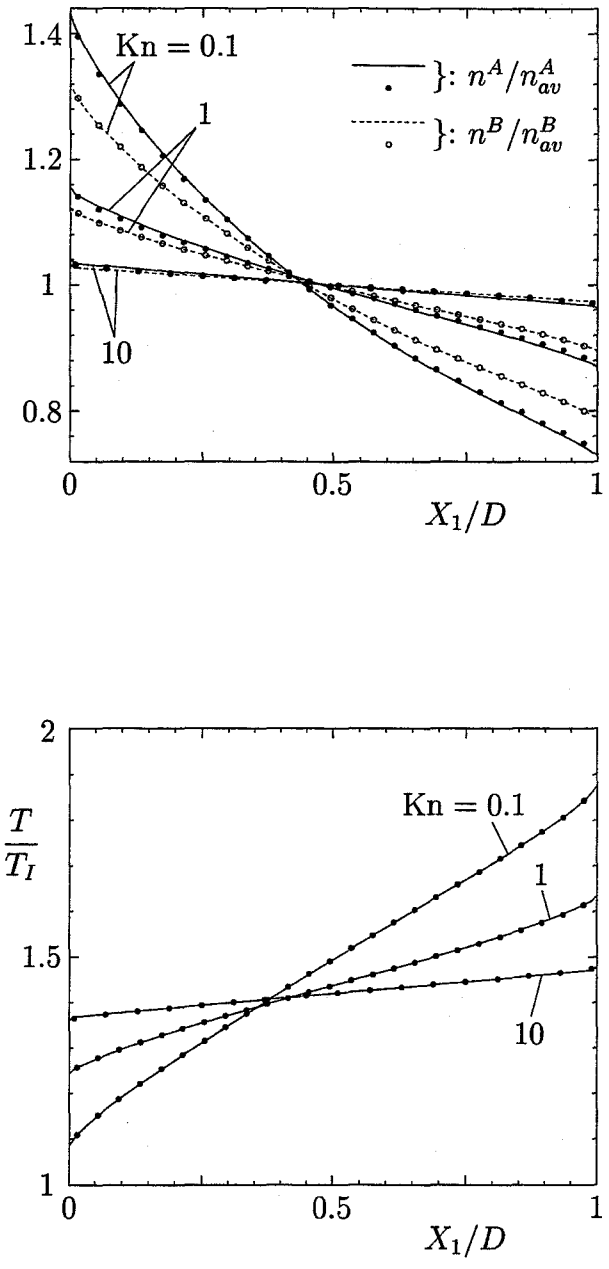

Figure 3.3: Profiles of the number densities n^A and n^B and of the temperature of the total mixture T for $m^B/m^A = 0.5$, $d^B_m/d^A_m = 1$, and $n^B_{av}/n^A_{av} = 10$. See the caption of Fig. 3.1.

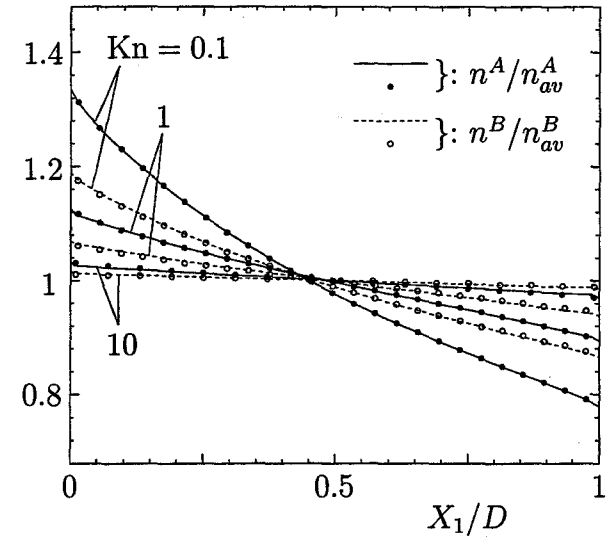

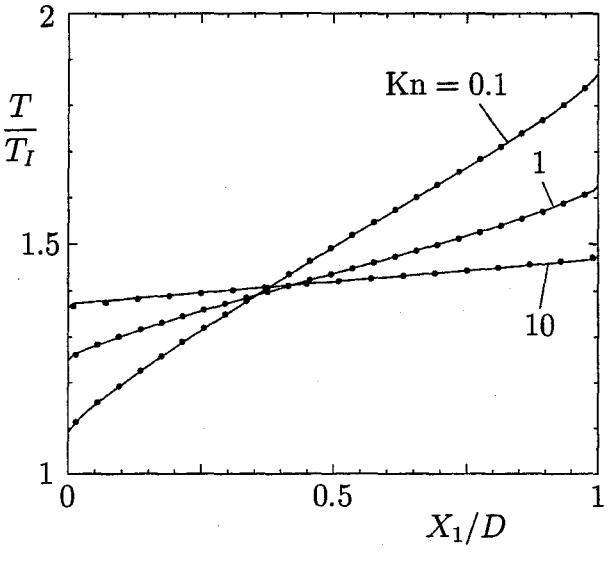

Figure 3.4: Profiles of the number densities n^A and n^B and of the temperature of the total mixture T for $m^B/m^A = 0.25$, $d^B_m/d^A_m = 0.5$, and $n^B_{av}/n^A_{av} = 0.1$. See the caption of Fig. 3.1.

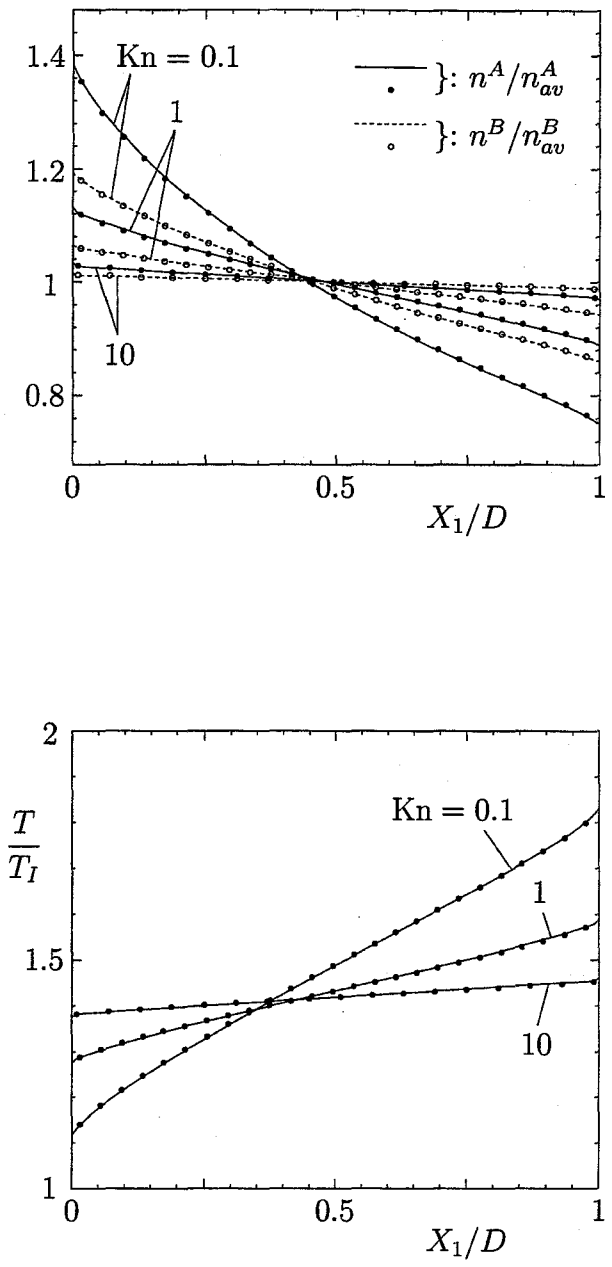

Figure 3.5: Profiles of the number densities n^A and n^B and of the temperature of the total mixture T for $m^B/m^A = 0.25$, $d^B_m/d^A_m = 0.5$, and $n^B_{av}/n^A_{av} = 1$. See the caption of Fig. 3.1.

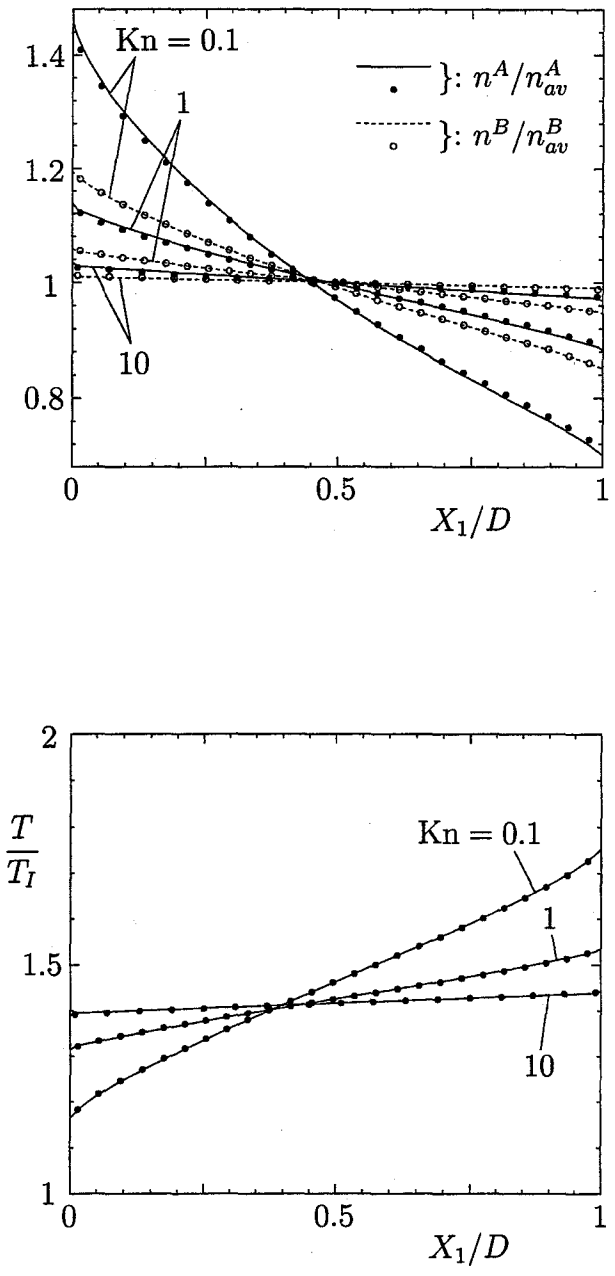

Figure 3.6: Profiles of the number densities n^A and n^B and of the temperature of the total mixture T for $m^B/m^A = 0.25$, $d^B_m/d^A_m = 0.5$, and $n^B_{av}/n^A_{av} = 10$. See the caption of Fig. 3.1.

density of the total mixture and on the diameter of the larger molecules (the molecules of A–component), the effective Knudsen number at the same Kn is larger for larger values of n_{av}^B/n_{av}^A. Therefore, the temperature jump on the walls at the same Kn is larger for larger n_{av}^B/n_{av}^A. In Figs. 3.1–3.6, the corresponding result obtained by the direct simulation Monte Carlo (DSMC) method[36] is also shown for comparison. The DSMC result shows good agreement with the finite-difference result.

The velocity distribution functions F^α at two points near the walls in the cases corresponding to Figs. 3.4–3.6 are shown in Figs. 3.7–3.9, respectively. That is, F^α at $\eta(2kT_I/m^A)^{-1/2} = 0.15$ and 1.35 are shown as functions of ξ_1. In the case of free-molecular gas (Kn $= \infty$), the velocity distribution functions for any X_1 are discontinuous at $\xi_1 = 0$. For large Kn (Kn $= 10$), though the discontinuity vanishes because of the molecular collision, the gradient near $\xi_1 = 0$ is still very steep. The change around $\xi_1 = 0$ becomes milder as the Knudsen number decreases. The corresponding result by the DSMC method is also shown in Figs. 3.7–3.9.

The data about grid systems are summarized here. Let us put $c_I^A = (2kT_I/m^A)^{1/2}$. We divided the interval $0 \leq X_1 \leq D$ into 100 uniform sections for Kn= 1 and 10 and into 100 nonuniform sections (minimum size $4 \times 10^{-6}D$ at $X_1 = 0$ and D; maximum size $0.0294D$ at $X_1 = D/2$) for Kn= 0.1. We used uniform grids for ξ_1: For Kn= 0.1 and 1, the grid size is $0.15c_I^A$ and the range is restricted to $-6c_I^A \leq \xi_1 \leq 6c_I^A$ ($m^B/m^A = 0.5$) or $-8.7c_I^A \leq \xi_1 \leq 8.7c_I^A$ ($m^B/m^A = 0.25$) for A–component and to $-8.4c_I^A \leq \xi_1 \leq 8.4c_I^A$ ($m^B/m^A = 0.5$) or $-12c_I^A \leq \xi_1 \leq 12c_I^A$ ($m^B/m^A = 0.25$) for B–component; for Kn= 10, the grid size is $0.106c_I^A$ and the range is restricted to $-5.73c_I^A \leq \xi_1 \leq 4.45c_I^A$ ($m^B/m^A = 0.5$) or $-7.85c_I^A \leq \xi_1 \leq 6.58c_I^A$ ($m^B/m^A = 0.25$) for A–component and to $-7.85c_I^A \leq \xi_1 \leq 6.58c_I^A$ ($m^B/m^A = 0.5$) or $-10.82c_I^A \leq \xi_1 \leq 9.55c_I^A$ ($m^B/m^A = 0.25$) for B–component. For η, we used nonuniform 14 grid points defined by $(2kT_I/m^\alpha)^{1/2}\sqrt{y_k}$ ($\alpha = A, B$) for Kn= 0.1 and 1 and $(2kT_I/m^\alpha)^{1/2}\sqrt{y_k/2}$ for Kn= 10, where y_k ($k = 1, ..., 14$) are the zeros of the Laguerre polynomial $L_{14}(y)$ (Chap. 2).

Finally, we give information about the DSMC computational system. We used 50 (Kn $= 10$) or 100 (Kn $= 0.1, 1$) uniform cells in the interval $0 \leq X_1 \leq D$. Let N^α be the average number of simulation particles per cell for α–component. Then, (N^A, N^B)=(1000, 100) for $n_{av}^B/n_{av}^A = 0.1$, (250, 250) for $n_{av}^B/n_{av}^A = 1$, and (100, 1000) for

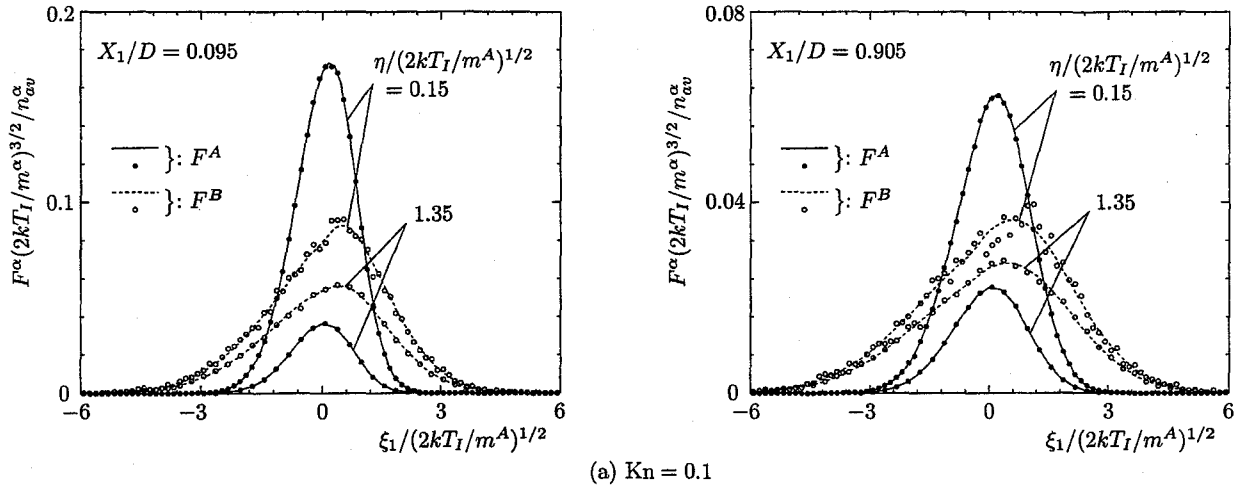

(a) Kn = 0.1

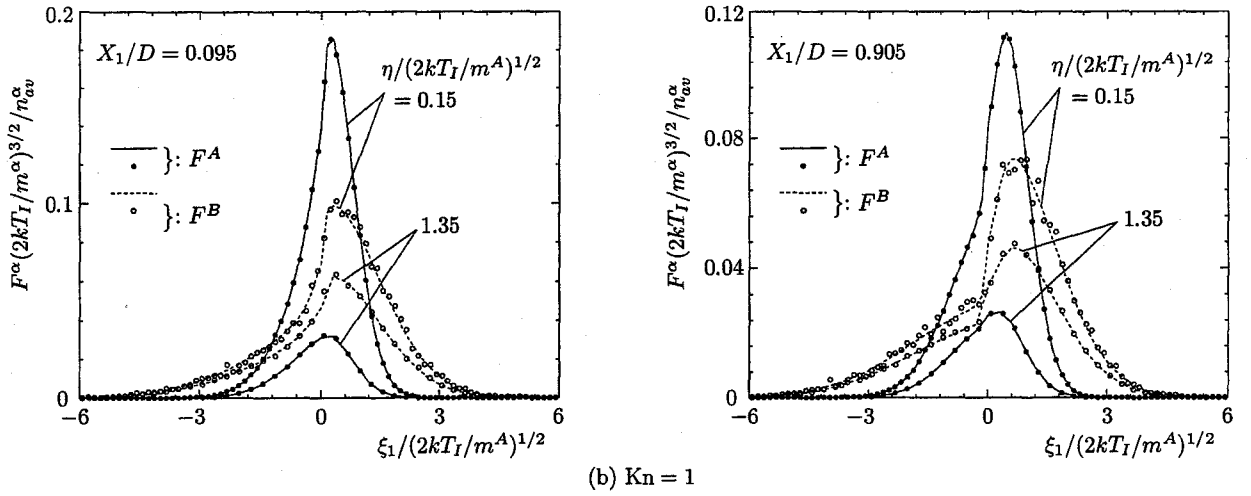

(b) Kn = 1

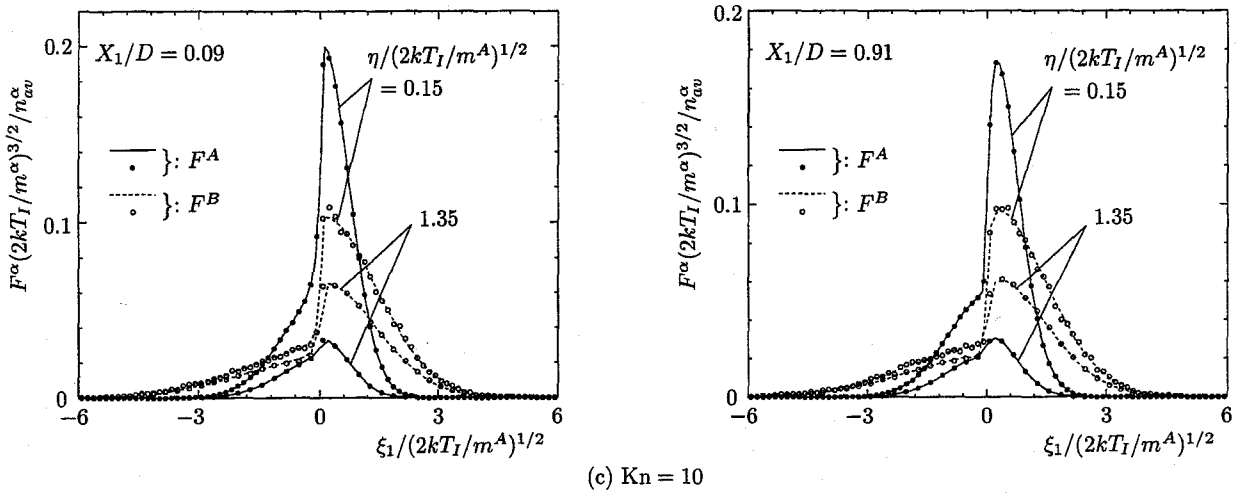

(c) Kn = 10

Figure 3.7: Velocity distribution functions F^A and F^B at two points near the walls for $m^B/m^A = 0.25$, $d^B_m/d^A_m = 0.5$, and $n^B_{av}/n^A_{av} = 0.1$ (cf. Fig. 3.4). (a) Kn = 0.1, (b) Kn = 1, (c) Kn = 10. Here, — and --- indicate the result by the finite-difference method, and • and ∘ that by the DSMC method. The F^α at $X_1/D = 0.095$ and 0.905 are shown in (a) and (b), while F^α at $X_1/D = 0.09$ and 0.91 are shown in (c).

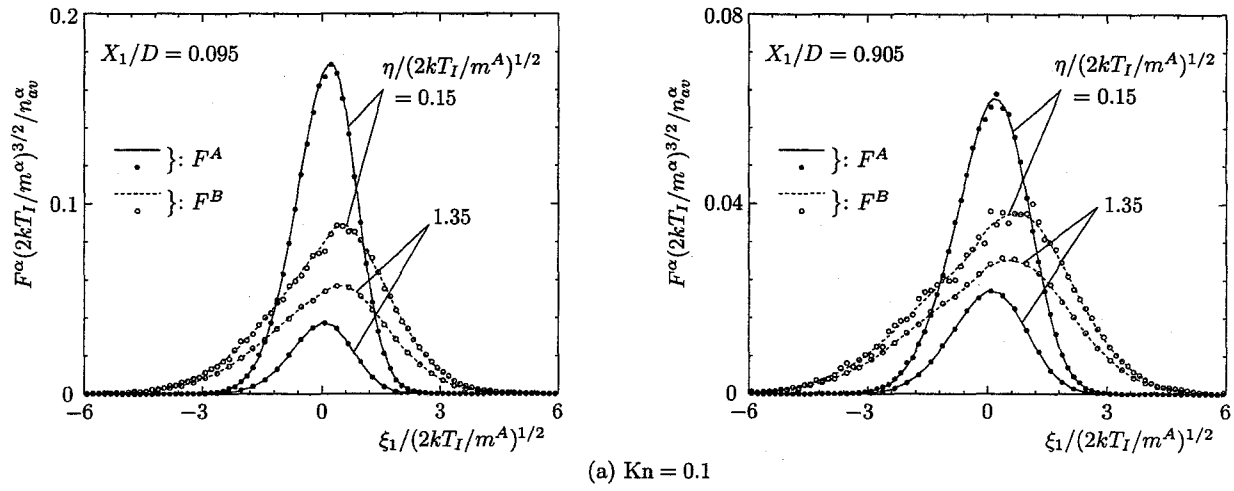

(a) Kn = 0.1

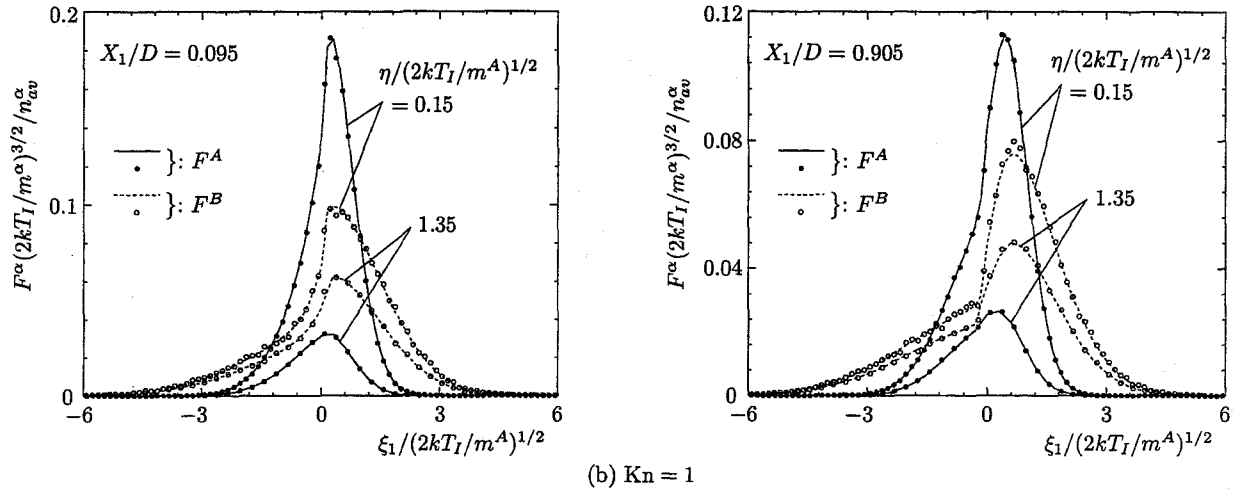

(b) Kn = 1

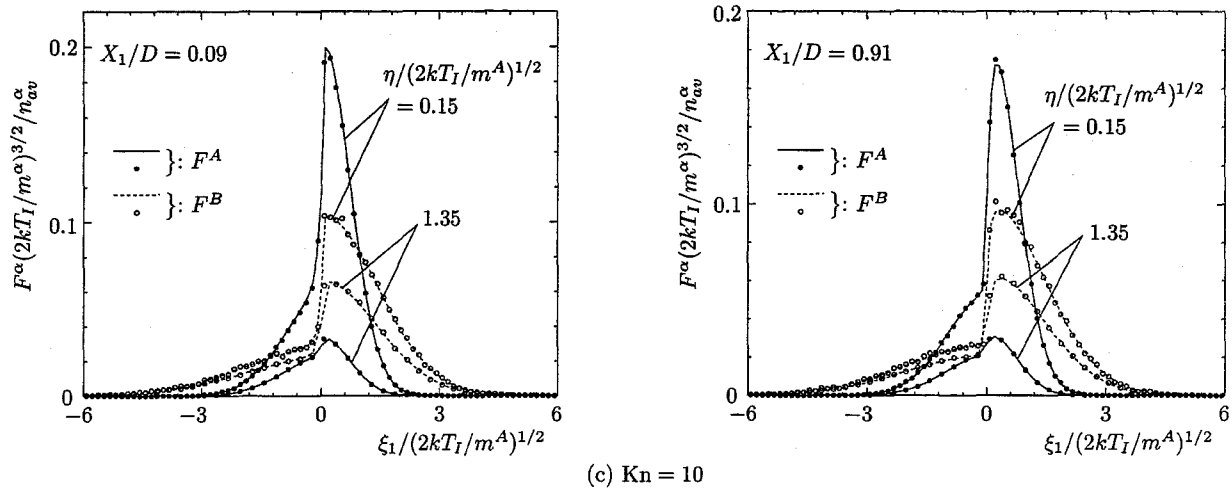

(c) Kn = 10

Figure 3.8: Velocity distribution functions F^A and F^B at two points near the walls for $m^B/m^A = 0.25$, $d^B_m/d^A_m = 0.5$, and $n^B_{av}/n^A_{av} = 1$ (cf. Fig. 3.5). (a) Kn = 0.1, (b) Kn = 1, (c) Kn = 10. See the caption of Fig. 3.7.

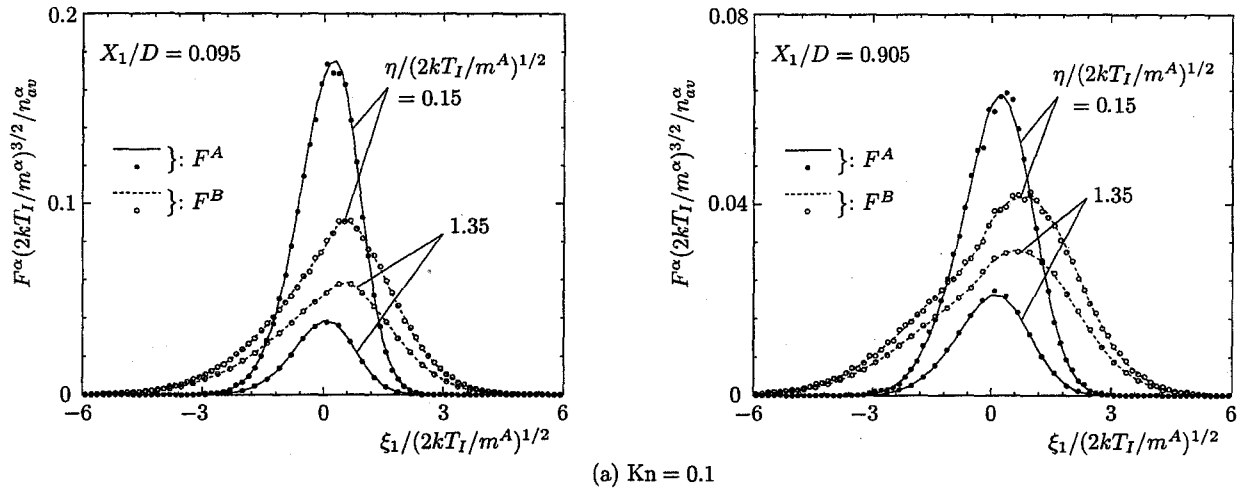

(a) Kn = 0.1

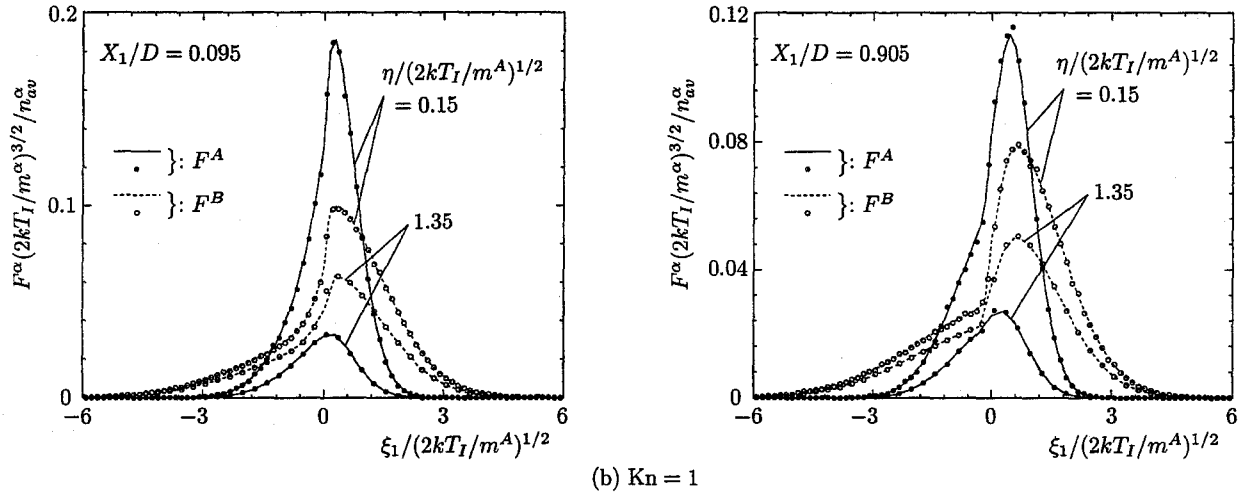

(b) Kn = 1

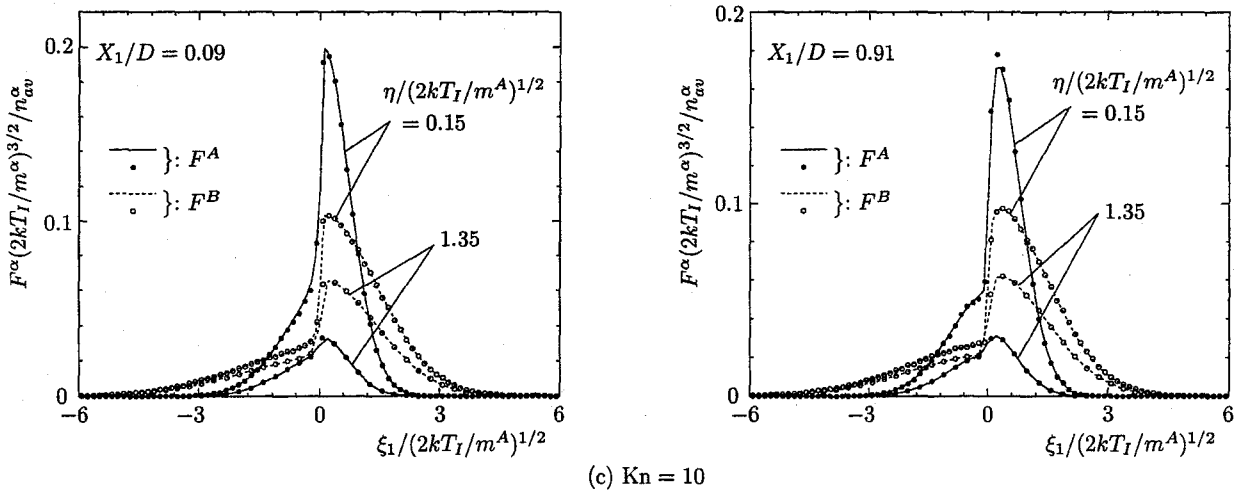

(c) Kn = 10

Figure 3.9: Velocity distribution functions F^A and F^B at two points near the walls for $m^B/m^A = 0.25$, $d^B_m/d^A_m = 0.5$, and $n^B_{av}/n^A_{av} = 10$ (cf. Fig. 3.6). (a) Kn = 0.1, (b) Kn = 1, (c) Kn = 10. See the caption of Fig. 3.7.

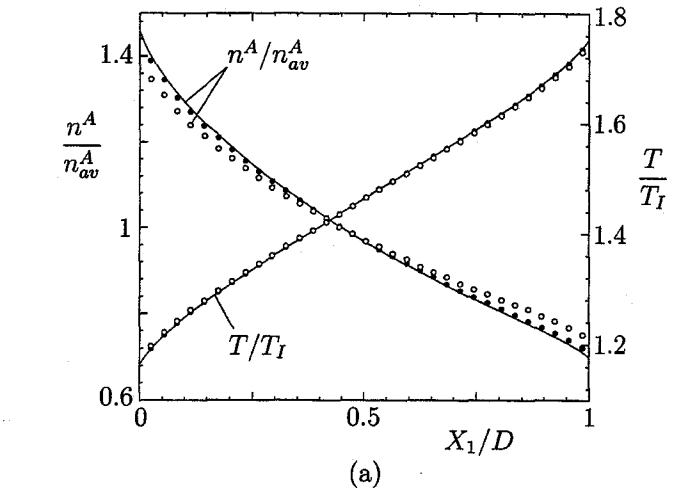

(a)

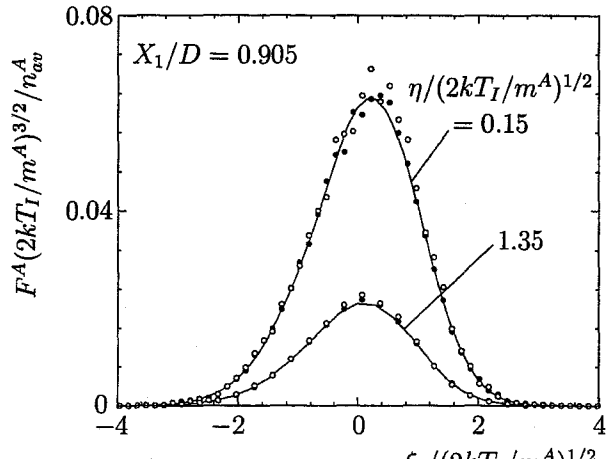

(b)

Figure 3.10: DSMC computations with two different numbers of simulation particles for $m^B/m^A = 0.25$, $d^B_m/d^A_m = 0.5$, Kn $= 0.1$, and $n^B_{av}/n^A_{av} = 10$. (a) Number density n^A and temperature T (cf. Fig. 3.6). (b) Velocity distribution function F^A at $X_1/D = 0.905$ (cf. Fig. 3.9). Here, — indicates the finite-difference result, ○ the DSMC result with $(N^A, N^B) = (25, 250)$, and • that with $(N^A, N^B) = (100, 1000)$.

$n_{av}^B/n_{av}^A = 10$ [(N^A, N^B)=(2000, 200) for $n_{av}^B/n_{av}^A = 0.1$ and (200, 2000) for $n_{av}^B/n_{av}^A = 10$ in the case of $m^B/m^A = 0.25$, $d_m^B/d_m^A = 0.5$, and Kn = 10]. The average of 2×10^4 samples taken at each 50 time steps is shown in Figs. 3.1–3.9. For small or large n_{av}^B/n_{av}^A, the total number of simulation particles increases because sufficient particles are necessary for the component with smaller number density (the same weight is used for both components in the present computation). We also carried out the DSMC computation with fewer particles, an example of which is shown in Fig. 3.10. That is, the result with (N^A, N^B)=(25, 250) of the case $m^B/m^A = 0.25$, $d_m^B/d_m^A = 0.5$, Kn = 0.1, and $n_{av}^B/n_{av}^A = 10$ is shown in the figure, together with the result with (N^A, N^B)=(100, 1000). Although it is smooth, the profile of n^A with (N^A, N^B)=(25, 250) deviates recognizably from that by the finite-difference method [Fig. 3.10(a)].

Appendixes

A Derivation of Eqs. (2.53) and (2.54)

The Christoffel–Darboux formula[99] for a system of orthonormal polynomials gives the following relation for the Laguerre polynomials:

$$(x-y)\sum_{s=0}^{H-1} L_s(x)L_s(y) = (c_{H-1,H-1}/c_{HH})[L_H(x)L_{H-1}(y) - L_H(y)L_{H-1}(x)]. \tag{A1}$$

Noting that $L_H(x) = c_{HH}\prod_{l=1}^{H}(x-y_l)$, where y_l are the zeros of $L_H(x)$, we put $y = y_k$ in Eq. (A1). Then, using the continuity of polynomials, we have

$$\prod_{l=1\ (\neq k)}^{H}(x-y_l) = \frac{1}{c_{H-1,H-1}L_{H-1}(y_k)}\sum_{l=0}^{H-1} L_l(y_k)L_l(x), \qquad (k=1,\ ...,\ H), \tag{A2}$$

for all $x > 0$.

Now let us consider Eq. (2.44) with $H^\alpha = H$ and suppose that $\zeta_r^{\alpha(k)} = \sqrt{y_k/\hat{m}^\alpha}$ [or $\hat{m}^\alpha(\zeta_r^{\alpha(k)})^2 = y_k$] [Eq. (2.52)]. For simplicity, let us put

$$\hat{m}^\alpha\zeta_r^2 \equiv x, \qquad \hat{F}_i^{\alpha(n)}(\zeta_1^{\alpha(j)},\zeta_r)\exp\left(\frac{\hat{m}^\alpha\zeta_r^2}{2}\right) \equiv f_{ij}^\alpha(x),$$
$$\hat{F}_{ijk}^{\alpha(n)}\exp\left(\frac{\hat{m}^\alpha(\zeta_r^{\alpha(k)})^2}{2}\right) = \hat{F}_{ijk}^{\alpha(n)}\exp\left(\frac{y_k}{2}\right) \equiv f_{ijk}^\alpha.$$

Then, Eq. (2.44) is written as

$$f_{ij}^\alpha(x) = \sum_{l=0}^{H-1} a_{ijl}^{\alpha(n)}L_l(x). \tag{A3}$$

On the other hand, from the choice of $a_{ijl}^{\alpha(n)}$ [see Eq. (2.47) and the sentences below it], $f_{ij}^\alpha(x)$ is expressed as

$$f_{ij}^\alpha(x) = \sum_{k=1}^{H} f_{ijk}^\alpha \prod_{s=1\ (\neq k)}^{H}\frac{x-y_s}{y_k-y_s}. \tag{A4}$$

By equating the RHS's of Eqs. (A3) and (A4) and using Eq. (A2), we obtain

$$\sum_{l=0}^{H-1} a_{ijl}^{\alpha(n)}L_l(x) = \sum_{k=1}^{H} f_{ijk}^\alpha \frac{1}{c_{H-1,H-1}L_{H-1}(y_k)\prod_{s=1\ (\neq k)}^{H}(y_k-y_s)}\sum_{s=0}^{H-1} L_s(y_k)L_s(x). \tag{A5}$$

If we integrate Eq. (A5) multiplied by $\exp(-x)L_m(x)$ with respect to x from 0 to infinity, we have, from the orthogonality relation (2.46), the following expression of $a_{ijm}^{\alpha(n)}$, i.e., Eqs. (2.53a) and (2.53b):

$$a_{ijm}^{\alpha(n)} = \sum_{k=1}^{H} f_{ijk}^{\alpha} \frac{L_m(y_k)}{c_{H-1,H-1} L_{H-1}(y_k) \prod_{s=1\ (\neq k)}^{H} (y_k - y_s)}. \tag{A6}$$

By the use of Eq. (2.53a), Eq. (A3) is written as

$$f_{ij}^{\alpha}(x) = \sum_{l=0}^{H-1} \Big(\sum_{k=1}^{H} w_{lk} \hat{F}_{ijk}^{\alpha(n)} \Big) L_l(x). \tag{A7}$$

Using the expression $L_l(x) = \sum_{m=0}^{l} c_{ml} x^m$ and changing the order of summations, we obtain

$$f_{ij}^{\alpha}(x) = \sum_{m=0}^{H-1} \Big(\sum_{k=1}^{H} \hat{F}_{ijk}^{\alpha(n)} \sum_{l=m}^{H-1} c_{ml} w_{lk} \Big) x^m. \tag{A8}$$

The comparison of Eq. (A8) with Eq. (2.48) gives

$$A_{ijm}^{\alpha(n)} = \sum_{k=1}^{H} \hat{F}_{ijk}^{\alpha(n)} \sum_{l=m}^{H-1} c_{ml} w_{lk}, \tag{A9}$$

which is equivalent to Eqs. (2.54a) and (2.54b).

B Integration of Eq. (2.66b)

Let us introduce the following integral:

$$\tilde{\Theta}_a^{kl}(x_0, x_1, z, \theta, \bar{\epsilon}) = \int_{-\infty}^{\infty} \int_{-\infty}^{\infty} J_1^l U(J_1; x_0, x_1) (\sqrt{\hat{m}^\beta} J_r^{(k)})^{2a} \exp\left(-\frac{(\sqrt{\hat{m}^\beta} J_r^{(k)})^2}{2} \right) dw' dw'', \tag{B1}$$

where

$$U(t; x_0, x_1) = \begin{cases} 1 & (x_0 < t < x_1), \\ 0 & (\text{otherwise}). \end{cases} \tag{B2}$$

Then, $\Theta_{pa}^k(z, \theta, \bar{\epsilon})$ in Eq. (2.66b) is expressed by a linear combination of $\tilde{\Theta}_a^{kl}(x_0, x_1, z, \theta, \bar{\epsilon})$, $(l = 0, 1, 2)$. For example, Θ_{1a}^k is expressed as follows:

$$\Theta_{1a}^k(z, \theta, \bar{\epsilon}) = [-\tilde{\Theta}_a^{k2}(0, 2h, z, \theta, \bar{\epsilon}) + 2h\tilde{\Theta}_a^{k1}(0, 2h, z, \theta, \bar{\epsilon})]/h^2. \tag{B3}$$

Therefore, the calculation of Eq. (2.66b) is reduced to that of Eq. (B1). The integration of Eq. (B1) can be carried out analytically and gives the following expression of $\tilde{\Theta}_a^{kl}$:

$$\begin{pmatrix} \tilde{\Theta}_a^{k2}(x_0, x_1, z, \theta, \bar{\epsilon}) \\ \tilde{\Theta}_a^{k1}(x_0, x_1, z, \theta, \bar{\epsilon}) \\ \tilde{\Theta}_a^{k0}(x_0, x_1, z, \theta, \bar{\epsilon}) \end{pmatrix} = \tilde{B}^k \begin{pmatrix} \tilde{Y}_a^{k2} \\ \tilde{Y}_a^{k1} \\ \tilde{Y}_a^{k0} \end{pmatrix}, \tag{B4}$$

where

$$\tilde{B}^k = \frac{1}{(\hat{m}^\beta)^2} \begin{pmatrix} \frac{\sin^2\theta}{\cos^3\theta} & 0 & 0 \\ 0 & \frac{\sin\theta}{\cos^2\theta} & 0 \\ 0 & 0 & \frac{1}{\cos\theta} \end{pmatrix} \begin{pmatrix} 1 & 2\zeta_r^{\alpha(k)}\cos\bar{\epsilon} & (\zeta_r^{\alpha(k)}\cos\bar{\epsilon})^2 \\ 0 & 1 & \zeta_r^{\alpha(k)}\cos\bar{\epsilon} \\ 0 & 0 & 1 \end{pmatrix} \times \begin{pmatrix} 1 & 2\sqrt{\hat{m}^\beta}\delta^{\beta\alpha}\frac{z}{\sin\theta} & \hat{m}^\beta\left(\delta^{\beta\alpha}\frac{z}{\sin\theta}\right)^2 \\ 0 & \sqrt{\hat{m}^\beta} & \hat{m}^\beta\delta^{\beta\alpha}\frac{z}{\sin\theta} \\ 0 & 0 & \hat{m}^\beta \end{pmatrix}, \tag{B5}$$

$$\delta^{\beta\alpha} = (\hat{m}^\beta - \hat{m}^\alpha)/(\hat{m}^\beta + \hat{m}^\alpha), \tag{B6}$$

$$\tilde{Y}_a^{kl} = \sum_{r=0}^{a} \binom{a}{r} \tilde{g}_{a-r} \times \tilde{q}_{2r+l}^k, \qquad (l = 0, 1, 2), \tag{B7}$$

$$\tilde{q}_s^k = E_s(\sqrt{\hat{m}^\beta} Z_1) - E_s(\sqrt{\hat{m}^\beta} Z_0), \tag{B8}$$

$$Z_i = x_i \cot\theta - \zeta_r^{\alpha(k)}\cos\bar{\epsilon} - \delta^{\beta\alpha}\frac{z}{\sin\theta}, \qquad (i = 0, 1). \tag{B9}$$

Here, $\binom{0}{0} = 1$; $E_s(x)$ is defined by

$$E_s(x) = \int_0^x t^s \exp(-t^2/2) dt, \tag{B10}$$

and has the following recursion formula:

$$E_s(x) = -x^{s-1}\exp(-x^2/2) + (s-1)E_{s-2}(x),$$
$$E_0(x) = \sqrt{\pi/2}\,\mathrm{erf}(x/\sqrt{2}), \qquad E_1(x) = 1 - \exp(-x^2/2),$$

where

$$\mathrm{erf}(x) = \frac{2}{\sqrt{\pi}} \int_0^x \exp(-t^2) dt, \tag{B11}$$

is the error function; and $\tilde{g}_s$ is defined by

$$\tilde{g}_s = \int_{-\infty}^{\infty} t^{2s} \exp(-t^2/2) dt, \tag{B12}$$

namely,

$$\tilde{g}_s = (2s-1)(2s-3)\cdots 5\cdot 3\cdot 1\cdot \tilde{g}_0, \qquad \tilde{g}_0 = \sqrt{2\pi}.$$

When $\beta = \alpha$, $\tilde{\Theta}_a^{kl}$ in Eq. (B1) does not depend on z because both of J_1 and $J_r^{(k)}$ are independent of z [cf. Eqs. (2.64a) and (2.64b)]. In this case, Eqs. (B4)–(B9) are reduced to the following:

$$\begin{pmatrix} \tilde{\Theta}_a^{k2}(x_0, x_1, \theta, \bar{\epsilon}) \\ \tilde{\Theta}_a^{k1}(x_0, x_1, \theta, \bar{\epsilon}) \\ \tilde{\Theta}_a^{k0}(x_0, x_1, \theta, \bar{\epsilon}) \end{pmatrix} = \tilde{B}^k \begin{pmatrix} \tilde{Y}_a^{k2} \\ \tilde{Y}_a^{k1} \\ \tilde{Y}_a^{k0} \end{pmatrix}, \tag{B13}$$

$$\tilde{B}^k = \frac{1}{(\hat{m}^\alpha)^2} \begin{pmatrix} \frac{\sin^2\theta}{\cos^3\theta} & 0 & 0 \\ 0 & \frac{\sin\theta}{\cos^2\theta} & 0 \\ 0 & 0 & \frac{1}{\cos\theta} \end{pmatrix} \begin{pmatrix} 1 & 2\sqrt{\hat{m}^\alpha}\zeta_r^{\alpha(k)}\cos\bar{\epsilon} & \hat{m}^\alpha(\zeta_r^{\alpha(k)}\cos\bar{\epsilon})^2 \\ 0 & \sqrt{\hat{m}^\alpha} & \hat{m}^\alpha\zeta_r^{\alpha(k)}\cos\bar{\epsilon} \\ 0 & 0 & \hat{m}^\alpha \end{pmatrix}, \quad \text{(B14)}$$

$$\tilde{Y}_a^{kl} = \sum_{r=0}^{a} \binom{a}{r} \tilde{g}_{a-r} \times \tilde{q}_{2r+l}^k, \qquad (l = 0, 1, 2), \quad \text{(B15)}$$

$$\tilde{q}_s^k = E_s(\sqrt{\hat{m}^\alpha}(x_1 \cot\theta - \zeta_r^{\alpha(k)}\cos\bar{\epsilon})) - E_s(\sqrt{\hat{m}^\alpha}(x_0 \cot\theta - \zeta_r^{\alpha(k)}\cos\bar{\epsilon})). \quad \text{(B16)}$$

C Integration of Eq. (2.66a)

Let us consider the following integral:

$$\tilde{\Gamma}_{ab}^{klm}(x_0, x_1, y_0, y_1, \theta, \bar{\epsilon}) = \sin\theta \int_0^\infty z K_1^l U(K_1; x_0, x_1)(\sqrt{\hat{m}^\alpha}K_r^{(k)})^{2b} \times \exp\left(-\frac{(\sqrt{\hat{m}^\alpha}K_r^{(k)})^2}{2}\right) \tilde{\Theta}_a^{km}(y_0, y_1, z, \theta, \bar{\epsilon}) dz. \quad \text{(C1)}$$

Then, $\Gamma_{pqab}^k(\theta, \bar{\epsilon})$ in Eq. (2.66a) is expressed by a linear combination of $\tilde{\Gamma}_{ab}^{klm}$ $(l, m = 0, 1, 2)$. Therefore, the computation of Γ_{pqab}^k is reduced to that of $\tilde{\Gamma}_{ab}^{klm}$. The $\tilde{\Gamma}_{ab}^{klm}$ can be expressed in the following form.

$$\begin{pmatrix} \tilde{\Gamma}_{ab}^{k22} & \tilde{\Gamma}_{ab}^{k21} & \tilde{\Gamma}_{ab}^{k20} \\ \tilde{\Gamma}_{ab}^{k12} & \tilde{\Gamma}_{ab}^{k11} & \tilde{\Gamma}_{ab}^{k10} \\ \tilde{\Gamma}_{ab}^{k02} & \tilde{\Gamma}_{ab}^{k01} & \tilde{\Gamma}_{ab}^{k00} \end{pmatrix} = \tilde{A}^k \begin{pmatrix} \tilde{X}_{ab}^{k32} & \tilde{X}_{ab}^{k31} & \tilde{X}_{ab}^{k30} \\ \tilde{X}_{ab}^{k22} & \tilde{X}_{ab}^{k21} & \tilde{X}_{ab}^{k20} \\ \tilde{X}_{ab}^{k12} & \tilde{X}_{ab}^{k11} & \tilde{X}_{ab}^{k10} \\ \tilde{X}_{ab}^{k02} & \tilde{X}_{ab}^{k01} & \tilde{X}_{ab}^{k00} \end{pmatrix}, \quad \text{(C2)}$$

where

$$\tilde{A}^k = \frac{1}{(\hat{\mu}^{\beta\alpha})^2} \exp\left(-\frac{\hat{m}^\alpha(\zeta_r^{\alpha(k)}\sin\bar{\epsilon})^2}{2}\right) \begin{pmatrix} \frac{\cos^2\theta}{\sin^3\theta} & 0 & 0 \\ 0 & \frac{\cos\theta}{\sin^2\theta} & 0 \\ 0 & 0 & \frac{1}{\sin\theta} \end{pmatrix} \times \begin{pmatrix} 1 & -3\sqrt{\hat{m}^\alpha}\zeta_r^{\alpha(k)}\cos\bar{\epsilon} & 3\hat{m}^\alpha(\zeta_r^{\alpha(k)}\cos\bar{\epsilon})^2 & -(\hat{m}^\alpha)^{3/2}(\zeta_r^{\alpha(k)}\cos\bar{\epsilon})^3 \\ 0 & \sqrt{\hat{m}^\alpha} & -2\hat{m}^\alpha\zeta_r^{\alpha(k)}\cos\bar{\epsilon} & (\hat{m}^\alpha)^{3/2}(\zeta_r^{\alpha(k)}\cos\bar{\epsilon})^2 \\ 0 & 0 & \hat{m}^\alpha & -(\hat{m}^\alpha)^{3/2}\zeta_r^{\alpha(k)}\cos\bar{\epsilon} \end{pmatrix}, \quad \text{(C3)}$$

$$\tilde{X}_{ab}^{klm} = \sum_{r=0}^{b} \binom{b}{r} (\sqrt{\hat{m}^\alpha}\zeta_r^{\alpha(k)}\sin\bar{\epsilon})^{2r} \times \tilde{p}_{a,2(b-r)+l}^{km}, \qquad (l = 0, 1, 2, 3;\ m = 0, 1, 2), \quad \text{(C4)}$$

$$\tilde{p}_{as}^{km} = \int_{\sqrt{\hat{m}^\alpha}Z_0}^{\sqrt{\hat{m}^\alpha}Z_1} \bar{z}^s \exp(-\bar{z}^2/2)\tilde{\Theta}_a^{km}(y_0, y_1, z, \theta, \bar{\epsilon}) d\bar{z}, \quad \text{(C5)}$$

$$z = \frac{\hat{m}^\alpha}{\hat{\mu}^{\beta\alpha}\sin\theta}\left(\frac{\bar{z}}{\sqrt{\hat{m}^\alpha}} - \zeta_r^{\alpha(k)}\cos\bar{\epsilon}\right), \quad \text{(C6)}$$

$$Z_i = x_i \tan\theta + \zeta_r^{\alpha(k)}\cos\bar{\epsilon}, \quad (i = 0, 1). \quad \text{(C7)}$$

The integration with respect to $\bar{z}$ in Eq. (C5) is carried out numerically. Then, the double integral with respect to $\bar{\epsilon}$ and θ in Eq. (2.65) is computed numerically.

When $\beta = \alpha$, Eq. (C1) is reduced to the following form, since $\tilde{\Theta}_a^{km}$ is independent of z.

$$\tilde{\Gamma}_{ab}^{klm}(x_0, x_1, y_0, y_1, \theta, \bar{\epsilon}) = \tilde{\Gamma}_b^{kl}(x_0, x_1, \theta, \bar{\epsilon}) \times \tilde{\Theta}_a^{km}(y_0, y_1, \theta, \bar{\epsilon}), \tag{C8}$$

where

$$\tilde{\Gamma}_b^{kl}(x_0, x_1, \theta, \bar{\epsilon}) = \sin\theta \int_0^\infty z K_1^l U(K_1; x_0, x_1)(\sqrt{\hat{m}^\alpha} K_r^{(k)})^{2b} \exp\left(-\frac{(\sqrt{\hat{m}^\alpha} K_r^{(k)})^2}{2}\right) dz. \tag{C9}$$

We can carry out this integration analytically to obtain the following expression of $\tilde{\Gamma}_b^{kl}$:

$$\begin{pmatrix} \tilde{\Gamma}_b^{k2}(x_0, x_1, \theta, \bar{\epsilon}) \\ \tilde{\Gamma}_b^{k1}(x_0, x_1, \theta, \bar{\epsilon}) \\ \tilde{\Gamma}_b^{k0}(x_0, x_1, \theta, \bar{\epsilon}) \end{pmatrix} = \tilde{A}^k \begin{pmatrix} \tilde{X}_b^{k3} \\ \tilde{X}_b^{k2} \\ \tilde{X}_b^{k1} \\ \tilde{X}_b^{k0} \end{pmatrix}, \tag{C10}$$

$$\tilde{X}_b^{kl} = \sum_{r=0}^{b} \binom{b}{r} (\sqrt{\hat{m}^\alpha} \zeta_r^{\alpha(k)} \sin\bar{\epsilon})^{2r} \times \tilde{p}_{2(b-r)+l}^k, \qquad (l = 0, 1, 2, 3), \tag{C11}$$

$$\tilde{p}_s^k = E_s(\sqrt{\hat{m}^\alpha} Z_1) - E_s(\sqrt{\hat{m}^\alpha} Z_0), \tag{C12}$$

$$Z_i = x_i \tan\theta + \zeta_r^{\alpha(k)} \cos\bar{\epsilon}, \qquad (i = 0, 1). \tag{C13}$$

Here, $\tilde{A}^k$ is given by Eq. (C3) with $\hat{\mu}^{\beta\alpha} = \hat{m}^\alpha$. With this expression of $\tilde{\Gamma}_b^{kl}$, we carry out the double integration with respect to $\bar{\epsilon}$ and θ in Eq. (2.65) numerically.

References

1 K. Aoki, S. Takata, and S. Kosuge, Phys. Fluids **10**, 1519 (1998).

2 Y. Sone and Y. Onishi, J. Phys. Soc. Jpn. **44**, 1981 (1978).

3 Y. Onishi and Y. Sone, J. Phys. Soc. Jpn. **47**, 1676 (1979).

4 Y. Sone, in *Advances in Kinetic Theory and Continuum Mechanics*, edited by R. Gatignol and Soubbaramayer (Springer-Verlag, Berlin, 1991), p. 29.

5 K. Aoki and Y. Sone, in *Advances in Kinetic Theory and Continuum Mechanics*, edited by R. Gatignol and Soubbaramayer (Springer-Verlag, Berlin, 1991), p. 43.

6 K. Aoki, K. Nishino, Y. Sone, and H. Sugimoto, Phys. Fluids A **3**, 2260 (1991).

7 H. Sugimoto and Y. Sone, Phys. Fluids A **4**, 419 (1992).

8 Y. Sone and H. Sugimoto, Phys. Fluids A **5**, 1491 (1993).

9 Y. Sone and H. Sugimoto, Phys. Fluids **7**, 2072 (1995).

10 S. Takata, Y. Sone, D. Lhuillier, and M. Wakabayashi, Computers Math. Applic. **35**, 193 (1998).

11 Y. Sone, S. Takata, and M. Wakabayashi, Phys. Fluids **6**, 1914 (1994).

12 Y. P. Pao, Phys. Fluids **14**, 306 (1971).

13 J. R. Thomas, Jr., T. S. Chang, and C. E. Siewert, Phys. Rev. Lett. **33**, 680 (1974).

14 T. Matsushita, Phys. Fluids **19**, 1712 (1976).

15 K. Aoki and C. Cercignani, Phys. Fluids **26**, 1163 (1983).

16 L. D. Koffman, M. S. Plesset, and L. Lees, Phys. Fluids **27**, 876 (1984).

17 C. Cercignani, W. Fiszdon, and A. Frezzotti, Phys. Fluids **28**, 3237 (1985).

18 T. Ytrehus and T. Aukrust, in *Rarefied Gas Dynamics*, edited by V. Boffi and C. Cercignani (Teubner, Stuttgart, 1986), Vol. 2, p. 271.

19 F. Boujot and Soubbaramayer, C. R. Acad. Sci. Paris Ser. II **307**, 323 (1988).

20 Y. Sone, T. Ohwada, and K. Aoki, in *Mathematical Aspects of Fluid and Plasma Dynamics*, Lecture Notes in Mathematics 1460, edited by G. Toscani, V. Boffi, and S. Rionero (Springer-Verlag, Berlin, 1991), p. 186.

21 K. Aoki and N. Masukawa, Phys. Fluids **6**, 1379 (1994).

22 H. Cabannes, Eur. J. Mech., B/Fluids **13**, 685 (1994).

23 A. d'Almeida and R. Gatignol, Eur. J. Mech., B/Fluids **16**, 401 (1997).

24 Y. Pao, J. Chem. Phys. **59**, 6688 (1973).

25 J. C. Hass and G. S. Springer, Trans. ASME Ser. C **95**, 263 (1973).

26 T. Matsushita, in *Rarefied Gas Dynamics*, edited by J. L. Potter (AIAA, New York, 1977), p. 1213.

27 T. Soga, Phys. Fluids **25**, 1978 (1982).

28 Y. Onishi, in *Rarefied Gas Dynamics*, edited by H. Oguchi (Univ. of Tokyo Press, Tokyo, 1984), p. 875.

29 Y. Onishi, in *Rarefied Gas Dynamics: Physical Phenomena*, edited by E. P. Muntz, D. P. Weaver and D. H. Campbell (AIAA, Washington, DC, 1989), p. 470.

30 Y. Onishi, in *Rarefied Gas Dynamics: Physical Phenomena*, edited by E. P. Muntz, D. P. Weaver and D. H. Campbell (AIAA, Washington, DC, 1989), p. 492.

31 D. Bedeaux, J. A. M. Smit, L. J. F. Hermans, and T. Ytrehus, Physica A **182**, 388 (1992).

32 P. L. Bhatnagar, E. P. Gross, and M. Krook, Phys. Rev. **94**, 511 (1954).

33 P. Welander, Ark. Fys. **7**, 507 (1954).

34 M. N. Kogan, Appl. Math. Mech. **22**, 597 (1958).

35 G. A. Bird, *Molecular Gas Dynamics* (Oxford University Press, Oxford, 1976).

36 G. A. Bird, *Molecular Gas Dynamics and the Direct Simulation of Gas Flows* (Oxford University Press, Oxford, 1994).

37 C. Cercignani, J. Math. Phys. **8**, 1653 (1967).

38 L. Arkeryd, C. Cercignani, and R. Illner, Comm. Math. Phys. **142**, 285 (1991).

39 S. Ukai, Transp. Theory Stat. Phys. **21**, 487 (1992).

40 L. Arkeryd and A. Nouri, Indiana Univ. Math. J. **44**, 815 (1995).

41 M. N. Kogan, *Rarefied Gas Dynamics* (Plenum, New York, 1969).

42 S. Chapman and T. G. Cowling, *The Mathematical Theory of Non-Uniform Gases*, 3rd ed. (Cambridge University Press, London, 1970).

43 F. Reif, *Fundamentals of Statistical and Thermal Physics* (McGraw-Hill, New York, 1965), p. 301.

44 In the present definition, p^α is not the partial pressure. Another definition of p^α and T^α, i.e., Eq. (1.8c) with u^α being replaced by u [see Eq. (1.9c)], is also used in the literature (e.g., Refs. 41 and 42).

45 C. Cercignani, *The Boltzmann Equation and Its Applications* (Springer-Verlag, New York, 1988).

46 H. Grad, in *Handbuch der Physik*, edited by S. Flügge (Springer-Verlag, Berlin, 1958), Vol. 12, p. 205.

47 Y. Sone, K. Aoki, and T. Doi, Transp. Theor. Stat. Phys. **21**, 297 (1992).

48 K. Aoki and T. Doi, in *Rarefied Gas Dynamics: Theory and simulations*, edited by B. D. Shizgal and D. P. Weaver (AIAA, Washington, DC, 1994), p 521.

49 T. Doi, K.Aoki, and Y. Sone, J. Vac. Soc. Jpn. **37**, 143 (1994) (in Japanese).

50 T. Doi, J. Vac. Soc. Jpn. **38**, 201 (1995) (in Japanese).

51 Y. Sone, J. Phys. Soc. Jpn. **45**, 315 (1978).

52 T. Ytrehus, in *Rarefied Gas Dynamics*, edited by J. L. Potter (AIAA, New York, 1977), p. 1197.

53 M. D. Arthur and C. Cercignani, Z. Angew. Math. Phys. **31**, 634 (1980).

54 Y. Sone and H. Sugimoto, in *Adiabatic Waves in Liquid-Vapor Systems*, edited by G. E. A. Meier and P. A. Thompson (Springer-Verlag, Berlin, 1990), p. 293.

55 Y. Sone and K. Aoki, *Molecular Gas Dynamics* (Asakura, Tokyo, 1994) (in Japanese).

56 T. Ytrehus and J. A. Alvestad, in *Rarefied Gas Dynamics*, edited by S. S. Fisher (AIAA, New York, 1981), p. 330.

57 Y. Sone, K. Aoki, and I. Yamashita, in *Rarefied Gas Dynamics*, edited by V. Boffi and C. Cercignani (Teubner, Stuttgart, 1986), Vol. 2, p. 236.

58 K. Aoki, Y. Sone, and T. Yamada, Phys. Fluids A **2**, 1867 (1990).

59 M. N. Kogan and A. A. Abramov, in *Rarefied Gas Dynamics*, edited by A. E. Beylich (VCH, Weinheim, 1991), p. 1251.

60 A. P. Kryukov, in *Rarefied Gas Dynamics*, edited by A. E. Beylich (VCH, Weinheim, 1991), p. 1278.

61 Y. Sone, F. Golse, T. Ohwada, and T. Doi, Eur. J. Mech., B/Fluids **17**, 277 (1998).

62 V. Garzó, A. Santos, and J. J. Brey, Phys. Fluids A **1**, 380 (1989).

63 The model in Ref. 62 reduces to the BGK model for a single component gas.

64 T. Doi, Doctoral Dissertation, Kyoto University (1997) (in Japanese).

65 F. B. Pidduck, Proc. Lond. Math. Soc. **15**, 89 (1915).

66 C. L. Pekeris, Proc. Nat. Acad. Sci. U.S.A. **41**, 661 (1955).

67 The actual evaluation of the constants $\hat{n}^A_{H0}$, $\hat{u}^A_{H0}$, and $\hat{T}^A_{H0}$ in the case (ii) was carried out on the basis of the model Boltzmann equation, not hard-sphere molecules.

68 Y. Sone, Y. Waniguchi, and K. Aoki, Phys. Fluids **8**, 2227 (1996).

69 The numerical results in Figs. 1.2 and 1.3 show that there arises a negative gradient in the profile of the temperature T of the total mixture (see also Figs. 1.5–1.7), though the temperatures of the two surfaces are the same ($T_I = T_{II}$). This is a special case of the phenomenon of the negative temperature gradient that was pointed out in Ref. 12 and discussed in Refs. 2,13,15,17,20, and 21 (the physical mechanism was clarified in Ref. 2).

70 S. Kosuge, K. Aoki, and S. Takata, Eur. J. Mech., B/Fluids **19**, (2000) (to be published).

71 H. M. Mott-Smith, Phys. Rev., 2nd Ser. **82**, 885 (1951).

72 H. W. Liepmann, R. Narashimha, and M. T. Chahine, Phys. Fluids **5**, 1313 (1962).

73 G. A. Bird, Phys. Fluids **13**, 1172 (1970).

74 W. Fiszdon, in *Rarefied Gas Flows: Theory and Experiment*, edited by W. Fiszdon (Springer, Vienna, 1981), p. 447.

75 C. Cercignani, A. Frezzotti, and P. Grosfils, Phys. Fluids **11**, 2757 (1999).

76 T. Ohwada, Phys. Fluids A **5**, 217 (1993).

77 Y. Sone, T. Ohwada, and K. Aoki, Phys. Fluids A **1**, 363 (1989).

78 T. Ohwada, Y. Sone, and K. Aoki, Phys. Fluids A **1**, 1588 (1989).

79 T. Ohwada and Y. Sone, Eur. J. Mech., B/Fluids **11**, 389 (1992).

80 T. Ohwada, Y. Sone, and K. Aoki, Phys. Fluids A **1**, 2042 (1989).

81 Y. Sone, S. Takata, and T. Ohwada, Eur. J. Mech., B/Fluids **9**, 273 (1990).

82 S. Takata, Y. Sone, and K. Aoki, Phys. Fluids A **5**, 716 (1993).

83 S. Takata and Y. Sone, Eur. J. Mech., B/Fluids **14**, 487 (1995).

84 T. Ohwada, in *Rarefied Gas Dynamics: Theory and Simulations*, edited by B. D. Shizgal and D. P. Weaver (AIAA, Washington, D.C., 1994), p. 482.

85 T. Ohwada, Phys. Fluids **8**, 2153 (1996).

86 T. Ohwada, in *Rarefied Gas Dynamics*, edited by C. Shen (Peking University Press, Beijing, 1997), p. 327.

87 R. E. Center, Phys. Fluids **10**, 1777 (1967).

88 L. N. Harnett and E. P. Muntz, Phys. Fluids **15**, 565 (1972).

89 A. S. Gmurczyk, M. Tarczyński, and Z. A. Walenta, in *Rarefied Gas Dynamics*, edited by R. Campargue (Commissariat a l'Energie Atomique, Paris, 1979), Vol. 1, p. 333.

90 M. M. Oberai, Phys. Fluids **9**, 1634 (1966).

91 M. M. Oberai and U. N. Sinha, in *Rarefied Gas Dynamics*, edited by M. Becker and M. Fiebig (DFVLR, Povz-Wahn, 1974), Vol. 1, B.25.

92 A. E. Beylich, Phys. Fluids **11**, 2764 (1968).

93 R. Fernández-Feria and J. Fernández de la Mora, J. Fluid Mech. **179**, 21 (1987).

94 K. Abe and H. Oguchi, Phys. Fluids **17**, 1333 (1974).

95 B. B. Hamel, in *Rarefied Gas Dynamics,* edited by J. L. Potter (AIAA, New York, 1977), Vol. 1, p. 171.

96 G. A. Bird, J. Fluid Mech. **31**, 657 (1968).

97 G. A. Bird, in *Rarefied Gas Dynamics,* edited by H. Oguchi (University of Tokyo Press, Tokyo, 1984), Vol. 1, p. 175.

98 A. A. Raines, in *Rarefied Gas Dynamics*, edited by R. Brun, R. Campargue, R. Gatignol, and J.-C. Lengrand (Cépaduès–Éditions, Toulouse, 1999), Vol. 2, p. 173.

99 M. Abramowitz and I. A. Stegun, *Handbook of Mathematical Functions* (Dover, New York, 1965), Chap. 22.

100 A. Ralston and P. Rabinowitz, *A First Course in Numerical Analysis, 2nd ed.* (McGraw-Hill, New York, 1978), Chap. 4.

101 A. V. Bobylev, A. Palczewski, and J. Schneider, SIAM J. Numer. Anal. **34**, 1865 (1997).

102 F. Rogier and J. Schneider, Transp. Ther. Stat. Phys. **23**, 313 (1994).

103 V. Panferov and A. Heintz, Math. Methods Appl. Sci. (to be published).

104 S. Kosuge, K. Aoki, and S. Takata, in *Rarefied Gas Dynamics,* edited by T. J. Bartel and M. Gallis (AIP, Melville, 2001) (to be published).

105 E. P. Gross and S. Ziering, Phys. Fluids **2**, 701 (1959).

106 P. Bassanini, C. Cercignani, and C. D. Pagani, Int. J. Heat Mass Transfer **10**, 447 (1967).

107 T. Ohwada, K. Aoki, and Y. Sone, in *Rarefied Gas Dynamics: Theoretical and Computational Techniques,* edited by E. P. Muntz, D. P. Weaver, and D. H. Campbell, (AIAA, Washington, DC, 1989), p. 70.

108 B. T. Yeh and A. Frohn, Phys. Fluids **16**, 330 (1973).

109 D. Braun and A. Frohn, Int. J. Heat Mass Transfer **19**, 1329 (1976).

Acknowledgements

The auther expresses his cordial thanks to Professor Kazuo Aoki for his kind guidance and valuable advice, and to Associate Professor Shigeru Takata for his continuous encouragement and helpful advice. At the same time, the auther is deeply grateful to Professor Yoshio Sone for his kind encouragement at suitable moments, and to Associate Professor Taku Ohwada for his creative works as good examples of Chap. 2 and Chap. 3 in the present study.